論文 / 著書情報
Article / Book Information

題目(和文)	強く駆動される非線形振動子と確率同期現象への位相縮約法によるアプローチ
Title(English)	Phase Reduction Approach to Strongly Driven Nonlinear Oscillators and Stochastic Synchrony
著者(和文)	紅林亘
Author(English)	Wataru Kurebayashi
出典(和文)	学位:博士（工学）, 学位授与機関:東京工業大学, 報告番号:甲第9665号, 授与年月日:2014年9月25日, 学位の種別:課程博士, 審査員:中尾　裕也,木村　康治,井村　順一,天谷　賢治,早川　朋久
Citation(English)	Degree:, Conferring organization: Tokyo Institute of Technology, Report number:甲第9665号, Conferred date:2014/9/25, Degree Type:Course doctor, Examiner:,,,,
学位種別(和文)	博士論文
Type(English)	Doctoral Thesis

DOCTORAL THESIS

Phase Reduction Approach to Strongly Driven Nonlinear Oscillators and Stochastic Synchrony

Wataru Kurebayashi
Graduate School of Information Science and Technology, Tokyo Institute of Technology

Abstract

Theoretical methods for analyzing synchronization of limit-cycle oscillators are in great demand in many fields of science and engineering. The aim of this thesis is to extend the class of external forcing for which synchronization dynamics can be analyzed. The first part deals with a new type of synchronization, called noise-induced synchronization, for which theoretical analysis has been limited to the case of white-noise forcing. Using an effective white-noise approximation, an extended quantitative method for analyzing colored-noise cases is proposed. In the second part, the fundamental theory for analyzing the synchronization dynamics itself, called the phase reduction method, is extended so that it can deal with strongly driven oscillators. This extension is not only useful for analyzing noise-induced synchronization, but also for analyzing other types of synchronization, e.g., injection locking and mutual synchronization of the oscillators. The validity and robustness of the proposed methods are confirmed by numerical simulations.

Contents

Chapter 1

Introduction

1.1 Background

Synchronization of oscillators is a ubiquitous phenomenon in nature. It has been studied in many fields of science and engineering, e.g., biology, chemistry, physics, mechanical engineering, and electrical engineering [1, 2, 3]. Since synchronization phenomena observed in various classes of systems generally shares basic mathematical mechanisms, theoretical analysis is useful for understanding synchronization mechanisms in such fields. By theoretical analysis, we can investigate various dynamical and statistical properties of synchronization (e.g., whether synchronization occurs, the accuracy of synchronization, and hysteresis). Indeed, theoretical synchronization analysis has been conducted for many classes of systems in various fields, e.g., neural networks [4, 5], oscillatory patterns in reaction-diffusion systems [6], oscillations in candle combustion [7], frogs' calling [8] and pedestrians on a bridge [9]. In such works, unknown nontrivial mechanisms underlying synchronization have been clarified by theoretical analysis. Thus, theoretical approaches provide powerful tools to understand synchronization mechanisms across the discipline. Therefore, basic theories useful for practical analysis should be valuable for researchers in many fields.

As such a basic theory, the phase reduction method [2] has played an essential role in theoretical synchronization analysis of limit-cycle oscillators particularly in physics and applied mathematics. Using the phase reduction method, we can simplify and reduce a high-dimensional limit-cycle oscillator subjected to a sufficiently weak perturbation $\sigma \boldsymbol{p}(t)$ ("sufficiently small" indicates $\sigma \ll 1$):

$$\dot{\boldsymbol{X}} = \boldsymbol{F}(\boldsymbol{X}) + \sigma \boldsymbol{p}(t), \tag{1.1}$$

to a one-dimensional *phase equation*:

$$\dot{\theta} = \omega + \sigma \boldsymbol{Z}(\theta) \cdot \boldsymbol{p}(t) + O(\sigma^2), \tag{1.2}$$

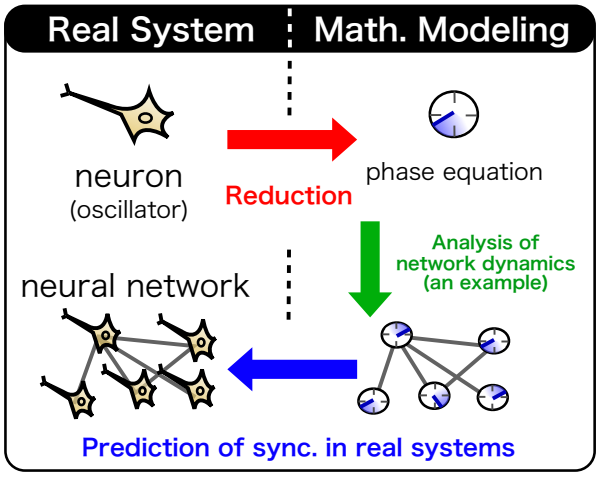

Figure 1.1: Schematic of theoretical synchronization analysis based on the phase reduction method. Using the phase reduction method, we reduce high-dimensional limit-cycle oscillators, e.g., neural oscillators, to one-dimensional phase equations (red arrow), so we can theoretically analyze their dynamics. For example, we can theoretically analyze collective dynamics in the network of phase equations (green arrow). From the theoretical result obtained by synchronization analysis of the phase equations, we can predict the actual collective dynamics in real network systems, e.g., neural networks (blue arrow).

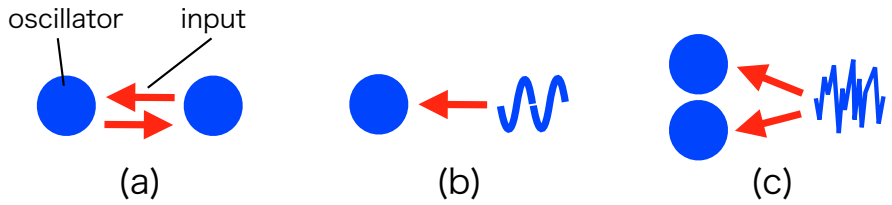

Figure 1.2: Three types of synchronization: (a) mutual synchronization, (b) injection locking, and (c) noise-induced synchronization.

where $\boldsymbol{X}(t) \in \mathbb{R}^n$ is an n-dimensional state variable of the oscillator, $\boldsymbol{F}(\boldsymbol{X}) \in \mathbb{R}^n$ is a vector field that has a stable limit-cycle orbit with period T and frequency $\omega := 2\pi/T$, $\sigma \boldsymbol{p}(t)$ is an input to the oscillator, σ is a scalar parameter that represents the strength of the input, $\theta(t)$ is a scalar variable called a phase, and $\boldsymbol{Z}(\theta)$ is a phase sensitivity function [2] that characterizes the response of the oscillator to the input. In the phase equation, the high-dimensional state $\boldsymbol{X}(t)$ of an oscillator is represented by the scalar phase variable $\theta(t)$. This equation has the advantage of being simple and easily analyzed, so it makes the theoretical synchronization analysis significantly easier (see Fig. 1.1 for a schematic of synchronization analysis based on this method). In addition, this equation is useful in engineering applications such as optimal design of oscillators, because the response of this equation to the input is explicitly characterized by a simple function $\boldsymbol{Z}(\theta)$ of a single variable θ only. Indeed, the phase reduction method has been applied, e.g., to optimal design of oscillator circuits [10, 11], optimal control of neurons [12, 13], system identification of interacting oscillators [14], and the evaluation and analysis of phase noise in oscillator circuits [15, 16, 17, 18, 19]. In particular, the phase reduction method has recently attracted much interest in electrical engineering [10, 11, 15, 16, 17, 18, 19]. Also in this thesis, we employ the phase reduction method as a theoretical basis. As discussed below, we extend this fundamental theory, i.e., the phase reduction method itself, in this thesis.

On the basis of the phase reduction method, various theoretical methods for synchronization analysis have been developed. In general, synchronization can be classified into the following three types [3] (see Fig. 1.2 for a schematic):

1. synchronization of limit-cycle oscillators interacting with each other via coupling (mutual synchronization),

2. synchronization of a limit-cycle oscillator to periodic external forcing applied to the oscillator (injection locking),

3. synchronization of uncoupled limit-cycle oscillators driven by common stochastic forcing or noise (noise-induced synchronization).

This thesis particularly focuses on the analysis of the mechanism of noise-induced synchronization, because noise-induced synchronization still remains largely unclear while the other two types of synchronization have been widely studied in the last four decades. Noise-induced synchronization has a quite different mechanism from the other two. In mutual synchronization or injection locking, the phase of an oscillator is locked to the phase of other oscillators or periodic external forcing, while the oscillator is not locked to external forcing but always fluctuates in noise-induced synchronization. Thus, noise-induced synchronization should be treated not only from a viewpoint of dynamical systems theory, but also from stochastic dynamics. On the basis of stochastic dynamics, Teramae and Tanaka [20] have proven that noise-induced synchronization of limit-cycle oscillators always occurs when the oscillators are driven by common weak white noise except for a special case. This proof has been extended to the case of general colored noise by Teramae and Tanaka [21] and confirmed in a more rigorous analysis by Goldobin, Teramae, Nakao, and Ermentrout [22]. Indeed, noise-induced synchronization can be ubiquitously observed in many classes of systems, e.g., neurons [23, 24, 25, 26, 27, 28], electric circuits [29], electronic devices [30], microbial cells [31], lasers [32], and chaotic dynamical systems [33, 34, 35]. Thus, theoretical methods for analyzing noise-induced synchronization are useful for researchers in many fields ranging from biology to electrical engineering.

As one of such theoretical methods, Nakao, Arai, and Kawamura [36] proposed a quantitative method for theoretically predicting various statistical properties of noise-induced synchronization from the properties of the oscillators and common noise. This method provides us with various useful information about the noise-induced synchronization, i.e., not only if noise-induced synchronization occurs, but also the accuracy of synchronization and the formation of various synchronization patterns including fully synchronized and clustered states. The key contribution of this work is the characterization of statistical properties of noise-induced synchronization by the probability density function of phase differences, which can be calculated from the properties of the oscillators and common noise. This probability density function can nicely characterize stochastic dynamics of the phase difference between two oscillators driven by common noise. We can predict what synchronization patterns are induced, from the shape of this probability density function, e.g, the number and height of peaks and the tail of the distribution, so we can clearly understand the relation between the synchronization patterns and the dynamical properties of the oscillators. Therefore, this method is useful for understating underlying mechanism of noise-induced synchronization in various systems.

However, the theoretical method by Nakao et al. [36] is valid only for the case that the oscillators are driven by weak white noise, so we cannot apply this method to various synchronization and clustering phenomena in nature when the common noise is temporally correlated or not sufficiently small. The aim of this thesis is to overcome these two limitations on the external forcing, i.e.,

1. limitation to white noise (temporally uncorrelated noise),

2. limitation to sufficiently weak forcing.

The first limitation arises because the Fokker-Planck equation is used for deriving the probability density function of the phase differences in Ref. [36]. Using the Fokker-Planck equation, we can analytically derive the stationary probability density function of a dynamical variable described by a Langevin equation driven by white noise, while such a useful tool has not been developed for the case of colored noise. However, the temporal correlation of common noise often plays an important role in noise-induced synchronization in nature. For example, it is theoretically confirmed that the temporal correlation in the spikes of neurons significantly affects the propagation of synchronized firings in neural circuits [37]. In addition, it is reported that oscillatory correlation enhances noise-induced synchronization [38]. It is clear from these examples that the temporal correlation of common noise to be of great importance in theoretical analysis. Thus, in order to overcome the first limitation, we have to develop an approximation theory for theoretically treating limit-cycle oscillators driven by colored noise.

On the other hand, the second limitation results from a more fundamental problem. It is because a basic theory for synchronization analysis, i.e., the phase reduction method, assumes that the perturbation to the oscillator is sufficiently weak. This limitation will impose a burden in theoretically analyzing not only noise-induced synchronization, but also mutual synchronization and injection locking. We cannot assume that the external forcing and interactions are sufficiently weak in practical applications, e.g., in biology and electrical engineering, so this limitation will severely hinder the applicability of the synchronization analysis. Indeed, it has been reported that we can observe nontrivial behavior in strongly driven limit-cycle oscillators [39, 40, 41]. In order to overcome this limitation, we have to extend the phase reduction method itself to the case of strong perturbations. In the history of nonlinear science, the phase reduction method has played an important role in the theoretical analysis of synchronization phenomena. Therefore, if we can extend the phase reduction method, this extension enables us to thoroughly extend the conventional theoretical methods for synchronization analysis. In this sense, this extension has been an open question in nonlinear science.

1.2 Organization of This Thesis

In Table 1.1, we summarize the relation between this thesis and the conventional theories. Theoretical methods for analyzing mutual synchronization of weakly coupled oscillators and injection locking to weak periodic forcing have already been established in the conventional theories in the last four decades. In addition, theoretical analysis for noise-induced synchronization has been developed in Ref. [36], but it is limited to the case of white noise. Thus, we establish synchronization analysis for colored-noise-induced synchronization in Chapters 2. In Chapter 3, we propose a design and control method of noise-induced synchronization patterns by applying the theory pro-

posed in Chapter 2. Since these theories are based on the phase reduction method that assumes weak external forcing, we cannot apply them to strongly driven oscillators. To overcome this problem, we extend the phase reduction method to the case of strong forcing in Chapter 4. Using the extended phase reduction method, we theoretically analyze injection locking of a limit-cycle oscillator subjected to strong periodic external forcing.

Table 1.1: Relation between this thesis and the conventional theories.

Input strength		Weak	Strong
Mutual sync.		Conv. Theory	**(Chap. 4)**
Injection locking		Conv. Theory	**Chap. 4**
Noise-induced sync.	(white noise)	Conv. Theory	**(Chap. 4)**
	(colored noise)	**Chap. 2 and 3**	**(Chap. 4)**

1.2.1 Synchronization by Colored Noise (Chap. 2 and 3)

In Chapter 2, we propose a general formulation of synchronization in an ensemble of uncoupled oscillators driven by common colored noise with an arbitrary power spectrum. To explore statistical properties of such colored-noise-induced synchronization, we derive the probability density function of phase differences between two oscillators in the ensemble. The key contribution of this chapter is to extend a white-noise approximation method proposed by Nakao, Teramae, Goldobin, and Kuramoto [42]. The effective white-noise approximation is a useful tool for analyzing stochastic oscillator dynamics, because it enables us to use the Fokker-Planck equation even in the case of colored noise. Roughly speaking, this technique approximates an oscillator subjected to colored noise by an augmented oscillator (i.e., the original oscillator coupled to a linear filter that generates colored noise) subjected to white noise (see Fig. 1.3 for a schematic). In the derivation of the probability density function of phase differences, it is useful to employ the effective white-noise approximation of limit-cycle oscillators driven by colored noise, but the original method proposed by Nakao et al. cannot be used for this purpose, because it is limited to the case of a single oscillator. We extend the white-noise approximation method for a single oscillator [42] into a two-oscillator system, so we can theoretically analyze stochastic dynamics of two uncoupled oscillators driven by common colored noise. This analytical result theoretically predicts various synchronized and clustered states induced by colored noise, indicating that these phenomena have a quite different synchronization mechanism from the case of white noise.

Chapter 3 is an application of the theory proposed in Chapter 2. We propose a method for controlling synchronization patterns of limit-cycle oscillators by common noisy inputs, i.e., by utilizing noise-induced synchronization. Here, the term synchronization pattern represents various statisti-

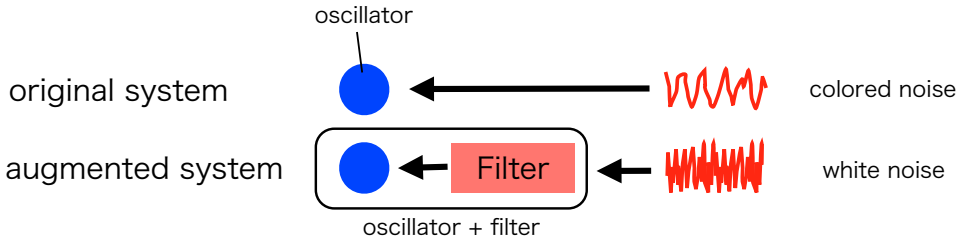

Figure 1.3: Schematic of effective white-noise approximation in limit-cycle oscillators driven by colored noise.

cal properties of noise-induced synchronization in an ensemble of oscillators, e.g., the accuracy of synchronization, the number and size of synchronized groups or clusters, the fluctuations around synchronized states, and so on. The key contribution of this chapter is to propose a theoretical basis useful for optimizing noise-induced synchronization in practical applications. The application of noise-induced synchronization mainly aims to save energy consumption. Utilizing common environmental noise for synchronization as in plants [43, 44], we can realize synchronization without injecting, e.g., periodic signals to the oscillators. Indeed, Yasuda et al. proposed an energy-efficient synchronization control method in wireless sensor networks by common environmental noise [45]. In such applications, the signal processing in each oscillator will play a key role for realizing the optimal noise-induced synchronization pattern in each application. For this purpose, we propose an optimization method for linear filters that process common noisy signals based on an objective function defined for each application. The objective function represents some statistical quantity that characterizes synchronization patterns, e.g., the degree of synchronization or clustering, and the percentage of oscillators in an exact synchronized state, so we can optimize the linear filter with respect to each practical application. In this method, we can realize various synchronization patterns, including fully synchronized and clustered states, by using linear filters that generate appropriate common noisy signals from given noise. The optimal linear filter can be determined from the linear phase response property of the oscillators and the power spectrum of the given noise. The validity of the proposed method is confirmed by numerical simulations.

1.2.2 Synchronization by Strong Forcing (Chap. 4)

Chapter 4 proposes a generalized phase reduction method that enables us to theoretically explore a broader class of strongly perturbed limit-cycle oscillators. The phase reduction method for limit-cycle oscillators subjected to weak perturbations has significantly contributed to theoretical investigations of rhythmic phenomena. We here propose a generalized phase reduction method that

is also applicable to strongly perturbed limit-cycle oscillators. The key contribution of this chapter is to introduce a generalized phase and to derive a generalized phase equation by a perturbation approximation in two small parameters. The fundamental assumption of our method is that the perturbations to the oscillator $\boldsymbol{I}(t)$ can be decomposed into a large-amplitude component $\boldsymbol{q}(\epsilon t)$ varying slowly as compared to the amplitude relaxation time and remaining weak fluctuations $\sigma \boldsymbol{p}(t)$:

$$\boldsymbol{I}(t) = \boldsymbol{q}(\epsilon t) + \sigma \boldsymbol{p}(t), \tag{1.3}$$

where ϵ and σ are sufficiently small parameters satisfying

$$\frac{\epsilon}{\lambda(\boldsymbol{q}(\epsilon t))^2} \ll 1, \quad \frac{\sigma}{\lambda(\boldsymbol{q}(\epsilon t))} \ll 1, \tag{1.4}$$

and $\lambda(\boldsymbol{q}(\epsilon t))$ is the second largest Floquet exponent (see Chapter 4). Under this assumption, we introduce a generalized phase parameterized by the slowly varying large-amplitude component $\boldsymbol{q}(\epsilon t)$ and derive a closed equation for the generalized phase describing the oscillator dynamics by a perturbation approximation in ϵ and σ. In contrast to the conventional phase equation derived by the first-order perturbation approximation in σ only, the generalized phase equation is valid to the first order in ϵ and σ, so it robustly works even for relatively strong inputs as compared to the conventional equation. The proposed method enables us to explore a broader class of rhythmic phenomena, in which the shape and frequency of the oscillation may vary largely because of the perturbations. We illustrate our method by analyzing the synchronization dynamics of limit-cycle oscillators driven by strong periodic signals. It is shown that the proposed method accurately predicts the synchronization properties of the oscillators, while the conventional method does not.

Chapter 2

Synchronization Induced by Common Colored Noise

2.1 Introduction

In this section, we propose a quantitative theory for characterizing and predicting the statistical property of synchronization induced by common colored noise. When driven by common noise, many nonlinear dynamical systems can synchronize. This phenomenon is called noise-induced synchronization, which is observed in various kinds of the nonlinear dynamical systems, for example, neural networks [23, 27], electric circuits [29], electronic devices [30], microbial cells [31] and lasers [32]. It has been theoretically proven that limit cycle oscillators can synchronize driven by common noise [20]. Many studies have investigated the synchronization property in case of various types of drive noises, for example, Gaussian white noise [36, 46, 47] and Poisson impulses [48]. In ref. [36], using a formulation of limit cycle oscillators driven by common and independent Gaussian white noises, Nakao et al. analytically obtained the probability density function (PDF) of phase differences between two oscillators, which enables us to effectively characterize the synchronization property. However, although there are some numerical studies [49, 50], analytical conventional studies are limited to the case that drive signals are white noise (temporally uncorrelated noise). If we can assume that the drive signal is white noise, we can use the Fokker-Planck approximation [51] to explore statistical properties of oscillator ensembles. However, such an ideal condition is rare in the real world. For example, in neural circuits, it is known that colored noise with negative autocorrelation plays a key role to propagate synchronous activities [37]. However, it still remains unclear how the oscillators behave if they are driven by common colored noise.

Recently, it has been clarified how a limit cycle oscillator behaves if it is driven by colored

non-Gaussian noise [21, 42, 22]. In this section, utilizing effective white-noise Langevin description proposed in ref. [42], we extend the formulation in ref. [36] to colored noise that has an arbitrary power spectrum. We then analytically derive the PDF of the phase difference between the oscillators if these oscillators are driven by common colored noise. We also conducted numerical simulations to verify our analytical results. The results show that the PDF of the phase difference explicitly depends on the power spectrum of the drive noise.

2.2 Model

We used the following system that consists of N identical limit cycle oscillators subject to common and independent multiplicative colored noises. The dynamics of the jth oscillator is described by

$$\dot{\boldsymbol{X}}^{(j)} = \boldsymbol{F}(\boldsymbol{X}^{(j)}) + \sqrt{D}\boldsymbol{G}(\boldsymbol{X}^{(j)})\boldsymbol{\xi}(t) + \sqrt{\epsilon}\boldsymbol{H}(\boldsymbol{X}^{(j)})\boldsymbol{\eta}^{(j)}(t), \tag{2.1}$$

for $j = 1, \ldots, N$, where $\boldsymbol{X}^{(j)} \in \mathbb{R}^n$ is the n-dimensional state variable of the jth oscillator; $\boldsymbol{F}(\boldsymbol{X}^{(j)}) \in \mathbb{R}^n$ is an unperturbed vector field that has a stable T-periodic limit cycle orbit $\boldsymbol{S}(t)$; $\boldsymbol{\xi}(t) \in \mathbb{R}^m$ is the common noise, which drives all of the oscillators; $\boldsymbol{\eta}^{(j)}(t) \in \mathbb{R}^m$ $(j = 1, \ldots, N)$ is the independent noise, which is received independently by each oscillator; $\boldsymbol{G}(\boldsymbol{X}^{(j)}) \in \mathbb{R}^{n\times m}$ and $\boldsymbol{H}(\boldsymbol{X}^{(j)}) \in \mathbb{R}^{n\times m}$ represent how the oscillators are coupled to the common and independent noises; D and ϵ are parameters to control the intensities of the common and independent noises. We introduced the following three assumptions:

1. $\boldsymbol{\xi}(t) \in \mathbb{R}^m$ and $\boldsymbol{\eta}^{(j)}(t) \in \mathbb{R}^m$ are independent, identically distributed zero-mean colored noises, namely,

$$\begin{aligned} &\langle \boldsymbol{\xi}(t) \rangle = \boldsymbol{0},\ \langle \boldsymbol{\eta}^{(j)}(t) \rangle = \boldsymbol{0}, \\ &\langle \boldsymbol{\xi}(t)\boldsymbol{\eta}^{(j)}(s)^\top \rangle = \boldsymbol{O},\ \langle \boldsymbol{\eta}^{(j)}(t)\boldsymbol{\eta}^{(k)}(s)^\top \rangle = \boldsymbol{O}, \end{aligned} \tag{2.2}$$

   where $\top$ denotes the transpose.

2. $\boldsymbol{\xi}(t)$ and $\boldsymbol{\eta}^{(j)}(t)$ can be approximated as the convolution of an arbitrary filter function and white noise.

3. $\boldsymbol{\xi}(t)$ and $\boldsymbol{\eta}^{(j)}(t)$ have correlation times shorter than the time scale of the phase diffusion $(\sim O(D^{-\frac{1}{2}}, \epsilon^{-\frac{1}{2}}))$.

To characterize the statistical properties of the drive noises $\boldsymbol{\xi}(t)$ and $\boldsymbol{\eta}^{(j)}(t)$, we define correlation matrices $\boldsymbol{C}_\xi(\tau) \in \mathbb{R}^{m\times m}$ and $\boldsymbol{C}_\eta(\tau) \in \mathbb{R}^{m\times m}$ as

$$\boldsymbol{C}_\xi(\tau) = \langle \boldsymbol{\xi}(t)\boldsymbol{\xi}(t-\tau)^\top \rangle_t, \tag{2.3}$$

and

$$\boldsymbol{C}_\eta(\tau) = \langle \boldsymbol{\eta}^{(j)}(t)\boldsymbol{\eta}^{(j)}(t-\tau)^\top \rangle_t, \tag{2.4}$$

for $j = 1, \ldots, N$), where $\langle\cdot\rangle_t$ represents $\int_{-\infty}^{+\infty} dt \cdot$. For the sake of simplicity, we assumed that all independent noises $\boldsymbol{\eta}^{(j)}(t)$ have the same statistical property characterized by $\boldsymbol{C}_\eta(\tau)$. The ($i$, j)th element of $\boldsymbol{C}_\xi(\tau)$ is the cross correlation function of the ith and jth elements of the common noise $\boldsymbol{\xi}(t)$. The diagonal elements of $\boldsymbol{C}_\xi(\tau)$ are autocorrelation functions. In the same way, we can characterize the statistical property of $\boldsymbol{\eta}^{(j)}(t)$ by using $\boldsymbol{C}_\eta(\tau)$.

2.3 Phase Reduction

Under the assumption that the noise intensity is sufficiently weak ($D \ll 1$ and $\epsilon \ll 1$), we can apply the phase reduction method [2, 22] to Eq. (2.1). By introducing a phase variable $\phi^{(j)}$, eq. (2.1) is reduced to the following phase equation:

$$\dot{\phi}^{(j)} \quad = \quad \omega + \sqrt{D}\boldsymbol{Z}_{\mathrm{G}}(\phi^{(j)}) \cdot \boldsymbol{\xi}(t) + \sqrt{\epsilon}\boldsymbol{Z}_{\mathrm{H}}(\phi^{(j)}) \cdot \boldsymbol{\eta}^{(j)}(t) + O(D, \epsilon), \tag{2.5}$$

where $\phi^{(j)}(t) \in [-\pi, +\pi]$ is a phase variable that corresponds to the state of the jth oscillator $\boldsymbol{X}^{(j)}$, ω ($= 2\pi T^{-1}$) is the natural frequency, and $\boldsymbol{Z}_G(\phi^{(j)})$ and $\boldsymbol{Z}_H(\phi^{(j)})$ are the phase sensitivity functions that represent the linear response of the phase variable $\phi^{(j)}$ to the drive noises [2, 22]. The phase sensitivity functions $\boldsymbol{Z}_G(\phi^{(j)})$ and $\boldsymbol{Z}_H(\phi^{(j)})$ are defined as follows:

$$\boldsymbol{Z}_G(\phi^{(j)}) = \nabla_{\boldsymbol{X}}\phi^{(j)}|_{\boldsymbol{X}=\boldsymbol{S}(\phi^{(j)})} \cdot \boldsymbol{G}(\boldsymbol{S}(\phi^{(j)})), \tag{2.6}$$

$$\boldsymbol{Z}_H(\phi^{(j)}) = \nabla_{\boldsymbol{X}}\phi^{(j)}|_{\boldsymbol{X}=\boldsymbol{S}(\phi^{(j)})} \cdot \boldsymbol{H}(\boldsymbol{S}(\phi^{(j)})). \tag{2.7}$$

As discussed in Ref. [22], the $O(D, \epsilon)$ term is necessary to describe the exact phase dynamics, while the phase diffusion is not affected by the $O(D, \epsilon)$ term. As we will focus on the phase diffusion in the following sections, we do not take this term into account.

2.4 Effective Langevin Description

To quantify the synchronization property without loss of generality, we consider the relationship of only two oscillators, that is, the two-body problem of $\phi^{(1)}(t)$ and $\phi^{(2)}(t)$, and define the phase difference θ ($:= \phi^{(1)} - \phi^{(2)}$). As we focus on the stochastic dynamics of θ, we define $f(\theta, t)$ as the PDF of the phase difference θ. Utilizing the effective white-noise Langevin description [42], the evolution of $f(\theta, t)$ is described by the following effective Fokker-Planck equation:

$$\frac{\partial f}{\partial t} + \frac{\partial}{\partial \theta}v^{(1)}(\theta)f - \frac{1}{2} \cdot \frac{\partial^2}{\partial \theta^2}v^{(2)}(\theta)f = 0, \tag{2.8}$$

where $v^{(1)}(\theta)$ and $v^{(2)}(\theta)$ are effective drift and diffusion coefficients. We have the drift coefficient $v^{(1)}(\theta) = 0$ because $\langle\dot{\theta}\rangle = \langle\dot{\phi}^{(1)} - \dot{\phi}^{(2)}\rangle = 0$. Meanwhile, the diffusion coefficient $v^{(2)}(\theta)$ is obtained as

$$\begin{aligned} v^{(2)}(\theta) &= \int_{-\infty}^{+\infty} d\tau \big\langle \big[\dot{\theta}(t) - \langle\dot{\theta}\rangle\big]\big[\dot{\theta}(t-\tau) - \langle\dot{\theta}\rangle\big]\big\rangle \\ &= \int_{-\infty}^{+\infty} d\tau \big\langle \big[\dot{\phi}^{(1)}(t) - \dot{\phi}^{(2)}(t)\big]\big[\dot{\phi}^{(1)}(t-\tau) - \dot{\phi}^{(2)}(t-\tau)\big]\big\rangle \end{aligned} \tag{2.9}$$

where $\langle\cdot\rangle$ represents the temporal average. For simplicity of notation, we define d_{jk} as

$$d_{jk} = \int_{-\infty}^{+\infty} d\tau \big\langle [\dot{\phi}^{(j)}(t) - \omega][\dot{\phi}^{(k)}(t-\tau) - \omega]\big\rangle. \tag{2.10}$$

Then, we obtain

$$v^{(2)}(\theta) = d_{11} + d_{22} - d_{12} - d_{21} = 2d_{11} - 2d_{12}. \tag{2.11}$$

The phase variable $\phi^{(j)}(t)$ can be expanded as

$$\phi^{(j)}(t) = \phi_0^{(j)}(t) + \sqrt{D}\phi_{D,1}^{(j)}(t) + \sqrt{\epsilon}\phi_{\epsilon,1}^{(j)}(t) + D\phi_{D,2}^{(j)}(t) + \epsilon\phi_{\epsilon,2}^{(j)}(t) + \cdots \tag{2.12}$$

by using $\sqrt{D}$ and $\sqrt{\epsilon}$ as expansion parameters, where $\phi_0^{(j)}(t)$, $\phi_{D,k}^{(j)}(t)$ and $\phi_{\epsilon,k}^{(j)}(t)$ $(k = 1, 2, \ldots)$ are approximate perturbed solutions of $\phi^{(j)}(t)$. We have

$$\phi_0^{(j)}(t) = \phi_0^{(j)}(0) + \omega t, \tag{2.13}$$

$$\dot{\phi}_{D,1}^{(j)}(t) = \boldsymbol{Z}_G(\phi_0^{(j)}(t)) \cdot \boldsymbol{\xi}(t), \tag{2.14}$$

$$\dot{\phi}_{\epsilon,1}^{(j)}(t) = \boldsymbol{Z}_H(\phi_0^{(j)}(t)) \cdot \boldsymbol{\eta}^{(j)}(t). \tag{2.15}$$

Using these perturbed solutions, eq. (2.5) can be written as

$$\dot{\phi}^{(j)} = \omega + \sqrt{D}\dot{\phi}_{D,1}^{(j)} + \sqrt{\epsilon}\dot{\phi}_{\epsilon,1}^{(j)} + O(D, \epsilon). \tag{2.16}$$

Using this approximation and the fact that $\langle\phi_{D,1}^{(j)}(t)\phi_{\epsilon,1}^{(k)}(t-\tau)\rangle = 0$ and $\langle\phi_{\epsilon,1}^{(j)}(t)\phi_{D,1}^{(k)}(t-\tau)\rangle = 0$, we obtain

$$\begin{aligned} d_{jk} &= D\int_{-\infty}^{+\infty} d\tau \big\langle \dot{\phi}_{D,1}^{(j)}(t)\dot{\phi}_{D,1}^{(k)}(t-\tau)\big\rangle \\ &\quad + \epsilon\int_{-\infty}^{+\infty} d\tau \big\langle \dot{\phi}_{\epsilon,1}^{(j)}(t)\dot{\phi}_{\epsilon,1}^{(k)}(t-\tau)\big\rangle + O(D^{\frac{3}{2}}, \epsilon^{\frac{3}{2}}). \end{aligned} \tag{2.17}$$

Thus, using Eq. (2.17), we can calculate d_{11} as follows:

$$d_{11} = \frac{D}{2\pi}\int_{-\infty}^{+\infty} d\tau \int_{-\pi}^{+\pi} d\phi \boldsymbol{Z}_G(\phi)^\top \boldsymbol{C}_\xi(\tau)\boldsymbol{Z}_G(\phi-\omega\tau) + \frac{\epsilon}{2\pi}\int_{-\infty}^{+\infty} d\tau \int_{-\pi}^{+\pi} d\phi \boldsymbol{Z}_H(\phi)^\top \boldsymbol{C}_\eta(\tau)\boldsymbol{Z}_H(\phi-\omega\tau) + O(D^{\frac{3}{2}}, \epsilon^{\frac{3}{2}}). \tag{2.18}$$

In the same way, d_{12} is given by

$$d_{12} = \frac{D}{2\pi}\int_{-\infty}^{+\infty} d\tau \int_{-\pi}^{+\pi} d\phi \boldsymbol{Z}_G(\phi)^\top \boldsymbol{C}_\xi(\tau)\boldsymbol{Z}_G(\phi-\theta-\omega\tau) + O(D^{\frac{3}{2}}, \epsilon^{\frac{3}{2}}). \tag{2.19}$$

The detailed derivations of Eqs. (2.18) and (2.19) are shown in Appendix (section A.1).

Finally, from Eqs. (2.11), (2.18) and (2.19), we have the efficient diffusion coefficient $v^{(2)}(\theta)$:

$$v^{(2)}(\theta) = 2D\big[g(0) - g(\theta)\big] + 2\epsilon h(0), \tag{2.20}$$

where $g(\theta)$ and $h(\theta)$ are correlation functions defined as

$$g(\theta) = \frac{1}{2\pi}\int_{-\infty}^{+\infty} d\tau \int_{-\pi}^{+\pi} d\phi \boldsymbol{Z}_G(\phi)^\top \boldsymbol{C}_\xi(\tau)\boldsymbol{Z}_G(\phi-\theta-\omega\tau), \tag{2.21}$$

$$h(\theta) = \frac{1}{2\pi}\int_{-\infty}^{+\infty} d\tau \int_{-\pi}^{+\pi} d\phi \boldsymbol{Z}_H(\phi)^\top \boldsymbol{C}_\eta(\tau)\boldsymbol{Z}_H(\phi-\theta-\omega\tau). \tag{2.22}$$

If we assume that the drive noise is white, namely, $\boldsymbol{C}_\xi(\tau) = \boldsymbol{C}_\eta(\tau) = \delta(\tau)\boldsymbol{E}_m$, eqs. (2.21) and (2.22) are exactly equivalent to eq. (6) in Ref. [36], where $\boldsymbol{E}_m$ is an $m \times m$ identity matrix. The results show that Eqs. (2.21) and (2.22) are a natural generalization of Eq. (6) in Ref. [36].

We obtain the explicit form of the Fokker-Planck equation of Eq. (2.8) from Eqs. (2.20)–(2.22). The stationary distribution of the phase difference $f_0(\theta)$ is given as the stationary solution of Eq. (2.8). Then, if we put $\partial f/\partial t = 0$ in Eq. (2.8), we obtain

$$f_0(\theta) = \frac{\nu}{v^{(2)}(\theta)} = \frac{\nu'}{D\big[g(0) - g(\theta)\big] + \epsilon h(0)}, \tag{2.23}$$

where ν and ν' $(= \nu/2)$ are normalization constants.

2.5 Fourier Representation

To understand the results obtained in the previous section, we rewrite the correlation functions defined in Eqs. (2.21) and (2.22) by using the Fourier representation. We introduced the Fourier series expansion of the phase sensitivity functions $\boldsymbol{Z}_G(\phi)$ and $\boldsymbol{Z}_H(\phi)$ as

$$\boldsymbol{Z}_G(\phi) = \sum_{l=-\infty}^{+\infty} \boldsymbol{Y}_{G,l} e^{il\phi}, \tag{2.24}$$

and

$$\boldsymbol{Z}_H(\phi) = \sum_{l=-\infty}^{+\infty} \boldsymbol{Y}_{H,l} e^{il\phi}, \tag{2.25}$$

where i denotes the imaginary unit and $\boldsymbol{Y}_{G,l} \in \mathbb{C}^m$ $(= \frac{1}{2\pi}\int_{-\pi}^{+\pi} d\phi \boldsymbol{Z}_G(\phi) e^{-il\phi})$ and $\boldsymbol{Y}_{H,l} \in \mathbb{C}^m$ $(= \frac{1}{2\pi}\int_{-\pi}^{+\pi} d\phi \boldsymbol{Z}_H(\phi) e^{-il\phi})$ are Fourier coefficients $(l = -\infty, \ldots, \infty)$.

Subsequently, we define $\boldsymbol{P}_\xi(\Omega) \in \mathbb{C}^{m\times m}$ and $\boldsymbol{P}_\eta(\Omega) \in \mathbb{C}^{m\times m}$ as the Fourier transforms of $\boldsymbol{C}_\xi(\tau)$ and $\boldsymbol{C}_\eta(\tau)$, that is,

$$\boldsymbol{P}_\xi(\Omega) = \int_{-\infty}^{+\infty} dt \boldsymbol{C}_\xi(t) e^{-i\Omega t}, \tag{2.26}$$

and

$$\boldsymbol{P}_\eta(\Omega) = \int_{-\infty}^{+\infty} dt \boldsymbol{C}_\eta(t) e^{-i\Omega t}. \tag{2.27}$$

Let us note that $\boldsymbol{P}_\xi(\Omega)$ and $\boldsymbol{P}_\eta(\Omega)$ are Hermitian matrices, namely, $\boldsymbol{P}_\xi(\Omega) = \boldsymbol{P}_\xi(\Omega)^\dagger$ and $\boldsymbol{P}_\eta(\Omega) = \boldsymbol{P}_\eta(\Omega)^\dagger$ because $\boldsymbol{C}_\xi(\tau) = \boldsymbol{C}_\xi(-\tau)^\top$ and $\boldsymbol{C}_\eta(\tau) = \boldsymbol{C}_\eta(-\tau)^\top$ from their definitions, where $\dagger$ denotes the adjoint. The (i,j)th elements of $\boldsymbol{P}_\xi(\Omega)$ and $\boldsymbol{P}_\eta(\Omega)$ represent the cross spectra of the ith and jth elements of $\boldsymbol{\xi}(t)$ and $\boldsymbol{\eta}^{(j)}(t)$. In particular, the diagonal elements of $\boldsymbol{P}_\xi(\Omega)$ and $\boldsymbol{P}_\eta(\Omega)$ represent the power spectra.

Using the Fourier representations defined above, we can obtain the Fourier representations of the correlation functions $g(\theta)$ and $h(\theta)$:

$$g(\theta) = \sum_{l=-\infty}^{+\infty} g_l e^{il\theta},\ h(\theta) = \sum_{l=-\infty}^{+\infty} h_l e^{il\theta}, \tag{2.28}$$

where

$$g_l := \boldsymbol{Y}_{G,l}^\dagger \boldsymbol{P}_\xi(l\omega) \boldsymbol{Y}_{G,l}, \tag{2.29}$$

and

$$h_l := \boldsymbol{Y}_{H,l}^\dagger \boldsymbol{P}_\eta(l\omega) \boldsymbol{Y}_{H,l}, \tag{2.30}$$

are Fourier coefficients $(l = -\infty, \ldots, \infty)$. The derivations of g_l and h_l will be shown in Appendix (section A.2).

These expressions clearly suggest that the correlation functions $g(\theta)$ and $h(\theta)$ only depend on $\boldsymbol{P}_\xi(\pm l\omega)$ and $\boldsymbol{P}_\eta(\pm l\omega)$ $(l = 0, 1, 2, \ldots)$, that is, the other frequency components can be neglected. In the next section, we will demonstrate that colored noise induces various synchronized and clustered states, which are clearly explained by Eq. (2.28).

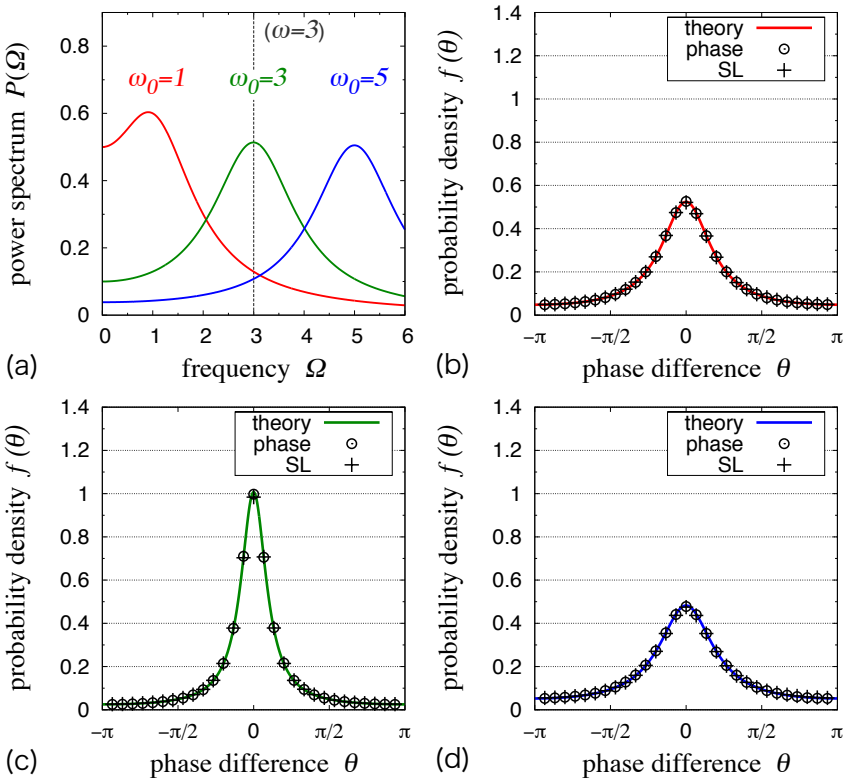

Figure 2.1: Simulation results of the Stuart-Landau oscillator (crosses) and the corresponding phase oscillator (open circles). (a) Power spectra of the common noises are shown for $\omega_0 = 1$, 3 and 5. The PDFs of θ show the frequency dependency of the synchronization property for (b) $\omega_0 = 1$, (c) $\omega_0 = 3$ $(= \omega)$, and (d) $\omega_0 = 5$.

2.6 Numerical Simulations

To demonstrate the validity of our results, we perform numerical experiments for two types of limit cycle oscillators. The first example is the Stuart-Landau oscillator, which takes the normal form of the supercritical Hopf bifurcation [2]:

$$\dot{x} = x - c_0 y - (x^2 + y^2)(x - c_2 y), \tag{2.31}$$

$$\dot{y} = y + c_0 x - (x^2 + y^2)(y + c_2 x), \tag{2.32}$$

where $\boldsymbol{X} = [x, y]^\top$ is a state variable and c_0 and c_2 are parameters. In the simulation, we fixed $c_0 = 1$, $c_2 = -2$, $\boldsymbol{G} = \boldsymbol{H} = \mathrm{diag}(1, 1)$, $D = 0.0095$ and $\epsilon = 0.0005$, where $\mathrm{diag}(\lambda_1, \ldots, \lambda_m)$ denotes an $m \times m$ diagonal matrix that has the diagonal elements $\lambda_1, \ldots, \lambda_m$. This model is reduced to the phase equation that has the natural frequency $\omega = c_0 - c_2 = 3$ and the phase sensitivity function $\boldsymbol{Z}(\phi) = \sqrt{2}[\sin(\phi + 3\pi/4), \sin(\phi + \pi/4)]^\top$.

In the simulation, we use a two-dimensional drive noise that has the correlation matrix $\boldsymbol{C}_{\mathrm{ex}}(\tau) \in \mathbb{R}^{2\times 2}$ defined as

$$\boldsymbol{C}_{\mathrm{ex}}(\tau) = \mathrm{diag}(C_{\mathrm{ex}}(\tau), C_{\mathrm{ex}}(\tau)), \tag{2.33}$$

$$C_{\mathrm{ex}}(\tau) = \frac{\gamma}{2} e^{-\gamma|\tau|} \cos \omega_0 \tau, \tag{2.34}$$

where ω_0 and γ are parameters that represent the peak frequency and the characteristic decay time. We define $P_{\mathrm{ex}}(\Omega)$, the Fourier transform of $C_{\mathrm{ex}}(\tau)$, as $P_{\mathrm{ex}}(\Omega) = \frac{\gamma^2}{2}\{[\gamma^2 + (\Omega + \omega_0)^2]^{-1} + [\gamma^2 + (\Omega - \omega_0)^2]^{-1}\}$. A drive noise characterized by $C_{\mathrm{ex}}(\tau)$ can be generated by the damped noisy harmonic oscillator (See Eqs. (43)–(49) in Ref. [42] for details).

We use the common noises with $(\omega_0, \gamma) = (1, 1)$, $(3, 1)$ and $(5, 1)$ and the independent noise with $(\omega_0, \gamma) = (0, 3)$. The power spectra of these common noises are shown in Fig. 2.1 (a). From Eq. (2.28), the correlation functions $g(\theta)$ and $h(\theta)$ are given by

$$g(\theta) = \left[\frac{1}{1 + (\omega_0 + 3)^2} + \frac{1}{1 + (\omega_0 - 3)^2}\right] \cos\theta, \tag{2.35}$$

$$h(\theta) = \cos\theta, \tag{2.36}$$

for $\omega_0 = 1$, 3 and 5, which correspond to the three types of the common noise. The derivations of $g(\theta)$ and $h(\theta)$ will be shown in Appendix (section A.3).

The correlation function $g(\theta)$ calculated above indicate that the effective intensity of the common noise depends on the peak frequency ω_0 and is maximal at $\omega_0 = \omega$. It means that the synchronous degree is maximized at $\omega_0 = \omega$. In Fig. 2.1 (b)–(d), we compared the results of the direct numerical simulation using the Stuart-Landau oscillator and its corresponding phase oscillator with the analytical results. All PDFs are well fitted by the theoretical curves. Our theory clearly predicts that the highest synchronous degree is realized at $\omega_0 = \omega$.

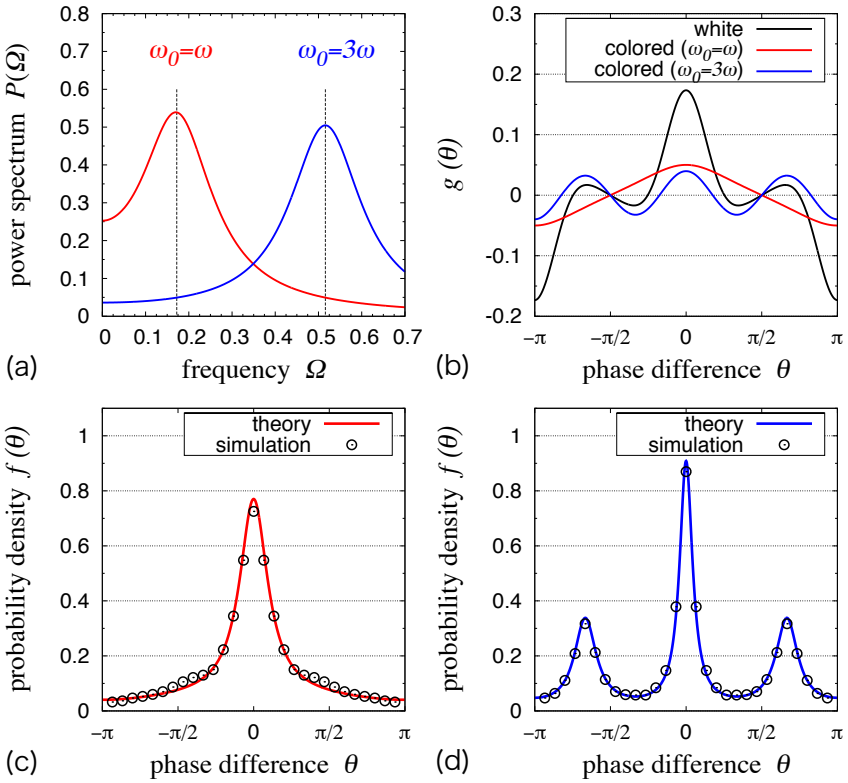

Figure 2.2: Simulation results of the FitzHugh-Nagumo oscillator. (a) Power spectra of the common noises are shown for $\omega_0 = \omega$ and 3ω. For these drive noises, (b) $g(\theta)$ $(= h(\theta))$ is shown. The PDFs of θ for (c) $\omega_0 = \omega$ (synchronized state) and for (d) $\omega_0 = 3\omega$ (3-cluster state) are shown.

The second example is the FitzHugh-Nagumo oscillator [52, 53]:

$$\dot{v} = v - \frac{v^3}{3} - u + I_0, \tag{2.37}$$

$$\dot{u} = \mu(v + a - bu), \tag{2.38}$$

where $\boldsymbol{X} = [v, u]^\top$ is a state variable and a, b, μ and I_0 are parameters. In the simulation, we fixed $a = 0.7$, $b = 0.8$, $\mu = 0.08$, $I_0 = 0.875$, $\boldsymbol{G} = \boldsymbol{H} = \mathrm{diag}(1, 0)$, $D = 0.045$ and $\epsilon = 0.005$. For these parameters, this oscillator has the natural frequency $\omega \simeq 0.1725$. This oscillator models bursting behavior of a neuron, and only the first variable v, which corresponds to the membrane potential of a neuron, is subject to noise.

In the simulation, we use the one-dimensional noise that has the correlation function $C_{\mathrm{ex}}(\tau)$. Unlike the first example, we use the same parameters (ω_0, γ) for both the common and independent noises. We used two parameter sets $(\omega_0, \gamma) = (\omega, 0.1)$ and $(3\omega, 0.1)$. The power spectra of these drive noises are shown in Fig. 2.2 (a). We obtain the correlation function $g(\theta)$ $(= h(\theta))$ numerically as shown in Fig. 2.2 (b).

In Fig. 2.2 (c) and (d), we compared the results of the direct numerical simulation with the analytical results. The numerical results are in good agreement with the theoretical results. As theoretically predicted, a 3-cluster state is realized as shown in Fig. 2.2 (d). If oscillators are driven by white noise, clustered states are induced only by multiplicative noise [36]. However, in case of colored noise, clustered states are induced not only by multiplicative noise but also by additive noise.

In the third example, we used the Hodgkin-Huxley oscillator [54], which enables us to demonstrate whether the theory is applicable to higher-dimensional limit cycle systems. We use two types of drive noise: chaotic noise generated by the Lorenz model [55] and high-pass noise generated by applying a high-pass filter to white noise. These power spectra are shown in Fig. 2.3 (a). Unlike the periodic noise characterized by $C_{\mathrm{ex}}(\tau)$, chaotic noise does not have a characteristic decay time, and high-pass noise has a vanishing spectrum as $\Omega \to 0$. In the simulation, for the sake of simplicity, we used the same type of drive noise for the common and independent noises, and we set $(D, \epsilon) = (0.02, 0.01)$ and $(0.0002, 0.0001)$ for the chaotic and high-pass noises, respectively. For the Lorenz model, we use the same parameters and normalization as in ref. [42]. Fig. 2.3 (b)–(d) compare the theoretical and numerical results, which show that our theory is also valid for these cases.

2.7 Summary and Discussions

In this section, we extended a formulation to analyze various synchronized and clustered states of uncoupled limit cycle oscillators driven by common and independent colored noises. Using this

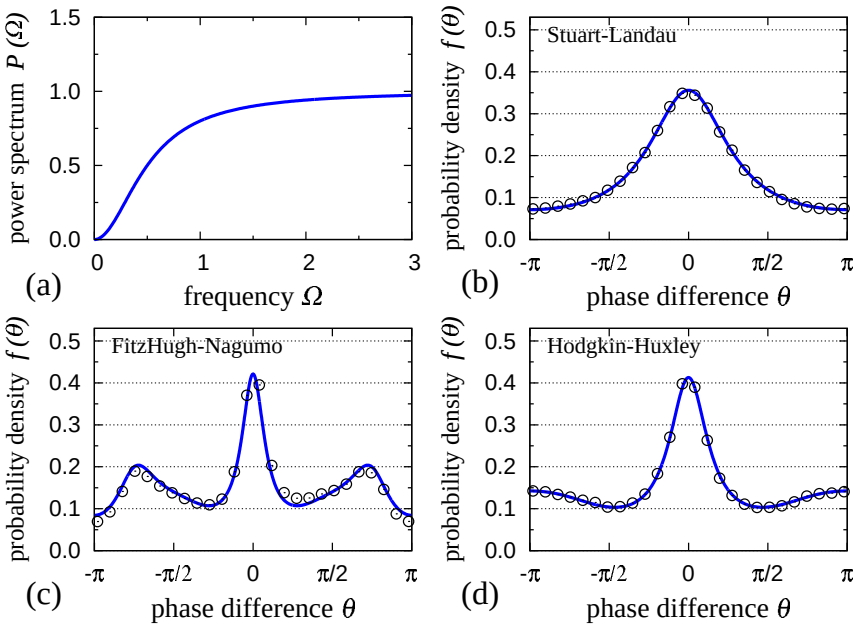

Figure 2.3: Simulation results of the limit cycle oscillators subject to chaotic noise (blue) and high-pass noise (red). (a) Power spectra of the drive noises. The PDFs of θ obtained by the theory (lines) and numerical simulations (crosses and circles) for (b) the Stuart-Landau oscillator, (c) the FitzHugh-Nagumo oscillator and (d) the Hodgkin-Huxley oscillator.

formulation, we derived the probability density function of the phase difference and rewrote it by the Fourier representation. The obtained expressions clearly show that the synchronization property depends on the power spectrum of the drive noises. Such dependency has already been reported experimentally. For example, in ref. [38], the reliability, or synchronization across trials, is explored in neuronal responses to periodic drive inputs with various frequencies. The reliability is maximized at a certain frequency, which is similar to our results shown in Fig. 2.1. Our results in this section supports the results in ref. [38] theoretically, because a neuron in a oscillatory state can be regarded as a noisy limit cycle oscillator.

Generally, noise in the real world often has a non-flat and characteristic power spectrum. In this sense, our formulation is a useful tool to estimate the synchronization property for both theoretical and practical aspects. Namely, the results obtained in this section can be applied to a wide range of purposes from mathematical modelings to technological problems.

Chapter 3

Design and Control of Noise-Induced Synchronization Patterns

3.1 Introduction

Various nonlinear dynamical systems tend to synchronize when driven by a common noisy input. This phenomenon, called noise-induced synchronization, is observed in many systems, for example, in neurons [23, 25, 27, 28], electric circuits [29], electronic devices [30], microbial cells [31], lasers [32], and chaotic dynamical systems [33, 34]. It has been clarified that noise-induced synchronization has quite a different mechanism from phase locking to periodic forcing, i.e., the oscillators are not entrained by the input but still exhibit mutual synchronization, characterized by coherent distributions of the phase differences. Analytical investigations of this phenomenon for limit-cycle oscillators can be performed by using the phase reduction method [2], and its properties have been widely studied in the last decade [20, 22, 36, 46, 48, 50, 56, 57, 58, 59, 60, 61, 62].

In contrast to phase locking that requires periodic forcing whose frequency is close to rational multiples of the natural frequency of the oscillators, noise-induced synchronization can occur even for white noise [20, 22, 36, 46, 48, 56, 57, 58, 59, 60, 61, 62]. Thus, noise-induced synchronization may more easily be realized than phase locking, because common environmental noise is ubiquitous in nature. Indeed, it is conjectured that some plants utilize common environmental noise for synchronization to realize biological functions [43, 44]. In such biological systems, some kind of filtering mechanisms for the environmental noise may also exist to improve noise-induced synchronization. Such filtering mechanisms, if any, would also be useful in practical applications such

as noise-induced synchronization of sensor networks [45]. The aim of this chapter is to provide a theoretical basis for optimizing noise-induced synchronization by filtering the given noise.

In our previous works [36, 59], we developed quantitative theories that predict global statistical properties of the noise-induced synchronization, such as formation of various synchronization patterns and fluctuations around these patterns, not only whether the oscillators synchronize with the others. The synchronization patterns are characterized by the probability density function (PDF) of the phase differences between the oscillators, which can be calculated from the phase response property of the oscillators and the statistical properties of the noisy inputs.

In this chapter, on the basis of ref. [59], we propose a method for designing and controlling various noise-induced synchronization patterns of limit-cycle oscillators, including the fully synchronized and clustered states. Since the synchronization pattern of the oscillators depends on the statistical properties of the noisy input, we can design the synchronization pattern by optimizing the noisy input so that some objective function, e.g., the degree of synchronization, is maximized. We develop an optimization method for the noisy input, namely, for a linear filter that transforms given noise into an appropriate noisy input so that the desired synchronization pattern is realized. The validity of the proposed method is confirmed by numerical simulations.

3.2 Model

We consider an ensemble of N uncoupled identical limit-cycle oscillators subjected to correlated noise and independent noise, described by the following Langevin equations:

$$\dot{\boldsymbol{X}}_j(t) = \boldsymbol{F}(\boldsymbol{X}_j) + \epsilon \boldsymbol{G}(\boldsymbol{X}_j)[I_j(t) + \zeta_j(t)], \tag{3.1}$$

for $j = 1, \ldots, N$. Here, $\boldsymbol{X}_j(t) \in \mathbb{R}^n$ is the state of the oscillator j at time t, $\boldsymbol{F}(\boldsymbol{X}_j) \in \mathbb{R}^n$ is a vector field representing the oscillator dynamics, $\boldsymbol{G}(\boldsymbol{X}_j) \in \mathbb{R}^n$ represents the coupling of the oscillator to the noisy inputs, $I_j(t) \in \mathbb{R}$ is the correlated noise, $\zeta_j(t) \in \mathbb{R}$ is the independent noise that drives each oscillator independently, and ϵ ($\ll 1$) is a small parameter that controls the strength of the noisy inputs. We assume that Eqs. (3.1) possesses a stable limit-cycle orbit $\boldsymbol{X}_0(t)$ with period T and frequency $\omega := 2\pi/T$ when $\epsilon = 0$. The correlated noise is generated from two given noisy signals by a linear filter as $I_j(t) = f * (\xi(t) + \eta_j(t))$, where the noise $\xi(t) \in \mathbb{R}$ is common to all oscillators, $\eta_j(t) \in \mathbb{R}$ is independently applied to each oscillator, $f(\tau) \in \mathbb{R}$ is a filter function that transforms the given noise to appropriate noise for realizing desired synchronization patterns, and the star ($*$) denotes convolution $f * \alpha(t) = \int_{-\infty}^{+\infty} f(\tau)\alpha(t-\tau)d\tau$. We introduced two independent noise terms $\eta_j(t)$ and $\zeta_j(t)$ to take into account the effect of external disturbances before and after filtering.

For example, the oscillators described by Eqs. (3.1) can be regarded as spiking neurons receiving artificial injection currents as in ref. [27]. In this case, the filtered noise $I_j(t)$ represents the injected

current to each neuron, and we may suppose $\eta_j(t) = 0$. The filter $f(\tau)$ is used for generating an appropriate injection current, and $\zeta_j(t)$ is independent noise inherent in each neuron, e.g., channel or synaptic noise. In the situation of ref. [45] where noise-induced synchronization of wireless sensor networks is considered, each oscillator described by Eqs. (3.1) corresponds to each sensor node. The sensor node measures a noisy environmental signal $\xi(t) + \eta_j(t)$, and the filter $f(\tau)$ implemented on each sensor node transforms the signal into an appropriate noisy input $I_j(t)$ that induces synchronization of the sensor nodes. We may suppose $\zeta_j(t) = 0$ in this case.

We assume that $\xi(t)$, $\eta_j(t)$, and $\zeta_j(t)$ are mutually independent zero-mean Gaussian noise, i.e., $\langle \xi(t) \rangle = \langle \eta_j(t) \rangle = \langle \zeta_j(t) \rangle = 0$ and $\langle \xi(t)\eta_j(t-\tau) \rangle = \langle \xi(t)\zeta_j(t-\tau) \rangle = \langle \eta_j(t)\eta_k(t-\tau) \rangle = \langle \zeta_j(t)\zeta_k(t-\tau) \rangle = \langle \eta_k(t)\zeta_\ell(t-\tau) \rangle = 0$ for any j, k, and ℓ ($j \neq k$), where $\langle \cdot \rangle$ denotes the ensemble average over realizations of $\xi(t)$, $\eta_j(t)$, and $\zeta_j(t)$. For simplicity, we assume that the statistical properties of $\eta_j(t)$ and $\zeta_j(t)$ do not depend on the oscillator index j. Their power spectra are given by $P_\xi(\Omega) := \int_{-\infty}^{+\infty} e^{-i\Omega\tau} \langle \xi(t)\xi(t-\tau) \rangle d\tau$, $P_\eta(\Omega) := \int_{-\infty}^{+\infty} e^{-i\Omega\tau} \langle \eta_j(t)\eta_j(t-\tau) \rangle d\tau$, and $P_\zeta(\Omega) := \int_{-\infty}^{+\infty} e^{-i\Omega\tau} \langle \zeta_j(t)\zeta_j(t-\tau) \rangle d\tau$. We also define the amplitude response of the filter $f(\tau)$ as $A(\Omega) := |\int_{-\infty}^{+\infty} e^{-i\Omega\tau} f(\tau) d\tau|$.

By the phase reduction method [2], we can reduce the high-dimensional oscillator dynamics described by Eqs. (3.1) to a one-dimensional phase equation for small ϵ,

$$\begin{aligned} \dot{\theta}_j = \omega &+ \epsilon Z(\theta_j)[f * (\xi_j(t) + \eta_j(t)) + \zeta_j(t)] \\ &+ \epsilon^2 \nu(\theta_j) + O(\epsilon^3), \end{aligned} \tag{3.2}$$

where $\theta_j(t) \in [0, 2\pi)$ is the phase of the oscillator j, $Z(\theta_j)$ is a sensitivity function that characterizes the response of the oscillator phase to noisy inputs, and $\nu(\theta_j)$ represents the effect of amplitude relaxation dynamics of stochastic limit-cycle oscillators [22, 66, 67] (this term eventually vanishes and does not play a role in the following argument). The sensitivity function $Z(\theta)$ is given as $Z(\theta) = \boldsymbol{G}^\top(\boldsymbol{X}) \nabla_{\boldsymbol{X}} \theta(\boldsymbol{X})|_{\boldsymbol{X}=\boldsymbol{X}_0(\theta/\omega)}$, where $\theta(\boldsymbol{X})$ is the isochron of the limit cycle and $\nabla_{\boldsymbol{X}} \theta(\boldsymbol{X})|_{\boldsymbol{X}=\boldsymbol{X}_0(\theta/\omega)}$ represents its gradient on the limit-cycle orbit at phase θ [2].

3.3 Characterization of Synchronization Patterns

As discussed in refs. [36, 59], the phase difference between two oscillators $\phi_{j,k} := \theta_j - \theta_k$ characterizes the noise-induced synchronized state. Since statistical properties of $\eta_j(t)$ and $\zeta_j(t)$ do not depend on the oscillator index j, the PDF of the phase difference $\phi_{j,k}$ does not depend on the indices j and k. Thus, in the following, we denote the phase difference by ϕ without the oscillator indices.

In our previous work [59], we obtained the stationary PDF $U(\phi)$ of the phase difference ϕ by employing effective white-noise approximation of the phase equations (3.2) subjected to correlated colored noise and by deriving an averaged Fokker-Planck equation for ϕ from the multivariate

Fokker-Planck equation for the phase variables $\{\theta_j\}$. It turns out that the correlation functions of the noise play an important role, and $U(\phi)$ is explicitly given by

$$U(\phi) = \frac{1}{\bar{u}} \cdot \frac{1}{g(0) - g(\phi) + h(0)}, \tag{3.3}$$

where $\bar{u} \in \mathbb{R}$ is a normalization constant determined by $\int_{-\pi}^{+\pi} U(\phi)d\phi = 1$, and $g(\phi) \in \mathbb{R}$ and $h(\phi) \in \mathbb{R}$ are correlation functions of the noise terms in Eqs. (3.2), defined as $g(\phi) = \int_{-\infty}^{+\infty} \langle Z(\theta(t)) f * \xi(t) Z(\theta(t-\tau)+\phi) f * \xi(t-\tau) \rangle d\tau$ and $h(\phi) = \int_{-\infty}^{+\infty} \langle Z(\theta(t))[f * \eta_j(t) + \zeta_j(t)] Z(\theta(t-\tau)+\phi)[f * \eta_j(t) + \zeta_j(t-\tau)] \rangle d\tau$. In Fourier representation, these functions can be written as $g(\phi) = \sum_{\ell=-\infty}^{+\infty} g_\ell e^{i\ell\phi}$ and $h(\phi) = \sum_{\ell=-\infty}^{+\infty} h_\ell e^{i\ell\phi}$, where the Fourier coefficients $g_\ell, h_\ell \in \mathbb{R}$ are given by

$$\begin{aligned} g_\ell &= |z_\ell|^2 |A(\ell\omega)|^2 P_\xi(\ell\omega), \\ h_\ell &= |z_\ell|^2 |A(\ell\omega)|^2 P_\eta(\ell\omega) + |z_\ell|^2 P_\zeta(\ell\omega), \end{aligned} \tag{3.4}$$

and $z_\ell := \frac{1}{2\pi} \int_{-\pi}^{+\pi} e^{-i\ell\theta} Z(\theta) d\theta$ is the Fourier coefficient of $Z(\theta)$. From Eqs. (3.3), we see that the PDF $U(\phi)$ is symmetric about $\phi = 0$ and has a maximum at $\phi = 0$. For example, a PDF $U(\phi)$ with a single peak at $\phi = 0$ represents the synchronized state of the oscillators, and $U(\phi)$ with k peaks represents the k-clustered state. Thus, when the amplitude response $A(\Omega)$ of the filter $f(\tau)$ enhances the k-th mode of the correlation function $g(\phi)$ in Eqs. (3.4), k-clustered distribution is emphasized in the PDF $U(\phi)$.

3.4 Design of Synchronization Patterns

Equation (3.3) indicates that we can design the stationary PDF of the phase difference $U(\phi)$, i.e., the synchronization pattern, by varying the correlation function $g(\phi)$. Therefore, given the power spectra $P_\xi(\Omega)$, $P_\eta(\Omega)$, $P_\zeta(\Omega)$, and the sensitivity function $Z(\theta)$, we can try to find an optimal filter $f(\tau)$ that gives $g(\phi)$. In this study, rather than explicitly specifying the precise PDF of the oscillators as the target, we aim to maximize its statistical property, e.g., the degree of synchronization or clustering. This is because such macroscopic properties, rather than precise functional forms of $U(\phi)$, are relevant in practical applications. Note also that we cannot generate arbitrary PDFs but only optimize the PDF given in the form of Eqs. (3.3).

To design the optimal filter $f(\tau)$, we introduce the following objective functional $R\{f\}$ of $f(\tau)$ characterizing the statistical property of $U(\phi)$ as a measure for choosing an optimal synchronization pattern:

$$R\{f\} = \int_{-\pi}^{+\pi} U(\phi; f) q(\phi) d\phi, \tag{3.5}$$

where we explicitly show the dependence of $U(\phi; f)$ on f. The function $q(\phi)$ determines what statistical property we focus on. We try to design synchronization patterns with desired statistical properties by choosing appropriate $q(\phi)$.

In the numerical simulations given below, we will use the following functions for designing the synchronization patterns: $q_1(\phi) = \cos\phi$, $q_2(\phi) = \delta(\phi)$, $q_3(\phi) = \cos 3\phi$, and $q_4(\phi) = \cos 2\phi$, where $\delta(\cdot)$ denotes the Dirac delta function. When we use $q_1(\phi)$, the objective functional $R\{f\}$ corresponds to the order parameter introduced in ref. [58], which characterizes the degree of noise-induced synchronization. When we use $q_2(\phi)$, the objective functional $R\{f\}$ corresponds to the maximum of the PDF $U(\phi)$ at $\phi = 0$, which also characterizes the degree of synchronization, but in a more strict way, i.e., it counts only the oscillator pairs with exactly zero phase difference. When we use $q_3(\phi)$, the objective functional $R\{f\}$ characterizes three-clustered states, in which three synchronized subgroups of oscillators are formed. Similarly, $q_4(\phi)$ characterizes two-clustered states.

In the following, we represent $q(\phi)$ as a Fourier series, $q(\phi) = \tilde{q}_0 + 2\sum_{\ell=1}^{\infty} \tilde{q}_\ell \cos \ell\phi$, where the coefficient $\tilde{q}_\ell \in \mathbb{R}$ represents the weight of the ℓ-th Fourier mode. Expanding $U(\phi)$ as $U(\phi) = \frac{1}{2\pi} + \sum_{\ell=1}^{\infty} \tilde{u}_\ell \cos \ell\phi$, Eqs. (3.5) can be written as $R\{f\} = \sum_{\ell=1}^{\infty} \tilde{q}_\ell \tilde{u}_\ell$. By finding optimal $\tilde{u}_\ell$ for given $\tilde{q}_\ell$, we can obtain a PDF $U(\phi)$ and a filter $f(\tau)$ that maximizes the objective functional $R\{f\}$.

3.5 Optimization of Filters

By maximizing the objective functional $R\{f\}$, we seek for the optimal filter $f(\tau)$. However, unconstrained maximization of $R\{f\}$ often leads to divergent $f(\tau)$. We also need to take into account that our present theory is not valid for strong noisy inputs, because the phase reduction method requires the input given to the oscillators to be sufficiently weak [2]. Thus, we should introduce some constraint on the filter function $f(\tau)$.

In this study, we formulate the constrained optimization problem of the objective functional $R\{f\}$ as follows:

$$\underset{f}{\text{maximize}} \qquad R\{f\}, \tag{3.6}$$

$$\text{subject to} \qquad \sigma^2 := \langle I_j(t)^2 \rangle = C, \tag{3.7}$$

where the condition Eqs. (3.7) constrains the variance σ^2 of the filtered noise $I_j(t)$ to be a constant C. Using the power spectra $P_\xi(\Omega)$ and $P_\eta(\Omega)$ and the amplitude response $A(\Omega)$ of the filter $f(\tau)$, the variance σ^2 can be written as

$$\sigma^2 = \int_{-\infty}^{+\infty} |A(\Omega)|^2 [P_\xi(\Omega) + P_\eta(\Omega)] d\Omega. \tag{3.8}$$

By solving the optimization problem described by Eqs. (3.6) and (3.7), we can, in principle, obtain the optimal filter $f(\tau)$ for maximizing the objective functional $R\{f\}$.

Actually, we should also take into account that the optimal solution of Eqs. (3.6) and (3.7) may not be implemented in practice. The optimal amplitude response $A(\Omega)$ obtained as above often has delta peaks at $\Omega = \ell\omega$ ($\ell \in \mathbb{Z}$), i.e., $|A(\Omega)|^2 = a_0\delta(\Omega) + \sum_{\ell=1}^{\infty} a_\ell[\delta(\Omega - \ell\omega) + \delta(\Omega + \ell\omega)]$ (a_ℓ is some coefficient and ω is the natural frequency of the oscillator), because the PDF $U(\phi)$ depends only on the harmonic components $P_\xi(0), P_\xi(\omega), P_\xi(2\omega), \ldots$ and $P_\eta(0), P_\eta(\omega), P_\eta(2\omega), \ldots$ of the noise (see Eqs. (3.3) and (3.4)). Such a delta-peaked amplitude response $A(\Omega)$ corresponds to a physically unrealistic filter that extracts only purely harmonic components from the noise, which leads to phase locking rather than noise-induced synchronization of the oscillators. Besides, such singular $A(\Omega)$ cannot be realized in practical implementation of the linear filter $f(\tau)$.

To overcome this problem, we restrict the class of $A(\Omega)$ and further assume that the square of the amplitude response is expressed as a finite sum of narrow-band basis functions as

$$|\tilde{A}(\Omega)|^2 := \sum_{\ell=-m}^{m} c_{|\ell|} W(\Omega - \ell\omega), \tag{3.9}$$

where c_ℓ ($\ell = 0, 1, 2, \ldots$) is a weight coefficient, $W(\Omega)$ represents a narrow-band basis function prespecified before the optimization process, e.g., a Gaussian function, and m is the maximum wavenumber of the filter. We assume that the basis function $W(\Omega)$ is localized in the range $|\Omega| < \omega$, i.e., $W(\Omega) \approx 0$ holds for $|\Omega| \geq \omega$. The parameter m should be sufficiently large to obtain a good filter. The restricted amplitude response $\tilde{A}(\Omega)$ is experimentally feasible, because $W(\Omega - \ell\omega)$ in Eqs. (3.9) can be implemented by a band-pass filter that passes frequencies around $\Omega = \ell\omega$.

We introduce a new parameter $\boldsymbol{\beta} = [\beta_0, \beta_1, \ldots, \beta_m]^\top \in \mathbb{R}^{m+1}$ as $\beta_0 = \sqrt{|b_0 c_0|}$ and $\beta_\ell = \sqrt{2|b_\ell c_\ell|}$ for $\ell = 1, \ldots, m$, where b_ℓ ($\ell = 0, 1, 2, \ldots$) is defined as $b_\ell = \int_{-\infty}^{+\infty} W(\Omega - \ell\omega)[P_\xi(\Omega) + P_\eta(\Omega)]d\Omega$. The optimization problem (3.6) and (3.7) with the above restriction can then be expressed as

$$\underset{\boldsymbol{\beta}}{\text{maximize}} \qquad \tilde{R}(\boldsymbol{\beta}) := \int_{-\pi}^{+\pi} \tilde{U}(\phi; \boldsymbol{\beta}) q(\phi) d\phi, \tag{3.10}$$

$$\text{subject to} \qquad \sigma^2 \approx ||\boldsymbol{\beta}||^2 = \sum_{l=0}^{m-1} |\beta_\ell|^2 = C, \tag{3.11}$$

where $\tilde{U}(\phi; \boldsymbol{\beta})$ is the PDF of the phase difference ϕ obtained by plugging Eqs. (3.9) into Eqs. (3.4), and Eqs. (3.11) follows from Eqs. (3.8) and (3.9) and the definition of $\boldsymbol{\beta}$. Thus, we can employ $\boldsymbol{\beta}$ as a design parameter of the optimization problem described by Eqs. (3.10) and (3.11).

3.6 Optimization Algorithm

To solve the optimization problem given by Eqs. (3.10) and (3.11), we use the gradient descent algorithm. We randomly choose an initial value $\boldsymbol{\beta}^{(0)}$ and iteratively calculate $\boldsymbol{\beta}^{(j)}$ for $j \geq 1$, where

$\boldsymbol{\beta}^{(j)}$ is the design parameter $\boldsymbol{\beta}$ at j-th iteration. At each iteration, we update $\boldsymbol{\beta}^{(j)}$ as

$$\tilde{\boldsymbol{\beta}}^{(j+1)} = \boldsymbol{\beta}^{(j)} + \alpha \nabla_{\boldsymbol{\beta}} \tilde{R}(\boldsymbol{\beta}^{(j)}) \tag{3.12}$$

and normalize it as $\boldsymbol{\beta}^{(j+1)} = \sqrt{C}\tilde{\boldsymbol{\beta}}^{(j+1)}/||\tilde{\boldsymbol{\beta}}^{(j+1)}||$, so that $\boldsymbol{\beta}^{(j)}$ satisfies the constraint (3.11). Here, α is a constant that controls the step size, and $\nabla_{\boldsymbol{\beta}}\tilde{R}(\boldsymbol{\beta}) \in \mathbb{R}^{m+1}$ represents the gradient of $\tilde{R}(\boldsymbol{\beta})$ with respect to $\boldsymbol{\beta}$, i.e., $\nabla_{\boldsymbol{\beta}}\tilde{R}(\boldsymbol{\beta}) = [\frac{\partial \tilde{R}(\boldsymbol{\beta})}{\partial \beta_0}, \ldots, \frac{\partial \tilde{R}(\boldsymbol{\beta})}{\partial \beta_m}]^\top$.

For simplicity of notation, we define $u(\phi) := 1/[g(0) - g(\phi) + h(0)]$. The normalization constant is given by $\bar{u} = \int_{-\pi}^{+\pi} u(\phi) d\phi$. Then, the gradient $\frac{\partial \tilde{R}(\boldsymbol{\beta}^{(j)})}{\partial \beta_\ell}$ in Eqs. (3.12) can be expressed as $\frac{\partial \tilde{R}(\boldsymbol{\beta})}{\partial \beta_\ell} = \int_{-\pi}^{+\pi} \frac{1}{\bar{u}^2}[\frac{\partial u(\phi)}{\partial \beta_\ell}\bar{u} - u(\phi)\frac{\partial \bar{u}}{\partial \beta_\ell}]q(\phi)d\phi$, and the gradients $(\partial u(\phi)/\partial \beta_\ell)$ and $(\partial \bar{u}/\partial \beta_\ell)$ can be calculated from Eqs. (3.3), (3.4) and (3.9) and the definition of $\boldsymbol{\beta}$ as $\frac{\partial u(\phi)}{\partial \beta_\ell} = 2u^2(\phi)\sum_{k=0}^{m-1} W(k\omega - \ell\omega)\frac{\beta_\ell |z_k|^2}{b_\ell}[P_\xi(k\omega)(\cos k\phi - 1) - P_\eta(k\omega)]$, $\frac{\partial \bar{u}}{\partial \beta_\ell} = \int_{-\pi}^{+\pi} \frac{\partial u(\phi)}{\partial \beta_\ell} d\phi$.

Because $W(\Omega)$ is localized in the range $|\Omega| < \omega$, the above expression can be simplified as follows: $\frac{\partial u(\phi)}{\partial \beta_\ell} = 2u^2(\phi)W(0)\frac{\beta_\ell |z_\ell|^2}{b_\ell}\left[P_\xi(\ell\omega)(\cos \ell\phi - 1) - P_\eta(\ell\omega)\right]$, which reduces the computational cost of the optimization process. Using the optimized $\boldsymbol{\beta}$, we can obtain the optimal amplitude response $\tilde{A}(\Omega)$ as the square root of Eqs. (3.9), whose coefficients $c_0, \ldots, c_m$ are given by $c_0 = \frac{|\beta_0|^2}{b_0}$, $c_\ell = \frac{|\beta_\ell|^2}{2b_\ell}$, for $\ell = 1, 2, \ldots, m$. Thus, using, e.g., the least-squares method [68], we can calculate the optimal filter $f(\tau)$ from the amplitude response $\tilde{A}(\Omega)$.

3.7 Numerical Simulations

To confirm the validity of our method, we performed numerical simulations using several examples of the objective functionals. In the first example, we use the FitzHugh-Nagumo (FHN) model of a periodically firing neuron. This model has a two-dimensional state variable (u, v), which obeys $\dot{v}(t) = v - v^3/3 - u + I_0 + I(t)$ and $\dot{u}(t) = \mu(v + c - du)$, $\mu = 0.08$, $c = 0.7$, $d = 0.8$, and $I_0 = 0.875$. The frequency of the oscillation is approximately $\omega = 0.173$ and the noisy input $I_j(t)$ is given to $v(t)$. The sensitivity function $Z(\theta)$ to $I(t)$ and its Fourier coefficients are shown in figs. 3.1 (a) and (b).

As the noisy inputs, we use the Ornstein-Uhlenbeck noise, whose power spectra are given by $P_\xi(\Omega) = \tilde{P}_{\mathrm{OU}}(\Omega; 0.5)$, $P_\eta(\Omega) = P_\zeta(\Omega) = 0.1 \cdot \tilde{P}_{\mathrm{OU}}(\Omega; 0.5)$, with $\tilde{P}_{\mathrm{OU}}(\Omega; \gamma) := \gamma^2/(\gamma^2 + \Omega^2)$ [fig. 3.1 (c)]. As the basis function $W(\Omega)$, we employ a rectangular function, $W(\Omega) = 1$ ($|\Omega| < \omega/2$), 0 (otherwise). The other parameters are set as follows: the coupling strength to the noise is $\epsilon = 0.01$, the variance of the filtered noise is $C = 10$, and the maximum wavenumber of the filter is $m = 5$ (because $|z_\ell|$ is small when $\ell \geq 6$). The parameter α used for the gradient descent is $\alpha = 0.5$. Note that the gradient descent algorithm finds only a local optimum and does not guarantee global optimality. In order to obtain the global optimum, the algorithm should be repeated from sufficiently many initial states $\boldsymbol{\beta}^{(0)}$.

Figure 3.2 shows the numerical results for the FHN model. For the functions $q_1(\phi)$ and $q_2(\phi)$ defined previously, synchronized states are successfully formed [figs. 3.2 (b) and (d)]. For the sinusoidal $q_1(\phi)$, we obtain a filter that emphasizes only the first Fourier mode [fig. 3.2 (a)] (see Eqs. (3.4)), which results in a bell-shaped PDF $U(\phi)$ [fig. 3.2 (b)]. For the delta-shaped $q_2(\phi)$, in contrast, we obtain a nontrivial filter that consists of multiple modes [fig. 3.2 (c)]. In this case, the PDF $U(\phi)$ has a sharper peak than that for $q_1(\phi)$ [fig. 3.2 (d)] and a more precisely synchronized state is realized. Note that the high-frequency components of $\tilde{A}(\Omega)$ in fig. 3.2 (c), which are stronger than the low-frequency components, do not significantly affect the statistical property of $I_j(t)$, because $P(\ell\omega)$ is sufficiently small for large ℓ. Therefore, we can safely neglect the high-frequency components of $\tilde{A}(\Omega)$ whose wavenumbers are larger than m. For the function $q_3(\phi)$, we obtain a filter that emphasizes only the third Fourier mode [fig. 3.2 (e)], which yields a three-clustered state as expected [fig. 3.2 (f)]. Note that we cannot form a two-clustered state in the FHN model, because the phase response property of this model has odd symmmetry, i.e., the second Fourier coefficient $|z_2|$ of $Z(\theta)$ is vanishingly small as shown in fig. 3.1 (b).

In the second experiment, we use the Hodgkin-Huxley (HH) model [54]. It also models periodic firing of a neuron, but it has more realistic, higher-dimensional dynamics without odd symmetry, in contrast to the FHN model. We apply the noisy input $I_j(t)$ as well as a constant input $I_0 = 10$ to the V variable (i.e., membrane potential) of the HH model. The oscillation frequency is approximately $\omega = 0.438$, and the sensitivity function and its Fourier coefficients are shown in figs. 3.3 (a) and (b). In addition to $q_1(\phi)$ and $q_2(\phi)$, we use $q_4(\phi)$ for optimization with the aim of forming two-clustered states. The power spectra $P_\xi(\Omega)$, $P_\eta(\Omega)$ and $P_\zeta(\Omega)$, the parameters C and α, and the basis function $W(\Omega)$ are the same as before. The noise intensity is $\epsilon = 0.1$ and the maximum wavenumber of the filter is $m = 4$ (because $|z_\ell|$ almost vanishes at $\ell = 5$).

Figure 3.4 shows the numerical results for the HH model. Synchronized states are successfully formed for $q_1(\phi)$ and $q_2(\phi)$ as shown in figs. 3.4 (b) and (d). When we use the delta-shaped $q_2(\phi)$, we obtain a nontrivial filter consisting of multiple modes [figs. 3.4 (c)] and the PDF $U(\phi)$ has a sharper peak than the case with the sinusoidal $q_1(\phi)$ [figs. 3.4 (d)]. In contrast to the FHN model, we can realize a two-clustered state as shown in figs. 3.4 (f), because $Z(\theta)$ of the HH model has a sufficiently large second Fourier component as shown in fig. 3.3 (b). Note that the realizability of a particular state is determined by the sensitivity function $Z(\theta)$ that characterizes the phase response property of the driven oscillator, rather than by the dimensionality or complexity of the oscillator model.

3.8 Summary and Discussion

We have proposed a method for designing and controlling various noise-induced synchronization patterns by filtering the input noise, including the synchronized and clustered states. By numerical

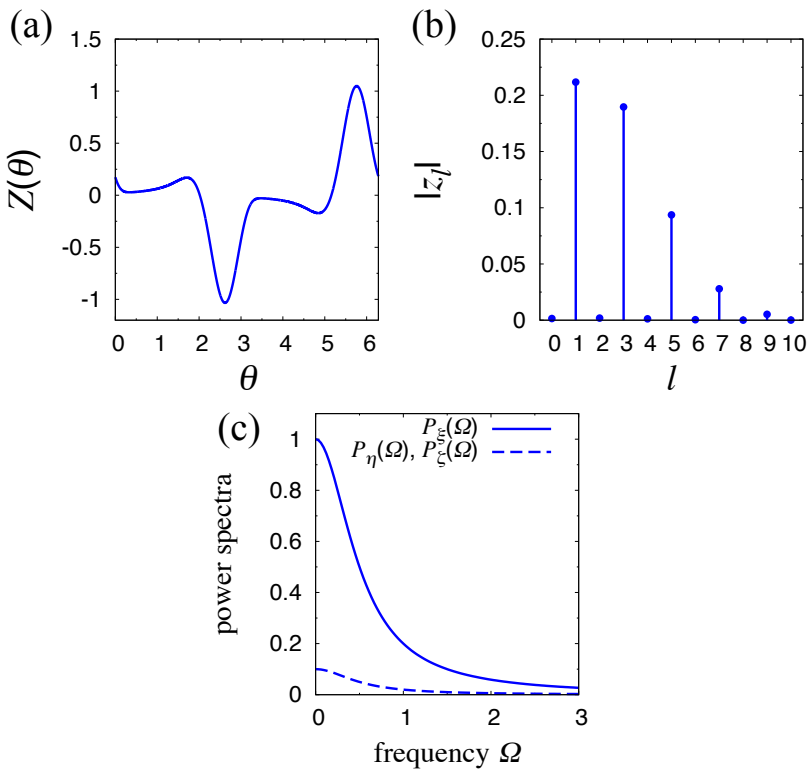

Figure 3.1: FitzHugh-Nagumo model. (a) Sensitivity function $Z(\theta)$, (b) Fourier coefficients $|z_\ell|$, and (c) power spectra of the noisy inputs $P_\xi(\Omega)$, $P_\eta(\Omega)$ and $P_\zeta(\Omega)$.

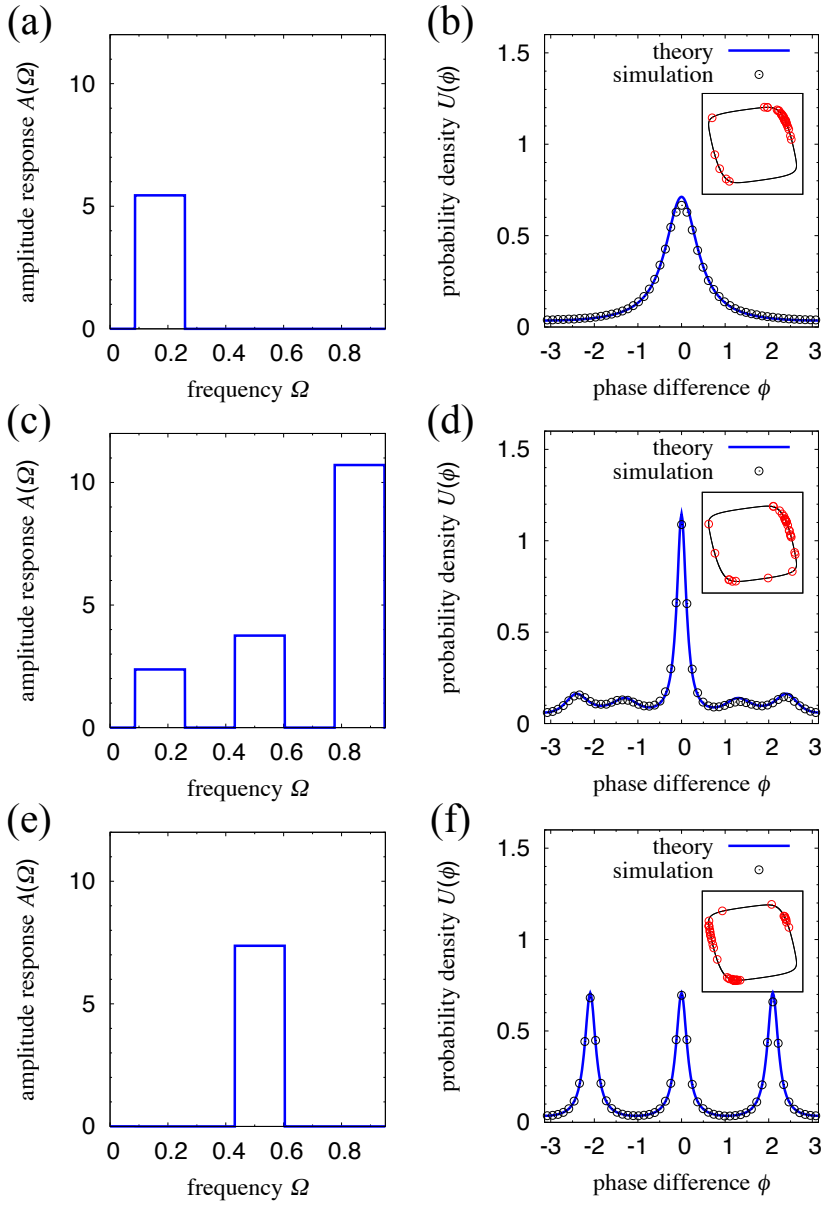

Figure 3.2: FitzHugh-Nagumo model. [(a), (c) and (e)] Amplitude response $A(\Omega)$ of the optimal filter designed by the proposed method and [(b), (d) and (f)] probability density function $U(\phi)$ of the phase difference ϕ for [(a) and (b)] $q_1(\phi)$, [(c) and (d)] $q_2(\phi)$, and [(e) and (f)] $q_3(\phi)$. The insets display snapshots of the oscillators in the v–u plane.

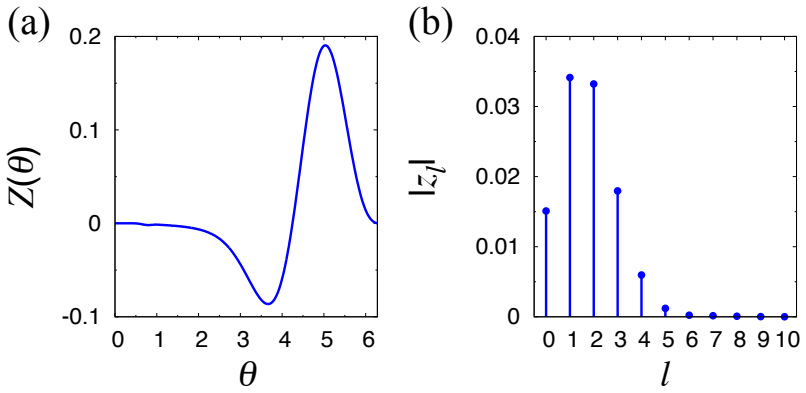

Figure 3.3: Hodgkin-Huxley model. (a) Sensitivity function $Z(\theta)$ and (b) Fourier coefficients.

simulations, the validity of the method has been confirmed for two types of limit-cycle oscillators. These results will provide a theoretical basis for optimizing noise-induced synchronization by filtering the input noise.

Though some previous works [64, 65] proposed optimization methods for the phase response property of the oscillator to enhance noise-induced synchronization, those works considered only the Lyapunov exponent of the phase (i.e., the exponential decay rate of the small phase difference between two oscillators), so that they could not fully characterize the synchronized states and could not be used to design various synchronization patterns as described in this chapter. More importantly, in contrast to previous works [64, 65] that gave the optimal phase response property of the oscillator, our present study provides a method to generate optimal noisy inputs to the oscillator, which can be implemented much more easily than designing the oscillator response. Thus, our method can be useful in various real-world applications, e.g., energy-efficient synchronization control in wireless sensor networks [45].

Finally, though we have not considered the effect of differences in the natural frequency of the oscillators [46, 60, 62] in this chapter, it is often significant in practical applications. Extension of the present method to non-identical oscillators will be an important future work.

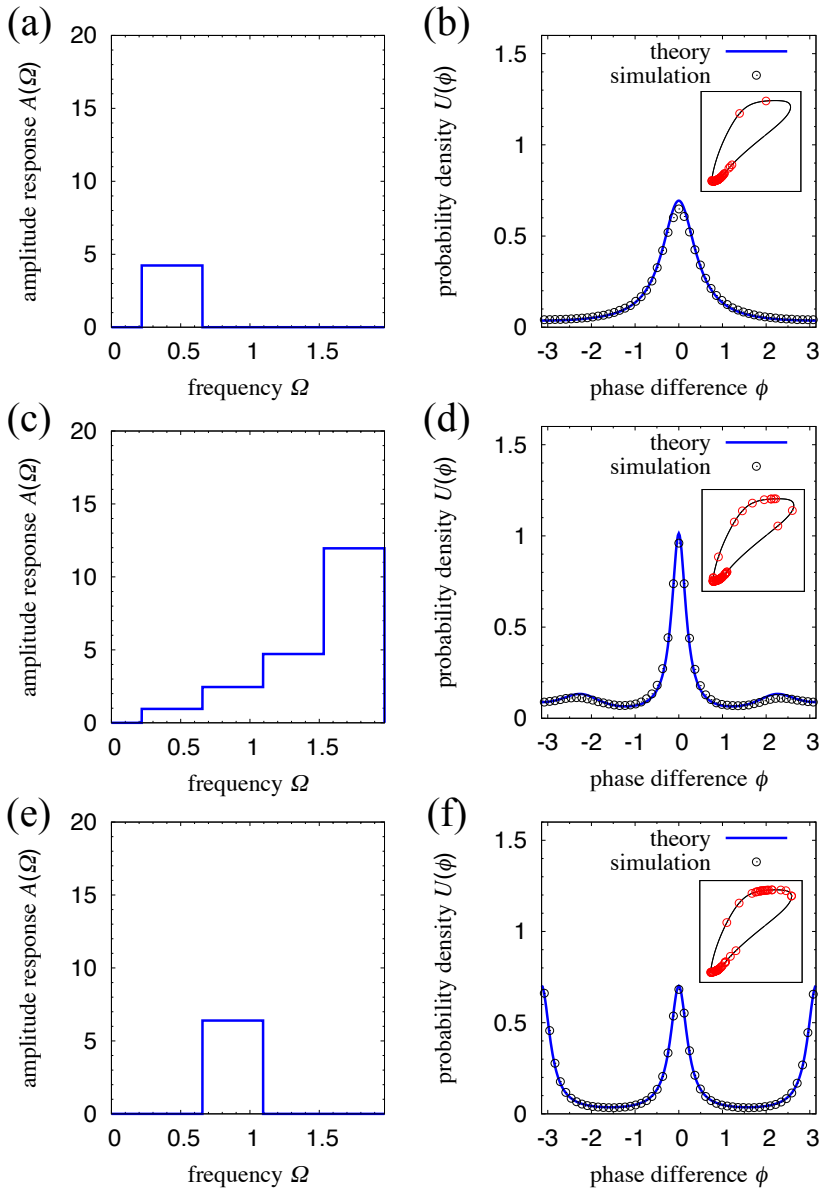

Figure 3.4: Hodgkin-Huxley model. [(a), (c) and (e)] Amplitude response $A(\Omega)$ of the optimal filter designed by the proposed method and [(b), (d) and (f)] probability density function $U(\phi)$ of the phase difference ϕ for [(a) and (b)] $q_1(\phi)$, [(c) and (d)] $q_2(\phi)$ and [(e) and (f)] $q_4(\phi)$. The insets display snapshots of the oscillators in the V–m plane, where m is a channel variable [54].

Chapter 4

Generalized Phase Reduction Method for Strong External Forcing

4.1 Intorduction

Rhythmic phenomena are ubiquitous in nature and of great interest in many fields of science and technology, including chemical reactions, neural networks, genetic circuits, lasers, and structural vibrations [1, 2, 3, 4, 70, 39, 5, 69]. These rhythmic phenomena often result from complex interactions among individual rhythmic elements, typically modeled as limit-cycle oscillators. In analyzing such systems, the phase reduction method [1, 2, 3, 4, 5, 69] has been widely used and considered an essential tool. It systematically approximates the high-dimensional dynamical equation of a perturbed limit-cycle oscillator by a one-dimensional reduced *phase equation*, with just a single *phase variable* θ representing the oscillator state.

A fundamental assumption of the conventional phase reduction method is that the applied perturbation is sufficiently weak; hence, the shape and frequency of the limit-cycle orbit remain almost unchanged. However, this assumption hinders the applications of the method to strongly perturbed oscillators because the shapes and frequencies of their orbits can significantly differ from those in the unperturbed cases. Indeed, strong coupling can destabilize synchronized states of oscillators that are stable in the weak coupling limit [40]. The effect of strong coupling can further lead to nontrivial collective dynamics such as quorum-sensing transition [39], amplitude death and bistability [40], and collective chaos [41]. Although not all of these collective phenomena are the subject of discussion in this study, our formulation will give an insight into a certain class

of them, e.g., bistability between phase-locked and drifting states [40]. The assumption of weak perturbations can also be an obstacle to modeling real-world systems, which are often subjected to strong perturbations.

Although the phase reduction method has recently been extended to stochastic [71], delay-induced [72], and collective oscillations [73], these extensions are still limited to the weakly perturbed regime. To analyze a broader class of synchronization phenomena exhibited by strongly driven or interacting oscillators, the conventional theory should be extended. This chapter proposes an extension of the phase reduction method to strongly perturbed limit-cycle oscillators, which enables us to derive a simple generalized phase equation that quantitatively describes their dynamics. We use it to analyze the synchronization dynamics of limit-cycle oscillators subjected to strong periodic forcing, which cannot be treated appropriately by the conventional method.

4.2 Model and Assumptions

We consider a limit-cycle oscillator whose dynamics depends on a time-varying parameter $\boldsymbol{I}(t) = [I_1(t), \ldots, I_m(t)]^\top \in \mathbb{R}^m$ representing general perturbations, described by

$$\dot{\boldsymbol{X}}(t) = \boldsymbol{F}(\boldsymbol{X}(t), \boldsymbol{I}(t)), \tag{4.1}$$

where $\boldsymbol{X}(t) = [X_1(t), \ldots, X_n(t)]^\top \in \mathbb{R}^n$ is the oscillator state and $\boldsymbol{F}(\boldsymbol{X}, \boldsymbol{I}) = [F_1(\boldsymbol{X}, \boldsymbol{I}), \ldots, F_n(\boldsymbol{X}, \boldsymbol{I})]^\top \in \mathbb{R}^n$ is an $\boldsymbol{I}$-dependent vector field representing the oscillator dynamics. For example, $\boldsymbol{X}$ and $\boldsymbol{I}$ can represent the state of a periodically firing neuron and the injected current, respectively [4, 69]. In this chapter, we introduce a generalized phase θ, which depends on the parameter $\boldsymbol{I}(t)$, of the oscillator. In defining the phase θ, we require that the oscillator state $\boldsymbol{X}(t)$ can be accurately approximated by using $\theta(t)$ with sufficiently small error, and that $\theta(t)$ increases at a constant frequency when the parameter $\boldsymbol{I}(t)$ remains constant. The former requirement is a necessary condition for the phase reduction, i.e., for deriving a closed equation for the generalized phase, and the latter enables us to derive an analytically tractable phase equation.

To define such θ, we suppose that $\boldsymbol{I}$ is constant until further notice. We assume that Eq. (A.12) possesses a family of stable limit-cycle solutions with period $T(\boldsymbol{I})$ and frequency $\omega(\boldsymbol{I}) := 2\pi/T(\boldsymbol{I})$ for $\boldsymbol{I} \in A$, where A is an open subset of $\mathbb{R}^m$ (e.g., an interval between two bifurcation points). An oscillator state on the limit cycle with parameter $\boldsymbol{I}$ can be parameterized by a phase $\theta \in [0, 2\pi)$ as $\boldsymbol{X}_0(\theta, \boldsymbol{I}) = [X_{0,1}(\theta, \boldsymbol{I}), \ldots, X_{0,n}(\theta, \boldsymbol{I})]^\top$. Generalizing the conventional phase reduction method [1, 2, 3, 4, 5], we define the phase θ such that, as the oscillator state $\boldsymbol{X}(t) = \boldsymbol{X}_0(\theta(t), \boldsymbol{I})$ evolves along the limit cycle, the corresponding phase $\theta(t)$ increases at a constant frequency $\omega(\boldsymbol{I})$ as $\dot{\theta}(t) = \omega(\boldsymbol{I})$ *for each* $\boldsymbol{I} \in A$. We assume that $\boldsymbol{X}_0(\theta, \boldsymbol{I})$ is continuously differentiable with respect to $\theta \in [0, 2\pi)$ and $\boldsymbol{I} \in A$.

We consider an extended phase space $\mathbb{R}^n \times A$, as depicted schematically in Fig. 4.1 (a). We

define C as a cylinder formed by the family of limit cycles $(\boldsymbol{X}_0(\theta, \boldsymbol{I}), \boldsymbol{I})$ for $\theta \in [0, 2\pi)$ and $\boldsymbol{I} \in A$, and define $U \subset \mathbb{R}^n \times A$ as a neighborhood of C. For each $\boldsymbol{I}$, we assume that any orbit starting from an arbitrary point $(\boldsymbol{X}, \boldsymbol{I})$ in U asymptotically converges to the limit cycle $\boldsymbol{X}_0(\theta, \boldsymbol{I})$ on C. We can then extend the definition of the phase into U, as in the conventional method [1, 2, 3, 4, 5], by introducing the *asymptotic phase* and *isochrons* around the limit cycle for each $\boldsymbol{I}$. Namely, we can define a generalized *phase function* $\Theta(\boldsymbol{X}, \boldsymbol{I}) \in [0, 2\pi)$ of $(\boldsymbol{X}, \boldsymbol{I}) \in U$ such that $\Theta(\boldsymbol{X}, \boldsymbol{I})$ is continuously differentiable with respect to $\boldsymbol{X}$ and $\boldsymbol{I}$, and $\frac{\partial \Theta(\boldsymbol{X}, \boldsymbol{I})}{\partial \boldsymbol{X}} \cdot \boldsymbol{F}(\boldsymbol{X}, \boldsymbol{I}) = \omega(\boldsymbol{I})$ holds everywhere in U, where $\frac{\partial \Theta}{\partial \boldsymbol{X}} = [\frac{\partial \Theta}{\partial X_1}, \ldots, \frac{\partial \Theta}{\partial X_n}]^\top \in \mathbb{R}^n$ is the gradient of $\Theta(\boldsymbol{X}, \boldsymbol{I})$ with respect to $\boldsymbol{X}$ and the dot $(\cdot)$ denotes an inner product. This $\Theta(\boldsymbol{X}, \boldsymbol{I})$ is a straightforward generalization of the conventional asymptotic phase [1, 2, 3, 4, 5] and guarantees that the phase of any orbit $\boldsymbol{X}(t)$ in U always increases with a constant frequency as $\dot{\Theta}(\boldsymbol{X}(t), \boldsymbol{I}) = \omega(\boldsymbol{I})$ at each $\boldsymbol{I}$. For any oscillator state on C, $\Theta(\boldsymbol{X}_0(\theta, \boldsymbol{I}), \boldsymbol{I}) = \theta$ holds. In general, the origin of the phase can be arbitrarily defined for each $\boldsymbol{I}$ as long as it is continuously differentiable with respect to $\boldsymbol{I}$. The assumptions that $\boldsymbol{X}_0(\theta, \boldsymbol{I})$ and $\Theta(\boldsymbol{X}, \boldsymbol{I})$ are continuously differentiable can be further relaxed for a certain class of oscillators, such as those considered in [74].

Now suppose that the parameter $\boldsymbol{I}(t)$ varies with time. To define θ that approximates the oscillator state with sufficiently small error, we assume that $\boldsymbol{I}(t)$ can be decomposed into a slowly varying component $\boldsymbol{q}(\epsilon t) \in A$ and remaining weak fluctuations $\sigma \boldsymbol{p}(t) \in \mathbb{R}^m$ as

$$\boldsymbol{I}(t) = \boldsymbol{q}(\epsilon t) + \sigma \boldsymbol{p}(t). \tag{4.2}$$

Here, the parameters ϵ and σ are assumed to be sufficiently small so that $\boldsymbol{q}(\epsilon t)$ varies slowly as compared to the relaxation time of a perturbed orbit to the cylinder C of the limit cycles, which we assume to be $O(1)$ without loss of generality, and the oscillator state $\boldsymbol{X}(t)$ always remains in a close neighborhood of $\boldsymbol{X}_0(\theta, \boldsymbol{q}(\epsilon t))$ on C, i.e., $\boldsymbol{X}(t) = \boldsymbol{X}_0(\theta(t), \boldsymbol{q}(\epsilon t)) + O(\epsilon, \sigma)$ holds (see Sec. A.4 (Appendix)). We also assume that $\boldsymbol{q}(\epsilon t)$ is continuously differentiable with respect to $t \in \mathbb{R}$. Note that the slow component $\boldsymbol{q}(\epsilon t)$ itself does not need to be small. Using the second largest Floquet exponent of the oscillator, we can derive the optimal decomposition of $\boldsymbol{I}(t)$ (see Sec. A.9 for a discussion).

4.3 Derivation of Phase Equation

Using the phase function $\Theta(\boldsymbol{X}, \boldsymbol{I})$, we introduce a generalized phase $\theta(t)$ of the limit-cycle oscillator (A.12) as $\theta(t) = \Theta(\boldsymbol{X}(t), \boldsymbol{q}(\epsilon t))$. This definition guarantees that $\theta(t)$ increases at a constant frequency when $\boldsymbol{I}(t)$ remains constant, and leads to a closed equation for $\theta(t)$. Expanding Eq. (A.12) in σ as

$$\dot{\boldsymbol{X}}(t) = \boldsymbol{F}(\boldsymbol{X}, \boldsymbol{q}(\epsilon t)) + \sigma \boldsymbol{G}(\boldsymbol{X}, \boldsymbol{q}(\epsilon t)) \boldsymbol{p}(t) + O(\sigma^2), \tag{4.3}$$

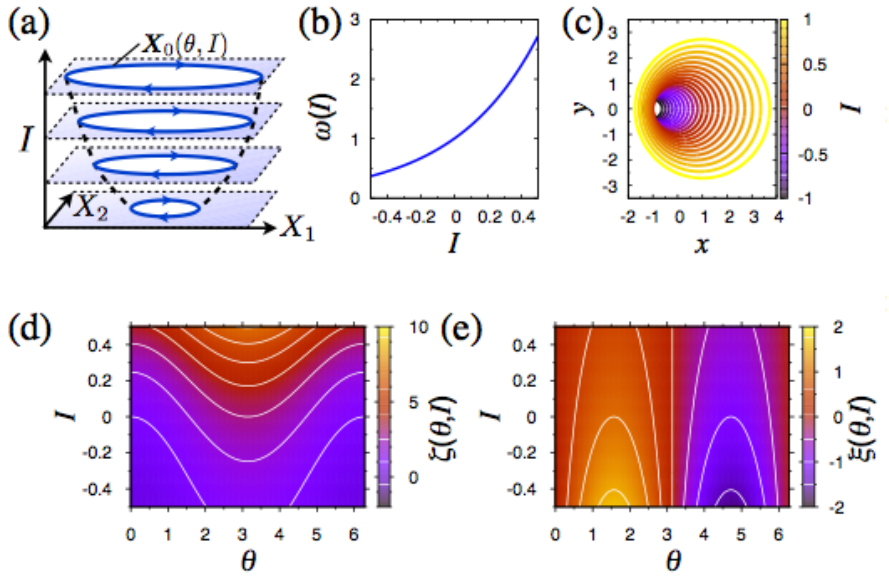

Figure 4.1: Phase dynamics of a modified Stuart-Landau oscillator. (a) A schematic diagram of the extended phase space $\mathbb{R}^n \times A$ with $n = 2$ and $m = 1$. (b) Frequency $\omega(I)$. (c) I-dependent stable limit-cycle solutions $\boldsymbol{X}_0(\theta, I)$. (d), (e) Sensitivity functions $\zeta(\theta, I)$ and $\xi(\theta, I)$.

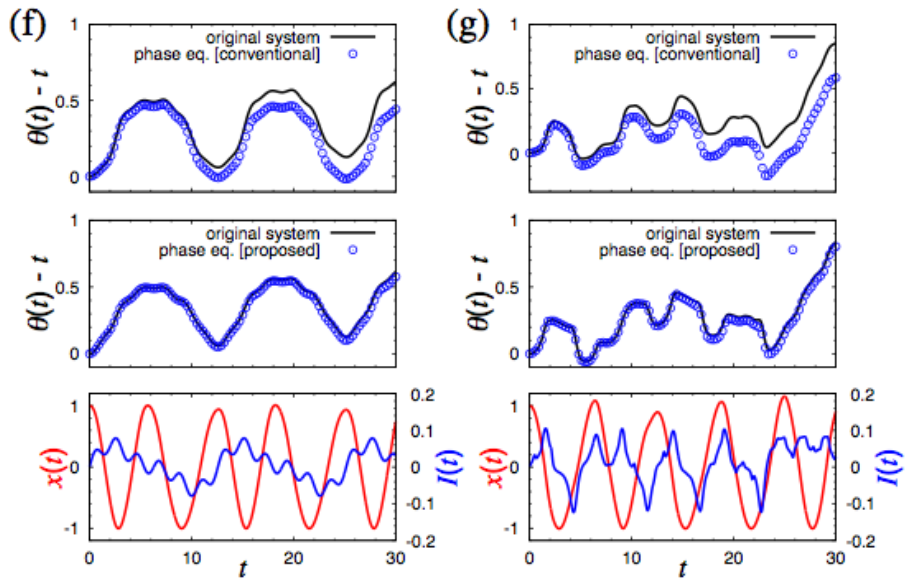

Figure 4.2: Phase dynamics of a modified Stuart-Landau oscillator. (f), (g) Time series of the phase $\theta(t)$ of the oscillator driven by (f) a periodically varying parameter $I^{(1)}(t)$ or (g) a chaotically varying parameter $I^{(2)}(t)$. For each of these cases, results of the conventional (top panel) and proposed (middle panel) methods are shown. Evolution of the conventional phase $\tilde{\theta}(t) = \Theta(\boldsymbol{X}(t), \boldsymbol{q}_c)$ and the generalized phase $\theta(t) = \Theta(\boldsymbol{X}(t), \boldsymbol{q}(\epsilon t))$ measured from the original system (lines) is compared with that of the conventional and generalized phase equations (circles). Time series of the state variable $x(t)$ (red) and time-varying parameter $I(t)$ (blue) are also depicted (bottom panel). The periodically varying parameter is given by $I^{(1)}(t) = q^{(1)}(\epsilon t) + \sigma p^{(1)}(t)$ with $q^{(1)}(\epsilon t) = 0.05\sin(0.5t) + 0.02\sin(t)$ and $\sigma p^{(1)}(t) = 0.02\sin(3t)$, and the chaotically varying parameter is given by $I^{(2)}(t) = q^{(2)}(\epsilon t) + \sigma p^{(2)}(t)$ with $q^{(2)}(\epsilon t) = 0.007 L_1(0.3t)$ and $\sigma p^{(2)}(t) = 0.001 L_2(t)$, where $L_1(t)$ and $L_2(t)$ are independently generated time series of the variable x of the chaotic Lorenz equation [3], $\dot{x} = 10(y - x)$, $\dot{y} = x(28 - z) - y$, and $\dot{z} = xy - 8z/3$.

and using the chain rule, we can derive

$$\dot{\theta}(t) = \omega(\boldsymbol{q}(\epsilon t)) + \sigma \frac{\partial \Theta(\boldsymbol{X}, \boldsymbol{I})}{\partial \boldsymbol{X}}|_{(\boldsymbol{X}(t), \boldsymbol{q}(\epsilon t))} \cdot \boldsymbol{G}(\boldsymbol{X}, \boldsymbol{q}(\epsilon t))\boldsymbol{p}(t) + \epsilon \frac{\partial \Theta(\boldsymbol{X}, \boldsymbol{I})}{\partial \boldsymbol{I}}|_{(\boldsymbol{X}(t), \boldsymbol{q}(\epsilon t))} \cdot \dot{\boldsymbol{q}}(\epsilon t) + O(\sigma^2), \tag{4.4}$$

where $\boldsymbol{G}(\boldsymbol{X}, \boldsymbol{I}) \in \mathbb{R}^{n \times m}$ is a matrix whose (i, j)-th element is given by $\frac{\partial F_i(\boldsymbol{X}, \boldsymbol{I})}{\partial I_j}$, $\frac{\partial \Theta}{\partial \boldsymbol{I}} = [\frac{\partial \Theta}{\partial I_1}, \ldots, \frac{\partial \Theta}{\partial I_m}]^\top \in \mathbb{R}^m$ is the gradient of $\Theta(\boldsymbol{X}, \boldsymbol{I})$ with respect to $\boldsymbol{I}$, and $\dot{\boldsymbol{q}}(\epsilon t)$ denotes $\frac{d\boldsymbol{q}(\epsilon t)}{d(\epsilon t)}$.

To obtain a closed equation for θ, we use the lowest-order approximation in σ and ϵ, i.e., $\boldsymbol{X}(t) = \boldsymbol{X}_0(\theta(t), \boldsymbol{q}(\epsilon t)) + O(\epsilon, \sigma)$. Then, by defining a *phase sensitivity function*

$$\boldsymbol{Z}(\theta, \boldsymbol{I}) := \frac{\partial \Theta(\boldsymbol{X}, \boldsymbol{I})}{\partial \boldsymbol{X}}|_{(\boldsymbol{X}_0(\theta, \boldsymbol{I}), \boldsymbol{I})} \in \mathbb{R}^n, \tag{4.5}$$

and two other sensitivity functions

$$\boldsymbol{\zeta}(\theta, \boldsymbol{I}) := \boldsymbol{G}^\top(\boldsymbol{X}_0(\theta, \boldsymbol{I}), \boldsymbol{I})\boldsymbol{Z}(\theta, \boldsymbol{I}) \in \mathbb{R}^m, \tag{4.6}$$

and

$$\boldsymbol{\xi}(\theta, \boldsymbol{I}) := \frac{\partial \Theta(\boldsymbol{X}, \boldsymbol{I})}{\partial \boldsymbol{I}}|_{(\boldsymbol{X}_0(\theta, \boldsymbol{I}), \boldsymbol{I})} \in \mathbb{R}^m, \tag{4.7}$$

we can obtain a closed equation for the oscillator phase $\theta(t)$ as

$$\dot{\theta}(t) = \omega(\boldsymbol{q}(\epsilon t)) + \sigma \boldsymbol{\zeta}(\theta, \boldsymbol{q}(\epsilon t)) \cdot \boldsymbol{p}(t) + \epsilon \boldsymbol{\xi}(\theta, \boldsymbol{q}(\epsilon t)) \cdot \dot{\boldsymbol{q}}(\epsilon t) + O(\sigma^2, \epsilon^2, \sigma\epsilon), \tag{4.8}$$

which is a generalized phase equation that we propose in this study. The first three terms in the right-hand side of Eq. (4.8) represent the instantaneous frequency of the oscillator, the phase response to the weak fluctuations $\sigma \boldsymbol{p}(t)$, and the phase response to deformation of the limit-cycle orbit caused by the slow variation in $\boldsymbol{q}(\epsilon t)$, respectively, all of which depend on the slowly varying component $\boldsymbol{q}(\epsilon t)$.

To address the validity of Eq. (4.8) more precisely, let $\lambda(\boldsymbol{I})$ (> 0) denote the absolute value of the second largest Floquet exponent of the oscillator for a fixed $\boldsymbol{I}$, which characterizes the amplitude relaxation timescale of the oscillator $(\approx 1/\lambda(\boldsymbol{I}))$. As argued in Appendix, we can show that the error terms in Eq. (4.8) remain sufficiently small when

$$\sigma / \lambda(\boldsymbol{q}(\epsilon t)) \ll 1, \tag{4.9}$$

and

$$\epsilon / \lambda(\boldsymbol{q}(\epsilon t))^2 \ll 1, \tag{4.10}$$

namely, when the orbit of the oscillator relaxes to the cylinder C sufficiently faster than the variations in $\boldsymbol{q}(\epsilon t)$.

Note that if we define the phase variable as $\tilde{\theta}(t) = \Theta(\boldsymbol{X}(t), \boldsymbol{q}_c)$ with some constant $\boldsymbol{q}_c$ instead of $\theta(t) = \Theta(\boldsymbol{X}(t), \boldsymbol{q}(\epsilon t))$, $\tilde{\theta}(t)$ gives the conventional phase. Then, we obtain the conventional phase equation $\dot{\tilde{\theta}}(t) = \omega_c + \sigma \boldsymbol{\zeta}_c(\tilde{\theta}) \cdot \boldsymbol{p}(t) + O(\sigma^2)$ with $\boldsymbol{q}(\epsilon t) = \boldsymbol{q}_c$ and $\sigma \boldsymbol{p}(t) = \boldsymbol{I}(t) - \boldsymbol{q}_c$. Here, $\omega_c := \omega(\boldsymbol{q}_c)$ is a natural frequency, $\boldsymbol{\zeta}_c(\tilde{\theta}) = \boldsymbol{\zeta}(\tilde{\theta}, \boldsymbol{q}_c) = \boldsymbol{G}(\boldsymbol{X}_0(\tilde{\theta}, \boldsymbol{q}_c), \boldsymbol{q}_c)^\top \boldsymbol{Z}(\tilde{\theta}, \boldsymbol{q}_c)$, and $\boldsymbol{Z}(\tilde{\theta}, \boldsymbol{q}_c)$ is the conventional phase sensitivity function at $\boldsymbol{I} = \boldsymbol{q}_c$ [2]. This equation is valid only when $\sigma/\lambda(\boldsymbol{q}_c) \ll 1$ (i.e., $||\boldsymbol{I}(t) - \boldsymbol{q}_c||/\lambda(\boldsymbol{q}_c) \ll 1$). By using the near-identity transformation [75], we can show that the conventional equation is actually a low-order approximation of the generalized equation (4.8) (see Sec. A.6 (Appendix)).

4.4 Sensitivity Functions

In practice, we need to calculate $\boldsymbol{\zeta}(\theta, \boldsymbol{I})$ and $\boldsymbol{\xi}(\theta, \boldsymbol{I})$ numerically from mathematical models or estimate them through experiments. We can show that the following relations hold (See Sec. A.5 for the derivation):

$$\boldsymbol{\xi}(\theta, \boldsymbol{I}) = -\frac{\partial \boldsymbol{X}_0(\theta, \boldsymbol{I})}{\partial \boldsymbol{I}}^\top \boldsymbol{Z}(\theta, \boldsymbol{I}), \tag{4.11}$$

$$\boldsymbol{\xi}(\theta, \boldsymbol{I}) = \boldsymbol{\xi}(\theta_0, \boldsymbol{I}) - \frac{1}{\omega(\boldsymbol{I})} \int_{\theta_0}^{\theta} [\boldsymbol{\zeta}(\theta', \boldsymbol{I}) - \bar{\boldsymbol{\zeta}}(\boldsymbol{I})] d\theta', \tag{4.12}$$

$$\bar{\boldsymbol{\zeta}}(\boldsymbol{I}) := \frac{1}{2\pi} \int_0^{2\pi} \boldsymbol{\zeta}(\theta, \boldsymbol{I}) d\theta = \frac{d\omega(\boldsymbol{I})}{d\boldsymbol{I}}, \tag{4.13}$$

where $\frac{\partial \boldsymbol{X}_0(\theta, \boldsymbol{I})}{\partial \boldsymbol{I}} \in \mathbb{R}^{n \times m}$ is a matrix whose (i, j)-th element is given by $\frac{\partial X_{0,i}(\theta, \boldsymbol{I})}{\partial I_j}$, $\theta_0 \in [0, 2\pi)$ is a constant, and $\bar{\boldsymbol{\zeta}}(\boldsymbol{I})$ is the average of $\boldsymbol{\xi}(\theta, \boldsymbol{I})$ with respect to θ over one period of oscillation. From mathematical models of limit-cycle oscillators, $\boldsymbol{Z}(\theta, \boldsymbol{I})$ can be obtained numerically by the adjoint method for each $\boldsymbol{I}$ [5, 69], and then $\boldsymbol{\zeta}(\theta, \boldsymbol{I})$ and $\boldsymbol{\xi}(\theta, \boldsymbol{I})$ can be computed from $\boldsymbol{\zeta}(\theta, \boldsymbol{I}) = \boldsymbol{G}^\top(\boldsymbol{X}_0(\theta, \boldsymbol{I}), \boldsymbol{I}) \boldsymbol{Z}(\theta, \boldsymbol{I})$ and Eqs. (4.11) and (4.12). Experimentally, $\boldsymbol{Z}(\theta, \boldsymbol{I})$ and $\boldsymbol{\zeta}(\theta, \boldsymbol{I})$ can be measured by applying small impulsive perturbations to $\boldsymbol{I}$, while $\boldsymbol{\xi}(\theta, \boldsymbol{I})$ can be obtained by applying small stepwise perturbations to $\boldsymbol{I}$.

To test the validity of the generalized phase equation (4.8), we introduce an analytically tractable model, a modified Stuart-Landau (MSL) oscillator The modified Stuart-Landau oscillator has a two-dimensional state variable $\boldsymbol{X}(t) = [x(t), y(t)]^\top$ and a vector field

$$\boldsymbol{F}(\boldsymbol{X}, \boldsymbol{I}) = \begin{pmatrix} e^{2I}(x - y - I) - ((x - I)^2 + y^2)(x - I) \\ e^{2I}(x + y - I) - ((x - I)^2 + y^2) y \end{pmatrix}, \tag{4.14}$$

with $\Theta(\boldsymbol{X}, I) = \tan^{-1}[y/(x - I)]$, $\omega(I) = e^{2I}$, $\boldsymbol{X}_0(\theta, I) = [I + e^I \cos\theta,\ e^I \sin\theta]^\top$, $\xi(\theta, I) = e^{-I} \sin\theta$, and $\zeta(\theta, I) = 2e^{2I} - e^I \cos\theta$ (see Fig. 4.1 for details). We numerically predict the phase $\theta(t)$ of a strongly perturbed MSL oscillator by both conventional and generalized phase equations,

and compare them with direct numerical simulations of the original system. In applying the conventional phase reduction, we set $q_c = \langle I(t)\rangle_t$, where $\langle\cdot\rangle_t$ denotes the time average. In Fig. 4.2, we can confirm that the generalized phase equation (4.8) accurately predicts the generalized phase $\Theta(\boldsymbol{X}(t), q(\epsilon t))$ of the original system, while the conventional phase equation does not well predict the conventional phase $\Theta(\boldsymbol{X}(t), q_c)$ because of large variations in $I(t)$.

4.5 Analysis of Phase Locking

As an application of the generalized phase equation (4.8), we analyze $k : l$ *phase locking* [76] of the system (A.12) to a periodically varying parameter $\boldsymbol{I}(t)$ with period T_I and frequency ω_I, in which the frequency tuning ($l\langle\dot{\theta}\rangle_t = k\omega_I$) occurs. Although the averaging approximation [77] for the phase difference $\tilde{\psi}(t) = l\theta(t) - k\omega_I$ is generally used to analyze the phase locking [2, 76], we cannot directly apply it in the present case because the frequency $\omega(\boldsymbol{q}(\epsilon t))$ can vary largely with time. Thus, generalizing the conventional definition, we introduce the phase difference as

$$\psi(t) = l\theta(t) - k\omega_I t - lh(t) \tag{4.15}$$

with an additional term $-lh(t)$ to remove the large periodic variations in $\psi(t)$ due to $\omega(\boldsymbol{q}(\epsilon t))$, where $h(t)$ is a T_I-periodic function defined as

$$h(t) = \int_0^t [\omega(\boldsymbol{q}(\epsilon t')) - T_I^{-1}\int_0^{T_I} \omega(\boldsymbol{q}(\epsilon t))dt]dt'. \tag{4.16}$$

By virtue of this term, temporal variations in $\dot{\psi}$ remain of the order $O(\epsilon, \sigma)$, i.e., $|\dot{\psi}| \ll 1$, which enables us to apply the averaging approximation to ψ.

Introducing a small parameter ν representing the magnitude of variations in ψ, one can derive a dynamical equation for ψ as

$$\dot{\psi}(t) \quad = \nu f(\psi, t), \tag{4.17}$$

where $\nu f(\psi, t) = lg(\psi/l + k\omega_I t/l + h(t), t) - k\omega_I - l\dot{h}(t)$ and $g(\theta, t)$ denotes the right-hand side of Eq. (4.8). Using first- and second-order averaging [77], we can introduce slightly deformed phase differences $\psi_{1,2}$ satisfying $\psi_{1,2}(t) = \psi(t) + O(\nu)$ and obtain the first- and second-order averaged equations,

$$\dot{\psi}_1(t) = \nu\bar{f}_1(\psi_1) + O(\nu^2), \tag{4.18}$$

$$\dot{\psi}_2(t) = \nu\bar{f}_1(\psi_2) + \nu^2\bar{f}_2(\psi_2) + O(\nu^3), \tag{4.19}$$

where $\bar{f}_1(\psi)$ and $\bar{f}_2(\psi)$ are given by

$$\bar{f}_1(\psi) = \frac{1}{lT_I}\int_0^{lT_I} f(\psi, t)dt, \tag{4.20}$$

$$\bar{f}_2(\psi) = \frac{1}{lT_I}\int_0^{lT_I} \left[\frac{\partial f(\psi, t)}{\partial \psi}u(\psi, t) - \bar{f}_1(\psi)\frac{\partial u(\psi, t)}{\partial \psi}\right] dt, \tag{4.21}$$

$$u(\psi, t) = \int_0^t [f(\psi, t') - \bar{f}_1(\psi)]dt'. \tag{4.22}$$

These averaged equations can be considered autonomous by neglecting the $O(\nu^2)$ and $O(\nu^3)$ terms, respectively. Averaged equations for the conventional phase equation can be derived similarly. Thus, if the averaged equation has a stable fixed point, $k : l$ phase locking is expected to occur. As demonstrated below, the first-order averaging of the generalized phase equation already predicts qualitative features of the phase-locking dynamics, while the second-order averaging gives more precise results when the parameter $\boldsymbol{I}(t)$ varies significantly.

As an example, we use the MSL oscillator and investigate their phase locking to periodic forcing. Figures A.1 and A.2 shows the results of the numerical simulations. We apply four types of periodically varying parameters and predict if the oscillator exhibits either $1 : 1$ or $1 : 2$ phase locking to the periodically varying parameter $q(\epsilon t)$ (small fluctuation $\sigma p(t)$ is also added for completeness). We derive averaged equations for the phase differences $\psi_{1,2}$ using the proposed and conventional methods, and compare the results with direct numerical simulations of the MSL oscillator. We find that our new method correctly predicts the stable phase-locking point already at first-order averaging, while the conventional method does not. In particular, the conventional method can fail to predict whether phase locking takes place or not, as shown in Figs. A.2 (g) and (h), even after the second-order averaging. In this case, the exponential dependence of the frequency $\omega(I)$ on the parameter I is the main cause of the breakdown of the conventional method (see Sec. A.6 for a discussion). Typical trajectories of $[x(t), y(t), q(\epsilon t)]^\top$ are plotted on the cylinder C of limit cycles in the extended phase space $[x, y, I]^\top$, which shows that the oscillator state migrates over C synchronously with the periodic forcing. The trajectories are closed when phase locking occurs.

4.6 Summary and Discussions

In summary, we proposed a generalized phase reduction method that enables us to theoretically explore a broader class of strongly perturbed limit-cycle oscillators. Although still limited to slowly varying perturbations with weak fluctuations, our method avoids the assumption of weak perturbations, which has been a major obstacle in applying the conventional phase reduction method to real-world phenomena. It will therefore facilitate further theoretical investigations of nontrivial synchronization phenomena of strongly perturbed limit-cycle oscillators [40, 41]. As a

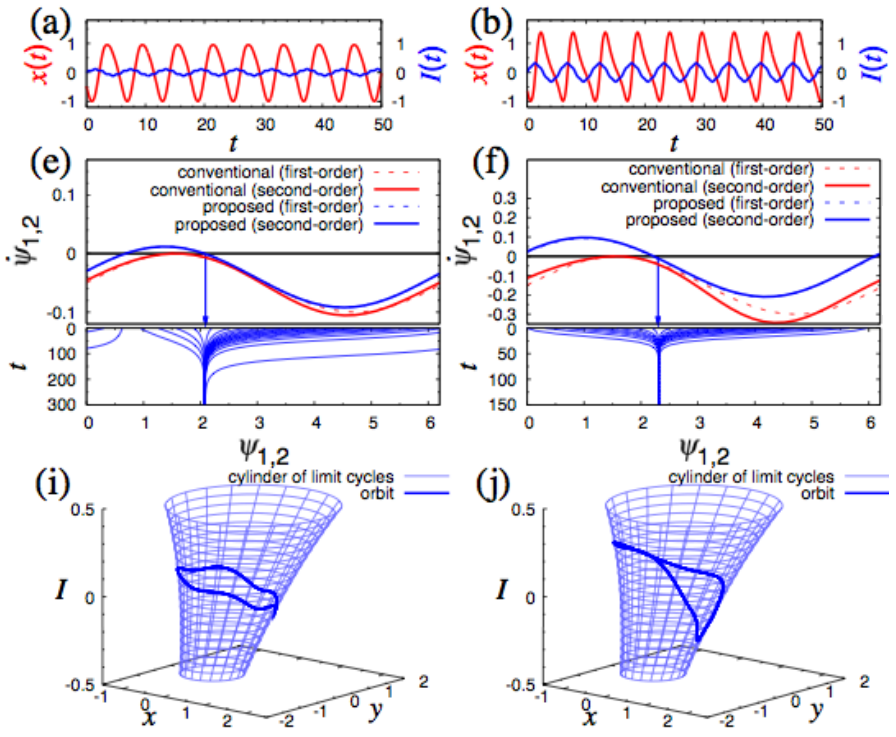

Figure 4.3: Phase locking of the modified Stuart-Landau oscillator. Four types of periodically varying parameters $I^{(j)}$ $(j = 3, 4)$ are applied, which lead to $1:1$ phase locking to $I^{(3)}(t)$ [(a), (e), and (i)] and $1:1$ phase locking to $I^{(4)}(t)$ [(b), (f), and (j)]. (a), (b) Time series of the state variable $x(t)$ of a periodically driven oscillator (red) and periodic external forcing (blue). (e), (f) Dynamics of the phase difference $\psi_{1,2}$ with an arrow representing a stable fixed point (top panel) and time series of $\psi_{1,2}$ with 20 different initial states (bottom panel). (i), (j) Orbits of a periodically driven oscillator (blue) on the cylinder of the limit cycles (light blue) plotted in the extended phase space. The parameter $I^{(j)}(t)$ is given by $I^{(j)}(t) = q^{(j)}(\epsilon t) + \sigma p^{(j)}(t)$, $q^{(j)}(\epsilon t) = \alpha^{(j)} \sin(\omega_I^{(j)} t)$ and $\sigma p^{(j)}(t) = 0.02 \sin(5\omega_I^{(j)} t)$ with $\alpha^{(3,4)} = 0.1$, 0.3, and $\omega_I^{(3,4)} = 1.05$, 1.10.

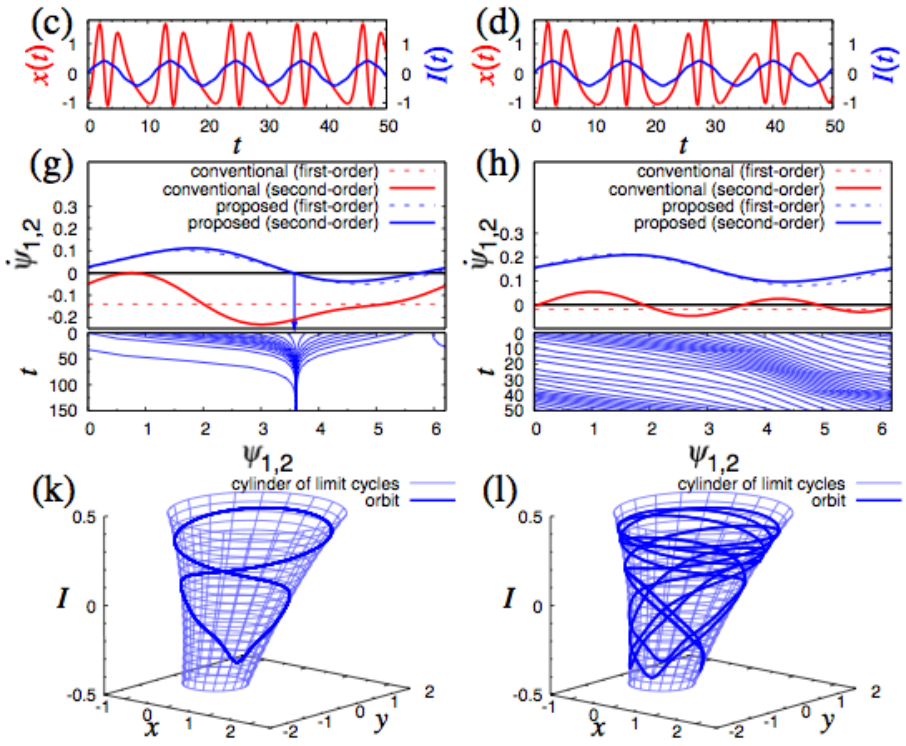

Figure 4.4: Phase locking of the modified Stuart-Landau oscillator. Four types of periodically varying parameters $I^{(j)}$ $(j = 5, 6)$ are applied, which lead to $1 : 2$ phase locking to $I^{(5)}(t)$ [(c), (g), and (k)] and and failure of phase locking to $I^{(6)}(t)$ [(d), (h), and (l)]. (c), (d) Time series of the state variable $x(t)$ of a periodically driven oscillator (red) and periodic external forcing (blue). (g), (h) Dynamics of the phase difference $\psi_{1,2}$ with an arrow representing a stable fixed point (top panel) and time series of $\psi_{1,2}$ with 20 different initial states (bottom panel). (k), (l) Orbits of a periodically driven oscillator (blue) on the cylinder of the limit cycles (light blue) plotted in the extended phase space. The parameter $I^{(j)}(t)$ is given by $I^{(j)}(t) = q^{(j)}(\epsilon t) + \sigma p^{(j)}(t)$, $q^{(j)}(\epsilon t) = \alpha^{(j)} \sin(\omega_I^{(j)} t)$ and $\sigma p^{(j)}(t) = 0.02 \sin(5\omega_I^{(j)} t)$ with $\alpha^{(5,6)} = 0.4$, 0.4, and $\omega_I^{(5,6)} = 0.57$, 0.51.

final remark, we point out that a phase equation similar to Eq. (4.8) has been postulated in a completely different context, to analyze the *geometric phase* in dissipative dynamical systems [78]. This formal similarity may provide an interesting possibility of understanding synchronization dynamics of strongly perturbed oscillators from a geometrical viewpoint.

Chapter 5

Conclusion

5.1 Summary of the Results

In Chapter 2, we proposed a quantitative theory for theoretically predicting the statistical properties of synchronization in an ensemble of uncoupled oscillators driven by common colored noise with an arbitrary power spectrum. In order to derive the probability density function of phase differences between two oscillators in the ensemble, we extended the white-noise approximation method for a single oscillator [42] into a two-oscillator system, so we can theoretically analyze stochastic dynamics of two uncoupled oscillators driven by common colored noise. This analytical result theoretically predicts various synchronized and clustered states induced by colored noise, which clearly showed find that these phenomena have a quite different synchronization mechanism from the case of white noise. We confirmed the validity of our theory through numerical simulations using the FitzHugh-Nagumo and Hodgkin-Huxley oscillators and common noise with various types of power spectrum.

In Chapter 3, we proposed a method for controlling synchronization patterns of limit-cycle oscillators by common noisy inputs, i.e., by utilizing noise-induced synchronization. We proposed a theoretical basis useful for optimizing noise-induced synchronization in practical applications, i.e., an optimization method for linear filters that process common noisy signals based on an objective function defined for each application. In this method, we can realize various synchronization patterns, including fully synchronized and clustered states, by using linear filters that generate appropriate common noisy signals from given noise. The optimal linear filter can be determined from the linear phase response property of the oscillators and the power spectrum of the given noise. The validity of the proposed method is confirmed by numerical simulations using the FitzHugh-Nagumo and Hodgkin-Huxley oscillators.

Chapter 4 proposed a generalized phase reduction method that is valid for strongly perturbed

limit-cycle oscillators. In order to derive the generalized phase equation, we introduced a generalized phase and conducted a perturbation approximation in two small parameters. The fundamental assumption of our method is that the perturbations to the oscillator $\boldsymbol{I}(t)$ can be decomposed into a large-amplitude component $\boldsymbol{q}(\epsilon t)$ varying slowly as compared to the amplitude relaxation time and remaining weak fluctuations $\sigma \boldsymbol{p}(t)$. Although the external forcing is still limited to a class of signals consisting of a slowly varying component and remaining weak fluctuations, the generalized phase reduction method considerably widens the applicability of theoretical synchronization analysis. We illustrated our method by analyzing the synchronization dynamics of limit-cycle oscillators driven by strong periodic signals. It was shown that the proposed method accurately predicts the synchronization properties of the oscillators, while the conventional method does not.

5.2 Future Works

This thesis extended the class of external forcing with which we can deal with in synchronization analysis. In particular, the extension of the phase reduction method to the case of strong forcing has great possibility of future works. In order to extend the theoretical methods for analyzing synchronization, we will be able to apply the generalized phase reduction to the following purposes:

1. A theoretical method for analyzing mutual synchronization via strong coupling between oscillators.

2. A theoretical method for analyzing the dynamics of oscillators driven by strong stochastic forcing, particularly, synchronization induced by strong common stochastic forcing.

In addition, as real-world applications of the generalized phase reduction, we will develop the following practical methods:

1. A system identification method for modeling an oscillatory system (e.g., neuron) from input-output data.

2. A system identification method for modeling a network system (e.g., neural network) composed by interacting oscillators from time series data.

3. A robust design method for oscillation circuits.

Acknowledgements

Over the past seven and a half years, I have received support and encouragement from a great number of individuals. Prof. H. Nakao is the supervisor of my doctoral thesis. Without his guidance, I could not have accomplished my works. He has taught me a way of life as an applied mathematician. I shall cherish his gift in the rest of my life. I am also grateful to Prof. K. Kimura, who has taught me the importance of probabilistic approaches and the spirit of educators. I appreciate Prof. J. Imura, Prof. K. Amaya, and Prof. T. Hayakawa for sincere reviews of my doctoral thesis and fruitful discussions. As collaborators of my supervisor, Prof. M. Hasegawa and Prof. K. Kotani provided me with fruitful discussions and instructions. Dr. S. Hata and Mr. S. Shirasaka helped me accomplish my works through kind encouragement and fruitful discussions.

I would like to give thanks to Prof. T. Ikeguchi, who is the supervisor of my master thesis. His guidance has taught me what a researcher should be and the importance and possibility of data science. I am also grateful to Prof. K. Fujiwara for kind encouragement and useful discussions. At the joint seminar on nonlinear problems, Prof. Y. Horio, Prof. M. Adachi, Prof. K. Jin'no, Prof. H. Kurokawa, Prof. A. Uchida, Prof. R. Hosaka, Prof. T. Kimura, Prof. T. Matsuura, Prof. H. Kato, Prof. Y. Shimada, Prof. K. Kuroda, and Prof. M. Kanno provided me with kind encouragement and instructions. I have no words to express my thanks to them.

Last but not least, I would like to give special thanks to my family and friends, who have supported me emotionally over the past seven and a half years.

Bibliography

[1] Winfree A. T., *The Geometry of Biological Time* (Springer, New York, 2001).

[2] Kuramoto Y., *Chemical Oscillations, Waves and Turbulence* (Dover, New York, 2003).

[3] Pikovsky A., Rosenblum M., and Kurths J., *Synchronization: A Universal Concept in Nonlinear Sciences* (Cambridge University Press, Cambridge, 2001).

[4] Hoppensteadt F. C. and Izhikevich E. M., *Weakly Connected Neural Networks* (Springer, New York, 1997).

[5] Ermentrout G. B. and Terman D. H., *Mathematical Foundations of Neuroscience* (Springer, New York, 2010).

[6] Nakao H., Yanagita T., and Kawamura Y., Phys Rev. X **4**, 021032 (2014).

[7] Kitahata H. et al., J. Phys. Chem. A **113**, 8164–8168 (2009).

[8] Aihara I., Phys. Rev. E **80**, 011918 (2009).

[9] Strogatz S. H. et al., Nature **438**, 43–44 (2005).

[10] Vytyaz I., Lee D. C., and Hanumolu P. K., *IEEE Trans. Circuits Syst.-I. Fundam. Theory Applicat.* **28**, 609–622, 2009.

[11] Maffezzoni P., Amore D. D., Daneshgar S., and Kennedy M. P., *IEEE Trans. Circuits Syst.-I. Fundam. Theory Applicat.* **57**, 2956–2966, 2010.

[12] Dasanayake I. and Li J.-S., *Phys. Rev. E*, **83**, 061916, 2011.

[13] Nabi A. and Moehlis J., *J. Math. Biol.*, **64**, 981–1004, 2012.

[14] Stankovski T., Duggento A., McClintock P. V. E., and Stefanovska A., *Phys. Rev. Lett.*, **109**, 024101, 2012.

[15] Demir A., Mehrotra A., and Roychowdhury J., *IEEE Trans. Circuits Syst.-I. Fundam. Theory Applicat.*, **47**, 655–674, 2000.

[16] Demir A., *IEEE Trans. Circuits Syst.-I. Fundam. Theory Applicat.*, **49**, 1782–1791, 2002.

[17] Demir A. and Roychowdhury J., *IEEE Trans. Comput.-Aided Des. Integer. Circuits Syst.*, **22**, 188–197, February 2003.

[18] Behera M., Kratyuk V., De S. K., Aluru N. R., and Mayaram K., *J. Microelectromech. Syst.*, **14**, 313–325, 2005.

[19] Demir A., *IEEE Trans. Circuits Syst.-I. Fundam. Theory Applicat.* **53**, 1869–1884, 2006.

[20] Teramae J.-N. and Tanaka D., Phys. Rev. Lett. **93**, 204103 (2004).

[21] Teramae J. and Tanaka D., Prog. Theor. Phys. **161**, 360 (2006).

[22] Goldobin D. S., Teramae J.-N., Nakao H. and Ermentrout G. B., Phys. Rev. Lett. **105**, 154101 (2010).

[23] Mainen Z. F. and Sejnowski T. J., Science **268**, 1503 (1995).

[24] Wang Y., Chik D. T. W. and Wang Z. D., Phys. Rev. E **61**, 740 (2000).

[25] Neiman A. B. and Russell D. F., Phys. Rev. Lett. **88**, 138103 (2002).

[26] Pakdaman K. and Mestivier D., Physica D **192**, 123 (2004).

[27] Galán R. F., Fourcaud-Trocmé N., Ermentrout G. B. and Urban N. N., J. Neurosci. **26**, 3646 (2006).

[28] Ermentrout G. B., Galán R. F., and Urban N. N., Trends in Neurosci. **31**, 428 (2008).

[29] Yoshida K., Sato K. and Sugamata A., J. Sound Vib. **290**, 34 (2006).

[30] Utagawa A., Asai T., Hirose T. and Amemiya Y., IEICE Trans. Fundam. **91**, 2475 (2008).

[31] Zhou T., Chen L. and Aihara K., Phys. Rev. Lett. **95**, 178103 (2005).

[32] Uchida A., McAllister R. and Roy R., Phys. Rev. Lett. **93**, 244102 (2004).

[33] Toral R., Mirasso C. R., Hernández-García E. and Piro O., Chaos **11**, 665 (2001).

[34] Zhou C. and Kurths J., Phys. Rev. Lett. **88**, 230602 (2002).

[35] Wang Y., Lai Y.-C., and Zheng Z., Phys. Rev. E **79**, 056210 (2009).

[36] Nakao H., Arai K. and Kawamura Y., Phys. Rev. Lett. **98**, 184101 (2007).

[37] Câteau H. and Reyes A. D., Phys. Rev. Lett. **96**, 058101 (2006).

[38] Fellous J. M., Houweling A. R., Modi R. H., Rao R. P. N., Tiesinga P. H. E. and Sejnowski T. J., J. Neurophysiol. **85**, 1782 (2001).

[39] Garcia-Ojalvo J., Elowitz M. B., and Strogatz S. H., Proc. Natl. Acad. Sci. USA **101**, 10955–10960 (2004); De Monte S., and d'Ovidio F., Danø S., and Sørensen P. G., Proc. Natl. Acad. Sci. **104**, 18377–18381 (2007); Taylor A. F., Tinsley M. R., Wang F., Huang Z., and Showalter K., Science **323**, 614–617 (2009); Danino T., Mondragón-Palomino O., Tsimring L., and Hasty J., Nature **463**, 326–330 (2010).

[40] Aronson D. G., Ermentrout G. B., and Kopell N., Physica D **41**, 403–449 (1990); Mirollo R. E. and Strogatz S. H., J. Stat. Phys. **50**, 245–262 (1990); Hansel D., Mato G., and Meunier C., Neural Comput. **7**, 307–337 (1995); Kiss I. Z., Wang W., and Hudson J. L., J. Phys. Chem. B **103**, 11433–11444 (1999); Bressloff P. C. and Coombes S., Neural Computation **12**, 91–129 (2000); Zhai Y., Kiss I. Z., and Hudson J. L., Phys. Rev. E **69**, 026208 (2004).

[41] Hakim V. and Rappel W. J., Physical Review A **46**, 7347-7350 (1992); Nakagawa N. and Kuramoto Y., Prog. Theor. Phys. **89**, 313-323 (1993); Nakao H. and Mikhailov A. S., Phys. Rev. E **79**, 036214 (2009).

[42] Nakao H., Teramae J.-N., Goldobin D. S. and Kuramoto Y., Chaos **20**, 3126 (2010).

[43] Satake A. and Iwasa Y., J. Ecol. **90**, 830–838 (2002).

[44] Lyles D., Rosenstock T. S., Hastings A., and Brown P. H., J. Theor. Biol. **259**, 701–713 (2009).

[45] Yasuda H. and Hasegawa M., IEICE Trans. Commun. **96**, 2749 (2013).

[46] Yoshimura K., Davis P. and Uchida A., Prog. Theor. Phys. **120**, 621 (2008).

[47] Nagai K. H. and Kori H., Phys. Rev. E **81**, 065202 (2010).

[48] Nakao H., Arai K., Nagai K., Tsubo Y. and Kuramoto Y., Physical Review E **72**, 26220 (2005).

[49] Yoshimura K., Valiusaityte I. and Davis P., Phys. Rev. E **75**, 026208 (2007).

[50] Hata S., Shimokawa T., Arai K. and Nakao H., Phys. Rev. E **82**, 036206 (2010).

[51] Risken H., *The Fokker-Planck Equation: Methods of Solution and Applications* (Springer Verlag, 1996).

[52] FitzHugh R., Biophys. J. **1**, 445 (1961).

[53] Nagumo J., Arimoto S. and Yoshizawa S., Proc. IRE **50**, 2061 (1962).

[54] Hodgkin A. and Huxley A., J. Physiol. **117**, 500 (1952).

[55] Lorenz E. N., J. Atmos. Sci. **20**, 130 (1963).

[56] Goldobin D. S. and Pikovsky A., Physica A **351**, 126 (2005).

[57] Goldobin D. S. and Pikovsky A., Phys. Rev. E **71**, 26220 (2005).

[58] Marella S. and Ermentrout G. B., Phys. Rev. E **77**, 041918 (2008).

[59] Kurebayashi W., Fujiwara K. and Ikeguchi T., Europhys. Lett. **97**, 50009 (2012).

[60] Burton S. D., Ermentrout G. B., and Urban N. N., J. Neurophysiol. **108**, 2115 (2012).

[61] Lai Y. M. and Porter M. A., Phys. Rev. E **88**, 012905 (2013).

[62] Zhou P., Burton S. D., Urban N. N., and Ermentrout G. B., Front. Comput. Neurosci. **113**, doi: 10.3389/fncom.2013.00113 (2013).

[63] Kawamura Y. and Nakao H., Phys. Rev. E **89**, 012912 (2014).

[64] Abouzeid A. and Ermentrout G. B., Phys. Rev. E **80**, 011911 (2009).

[65] Hata S., Arai K., Galán R. F. and Nakao H., Phys. Rev. E **84**, 016229 (2011).

[66] Yoshimura Y. and Arai K., Phys. Rev. Lett. **101**, 154101 (2008).

[67] Teramae J.-N., Nakao H. and Ermentrout G. B., Phys. Rev. Lett. **102**, 194102 (2009).

[68] Jackson L. B., *Digital Filters and Signal Processing* (Kluwer Academic Publishers, Norwell, 1996).

[69] Brown E., Moehlis J., and Holmes P., Neural Comput. **16**, 673–715 (2004).

[70] Wiesenfeld K., Bracikowski C., James G., and Roy R., Phys. Rev. Lett. **65**, 1749–1752 (1990); Strogatz S. H., Abrams D. M., McRobie A., Eckhardt B., and Ott E., Nature **438**, 43–44 (2005); Kiss I. Z., Rusin C. G., Kori H., and Hudson J. L., Science **316**, 1886–1889 (2007).

[71] Yoshimura K. and Arai K., Phys. Rev. Lett. **101**, 154101 (2008); Teramae J.-N., Nakao H., and Ermentrout G. B., Phys. Rev. Lett. **102**, 194102 (2009); Goldobin D. S., Teramae J.-N., Nakao H., and Ermentrout G. B., Phys. Rev. Lett. **105**, 154101 (2010).

[72] Novicẽnko V. and Pyragas K., Physica D **241**, 1090–1098 (2012); Kotani K., Yamaguchi I., Ogawa Y., Jimbo Y., Nakao H., Ermentrout G. B., Phys. Rev. Lett. **109**, 044101 (2012).

[73] Kawamura Y., Nakao H., Arai K., Kori H., and Kuramoto Y., Phys. Rev. Lett. **101**, 024101 (2008); Kawamura Y., Nakao H., and Kuramoto Y., Phys. Rev. E **84**, 046211 (2011).

[74] Izhikevich E. M., SIAM J. App. Math. **60**, 1789–1804 (2000).

[75] Keener J. P., *Principles of Applied Mathematics: Transformation and Approximation* (Addison Wesley, Boston, 1988).

[76] Ermentrout G. B., J. Math. Biol. **12**, 327–342 (1981).

[77] Sanders J. A. and Verhulst F., *Averaging Methods in Nonlinear Dynamical Systems* (Springer-Verlag, New York, 1985).

[78] Kepler T. B. and Kagan M. L., Phys. Rev. Lett. **66**, 847–849 (1991).

Chapter

Appendices

A.1 Derivations of Eqs. (2.18) and (2.19)

Substituting $\dot{\phi}^{(j)}_{D,1} = \boldsymbol{Z}_G(\phi^{(j)}_0(t)) \cdot \boldsymbol{\xi}(t)$ and $\dot{\phi}^{(j)}_{\epsilon,1} = \boldsymbol{Z}_H(\phi^{(1)}_0(t)) \cdot \boldsymbol{\eta}^{(1)}(t)$ into Eq. (2.17), we obtain

$$\begin{aligned} d_{11} &= D\int_{-\infty}^{+\infty} d\tau \big\langle [\boldsymbol{Z}_G(\phi^{(1)}_0(t))^\top \boldsymbol{\xi}(t)][\boldsymbol{Z}_G(\phi^{(1)}_0(t-\tau))^\top \boldsymbol{\xi}(t-\tau)] \big\rangle \\ &\quad + \epsilon \int_{-\infty}^{+\infty} d\tau \big\langle [\boldsymbol{Z}_H(\phi^{(1)}_0(t))^\top \boldsymbol{\eta}^{(1)}(t)][\boldsymbol{Z}_H(\phi^{(1)}_0(t-\tau))^\top \boldsymbol{\eta}^{(1)}(t-\tau)] \big\rangle \\ &\quad + O(D^{\frac{3}{2}}, \epsilon^{\frac{3}{2}}) \qquad \text{(A.1)} \\ &= D\int_{-\infty}^{+\infty} d\tau \big\langle \boldsymbol{Z}_G(\phi^{(1)}_0(t))^\top \boldsymbol{\xi}(t)\boldsymbol{\xi}(t-\tau)^\top \boldsymbol{Z}_G(\phi^{(1)}_0(t-\tau)) \big\rangle \\ &\quad + \epsilon \int_{-\infty}^{+\infty} d\tau \big\langle \boldsymbol{Z}_H(\phi^{(1)}_0(t))^\top \boldsymbol{\eta}^{(1)}(t)\boldsymbol{\eta}^{(1)}(t-\tau)^\top \boldsymbol{Z}_H(\phi^{(1)}_0(t-\tau)) \big\rangle \\ &\quad + O(D^{\frac{3}{2}}, \epsilon^{\frac{3}{2}}). \qquad \text{(A.2)} \end{aligned}$$

We rewrite $\boldsymbol{Z}_G(\phi)$, $\boldsymbol{Z}_H(\phi)$, $\boldsymbol{\xi}(t)$ and $\boldsymbol{\eta}^{(1)}(t)$ by using their elements and obtain

$$\begin{aligned} d_{11} &= D\int_{-\infty}^{+\infty} d\tau \sum_{k=1}^{m}\sum_{l=1}^{m} \big\langle Z_{H,k}(\phi^{(1)}_0(t))\xi_k(t)\xi_l(t-\tau)Z_{H,l}(\phi^{(1)}_0(t-\tau)) \big\rangle \\ &\quad + \epsilon \int_{-\infty}^{+\infty} d\tau \sum_{k=1}^{m}\sum_{l=1}^{m} \big\langle Z_{H,k}(\phi^{(1)}_0(t))\eta^{(1)}_k(t)\eta^{(1)}_l(t-\tau)Z_{H,l}(\phi^{(1)}_0(t-\tau)) \big\rangle \\ &\quad + O(D^{\frac{3}{2}}, \epsilon^{\frac{3}{2}}), \qquad \text{(A.3)} \end{aligned}$$

where $Z_{G,l}(\phi)$ and $Z_{H,l}(\phi)$ are the lth elements of $\boldsymbol{Z}_G(\phi)$ and $\boldsymbol{Z}_H(\phi)$, and $\xi_l(t)$ and $\eta^{(1)}_l(t)$ are the lth elements of $\boldsymbol{\xi}(t)$ and $\boldsymbol{\eta}^{(1)}(t)$.

We assume that the phase variable $\phi^{(1)}$ and the drive noises $\boldsymbol{\xi}(t)$ and $\boldsymbol{\eta}^{(1)}(t)$ are approximately independent. Under this assumption, the temporal average $\langle\cdot\rangle$ can be divided into two parts; $\langle\cdot\rangle_\phi$ ($:= (2\pi)^{-1}\int_{-\pi}^{+\pi} d\phi\,\cdot$) and $\langle\cdot\rangle_t$ ($:= \lim_{s\to\infty}(2s)^{-1}\int_{-s}^{+s} dt\,\cdot$). Thus, we obtain

$$\begin{aligned}
d_{11} &= D\int_{-\infty}^{+\infty} d\tau \sum_{k=1}^{m}\sum_{l=1}^{m} \big\langle Z_{G,k}(\phi_0^{(1)}(t)) Z_{G,l}(\phi_0^{(1)}(t-\tau))\big\rangle_\phi \big\langle \xi_k(t)\xi_l(t-\tau)\big\rangle_t \\
&\quad +\epsilon\int_{-\infty}^{+\infty} d\tau \sum_{k=1}^{m}\sum_{l=1}^{m} \big\langle Z_{H,k}(\phi_0^{(1)}(t)) Z_{H,l}(\phi_0^{(1)}(t-\tau))\big\rangle_\phi \big\langle \eta_k^{(1)}(t)\eta_l^{(1)}(t-\tau)\big\rangle_t \\
&\quad +O(D^{\frac{3}{2}},\epsilon^{\frac{3}{2}}) \\
&= \frac{D}{2\pi}\int_{-\infty}^{+\infty} d\tau \int_{-\pi}^{+\pi} d\phi \sum_{k=1}^{m}\sum_{l=1}^{m} Z_{G,k}(\phi) Z_{G,l}(\phi-\omega\tau) C_{\xi,kl}(\tau) \\
&\quad +\frac{\epsilon}{2\pi}\int_{-\infty}^{+\infty} d\tau \int_{-\pi}^{+\pi} d\phi \sum_{k=1}^{m}\sum_{l=1}^{m} Z_{H,k}(\phi) Z_{H,l}(\phi-\omega\tau) C_{\eta,kl}(\tau) \\
&\quad +O(D^{\frac{3}{2}},\epsilon^{\frac{3}{2}}),
\end{aligned} \tag{A.4}$$

where $C_{\xi,kl}$ and $C_{\eta,kl}$ are the (k,l)th elements of $\boldsymbol{C}_\xi(\phi)$ and $\boldsymbol{C}_\eta(\phi)$. Finally, we rewrite Eq. (A.4) by using $\boldsymbol{Z}_G(\phi)$, $\boldsymbol{Z}_H(\phi)$, $\boldsymbol{C}_\xi(\tau)$ and $\boldsymbol{C}_\eta(\tau)$ and obtain

$$\begin{aligned}
d_{11} &= \frac{D}{2\pi}\int_{-\infty}^{+\infty} d\tau \int_{-\pi}^{+\pi} d\phi \boldsymbol{Z}_G(\phi)^\top \boldsymbol{C}_\xi(\tau) \boldsymbol{Z}_G(\phi-\omega\tau) \\
&\quad +\frac{\epsilon}{2\pi}\int_{-\infty}^{+\infty} d\tau \int_{-\pi}^{+\pi} d\phi \boldsymbol{Z}_H(\phi)^\top \boldsymbol{C}_\eta(\tau) \boldsymbol{Z}_H(\phi-\omega\tau) \\
&\quad +O(D^{\frac{3}{2}},\epsilon^{\frac{3}{2}}).
\end{aligned} \tag{A.5}$$

In the same way, one can calculate d_{12} as follows. We use the fact that $\langle \phi_{\epsilon,1}^{(1)}(t)\phi_{\epsilon,1}^{(2)}(t-\tau)\rangle = 0$ and eliminate the phase variable of the second oscillator $\phi_0^{(2)}$ by substituting $\phi_0^{(2)} = \phi_0^{(1)} - \theta$ into $\phi_0^{(2)}$, and then, we obtain

$$\begin{aligned}
d_{12} &= D\int_{-\infty}^{+\infty} d\tau \big\langle [\boldsymbol{Z}_G(\phi_0^{(1)}(t))^\top \boldsymbol{\xi}(t)][\boldsymbol{Z}_G(\phi_0^{(2)}(t-\tau))^\top \boldsymbol{\xi}(t-\tau)]\big\rangle \\
&\quad +O(D^{\frac{3}{2}},\epsilon^{\frac{3}{2}}) \\
&= D\int_{-\infty}^{+\infty} d\tau \big\langle \boldsymbol{Z}_G(\phi_0^{(1)}(t))^\top \boldsymbol{\xi}(t)\boldsymbol{\xi}(t-\tau)^\top \boldsymbol{Z}_G(\phi_0^{(2)}(t-\tau))\big\rangle \\
&\quad +O(D^{\frac{3}{2}},\epsilon^{\frac{3}{2}}) \\
&= \frac{D}{2\pi}\int_{-\infty}^{+\infty} d\tau \int_{-\pi}^{+\pi} d\phi \boldsymbol{Z}_G(\phi)^\top \boldsymbol{C}_\xi(\tau) \boldsymbol{Z}_G(\phi-\theta-\omega\tau) \\
&\quad +O(D^{\frac{3}{2}},\epsilon^{\frac{3}{2}}).
\end{aligned} \tag{A.6}$$

A.2 Derivation of Eq. (2.28)

From Eq. (2.21), one can calculate the Fourier coefficient g_l as follows. We introduce a new variable χ ($:= \phi - \theta - \omega\tau$) and use the fact that $\boldsymbol{P}_\xi(\Omega)$ is a Hermitian matrix. Then, we obtain

$$\begin{aligned} g_l &= \frac{1}{2\pi}\int_{-\pi}^{+\pi} d\theta g(\theta) e^{-il\theta} \\ &= \frac{1}{2\pi}\int_{-\pi}^{+\pi} d\theta \frac{1}{2\pi}\int_{-\infty}^{+\infty} d\tau \int_{-\pi}^{+\pi} d\phi \boldsymbol{Z}_G(\phi)^\top \boldsymbol{C}_\xi(\tau)\boldsymbol{Z}_G(\phi-\theta-\omega\tau)e^{-il\theta} \\ &= \left(\frac{1}{2\pi}\int_{-\pi}^{+\pi} d\phi \boldsymbol{Z}_G(\phi)^\top e^{-il\phi}\right)\left(\int_{-\infty}^{+\infty} d\tau \boldsymbol{C}_\xi(\tau)e^{il\omega\tau}\right)\left(\frac{1}{2\pi}\int_{-\pi}^{+\pi} d\chi \boldsymbol{Z}_G(\chi)e^{il\chi}\right) \\ &= \boldsymbol{Y}_{G,l}^\top \overline{\boldsymbol{P}_\xi(l\omega)}\,\overline{\boldsymbol{Y}_{G,l}} = \boldsymbol{Y}_{G,l}^\dagger \boldsymbol{P}_\xi(l\omega)^\dagger \boldsymbol{Y}_{G,l} \\ &= \boldsymbol{Y}_{G,l}^\dagger \boldsymbol{P}_\xi(l\omega)\boldsymbol{Y}_{G,l}, \end{aligned} \tag{A.7}$$

where $\overline{\cdot}$ denotes the complex conjugate. From Eq. (2.22), h_l can be derived likewise.

A.3 Derivations of Correlation Functions

For the Stuart-Landau oscillator we used in the simulations, we can calculate the Fourier coefficients $\boldsymbol{Y}_{G,l}$ and $\boldsymbol{Y}_{H,l}$ as

$$\boldsymbol{Y}_{G,\pm1} = \boldsymbol{Y}_{H,\pm1} = \frac{1}{2}[1 \pm i, 1 \mp i]^\top, \tag{A.8}$$

$$\boldsymbol{Y}_{G,l} = \boldsymbol{Y}_{H,l} = \boldsymbol{0}\ (l \neq \pm 1). \tag{A.9}$$

Thus, from Eq. (2.28), the Fourier coefficient g_l is given by

$$g_{\pm1} = \boldsymbol{Y}_{G,\pm1}^\dagger \boldsymbol{Y}_{G,\pm1} P_{\mathrm{ex}}(\omega)|_{\gamma=1} = \frac{1}{2}\left[\frac{1}{1+(\omega_0+3)^2} + \frac{1}{1+(\omega_0-3)^2}\right], \tag{A.10}$$

and

$$g_l = 0 \quad (l \neq \pm 1) \tag{A.11}$$

where ω_0 is a parameter. In the same way, the Fourier coefficient h_l is given by $h_{\pm1} = \boldsymbol{Y}_{H,\pm l}^\dagger \boldsymbol{Y}_{H,\pm l} P_{\mathrm{ex}}(\omega)|_{\omega_0=0,\gamma=3} = \frac{1}{2}$ and $h_l = 0 \quad (l \neq \pm 1)$. Substituting g_l and h_l to Eq. (2.28), we can obtain the explicit forms of $g(\theta)$ and $h(\theta)$.

A.4 Derivation of the Generalized Phase Equation

In this section, we give a detailed derivation of the generalized phase equation (4.8) in the main article, which takes into account the effect of amplitude relaxation of the oscillator state to the

cylinder of limit cycles C. Our aim is to evaluate the order of error terms in the generalized phase equation (4.8). Our argument here is based on a formulation similar to Ref. [22] by Goldobin *et al.*, in which the effect of colored noise on limit-cycle oscillators is analyzed and an effective phase equation that accurately describes the oscillator state is derived by incorporating the effect of amplitude relaxation of the oscillator state to the unperturbed limit-cycle orbit.

As in the main article, we consider a limit-cycle oscillator whose dynamics depends on a time-varying parameter $\boldsymbol{I}(t)$ representing general perturbations, described by

$$\dot{\boldsymbol{X}}(t) = \boldsymbol{F}(\boldsymbol{X}(t), \boldsymbol{I}(t)). \tag{A.12}$$

For simplicity, we assume that the state variable $\boldsymbol{X}(t)$ is two-dimensional ($n = 2$), but the formulation can be straightforwardly extended to higher-dimensional cases.

Suppose that the parameter $\boldsymbol{I}$ is constant for the moment. As explained in the main article, we introduce an extended phase space $\mathbb{R}^n \times A$ and define a generalized phase θ and amplitude r as functions of $(\boldsymbol{X}, \boldsymbol{I})$ in U. Here, r gives the distance of the oscillator state $\boldsymbol{X}$ from the unperturbed stable limit cycle $\boldsymbol{X}_0(\theta, \boldsymbol{I})$. For each constant value of $\boldsymbol{I} \in A$, as argued in the Supplementary Information of Ref. [22], we can define a phase $\theta = \Theta(\boldsymbol{X}, \boldsymbol{I})$ and an amplitude $r = R(\boldsymbol{X}, \boldsymbol{I})$ such that

$$\frac{\partial \Theta(\boldsymbol{X}, \boldsymbol{I})}{\partial \boldsymbol{X}} \cdot \boldsymbol{F}(\boldsymbol{X}, \boldsymbol{I}) = \omega(\boldsymbol{I}), \tag{A.13}$$

$$\frac{\partial R(\boldsymbol{X}, \boldsymbol{I})}{\partial \boldsymbol{X}} \cdot \boldsymbol{F}(\boldsymbol{X}, \boldsymbol{I}) = -\lambda(\boldsymbol{I}) R(\boldsymbol{X}, \boldsymbol{I}), \tag{A.14}$$

where $\lambda(\boldsymbol{I})$ is the absolute value of the second Floquet exponent of Eq. (A.12) for each $\boldsymbol{I}$. We further assume that $\Theta(\boldsymbol{X}, \boldsymbol{I})$ and $R(\boldsymbol{X}, \boldsymbol{I})$ are continuously differentiable with respect to $\boldsymbol{X}$ and $\boldsymbol{I}$. Equations (A.13) and (A.14) guarantee that

$$\dot{\theta} = \omega(\boldsymbol{I}), \quad \dot{r} = -\lambda(\boldsymbol{I}) r \tag{A.15}$$

always hold for each $\boldsymbol{I}$. In the absence of perturbations, the amplitude $r = R(\boldsymbol{X}, \boldsymbol{I})$ decays to 0 exponentially, and the phase $\theta = \Theta(\boldsymbol{X}, \boldsymbol{I})$ increases constantly.

Now we suppose that the parameter $\boldsymbol{I}(t)$ can vary with time. As explained in the main article, we decompose the parameter $\boldsymbol{I}(t)$ into a slowly varying component $\boldsymbol{q}(\epsilon t)$ and remaining weak fluctuations $\sigma \boldsymbol{p}(t)$ as $\boldsymbol{I}(t) = \boldsymbol{q}(\epsilon t) + \sigma \boldsymbol{p}(t)$. We define a phase $\theta(t)$ and an amplitude $r(t)$ of the oscillator as follows:

$$\theta(t) = \Theta(\boldsymbol{X}(t), \boldsymbol{q}(\epsilon t)), \tag{A.16}$$

$$r(t) = R(\boldsymbol{X}(t), \boldsymbol{q}(\epsilon t)). \tag{A.17}$$

Since $\Theta(\boldsymbol{X}, \boldsymbol{I})$ and $R(\boldsymbol{X}, \boldsymbol{I})$ are continuously differentiable with respect to $\boldsymbol{X}$ and $\boldsymbol{I}$, we can derive

the dynamical equations for $\theta(t)$ and $r(t)$ as

$$\dot{\theta} = \left.\frac{\partial \Theta(\boldsymbol{X}, \boldsymbol{I})}{\partial \boldsymbol{X}}\right|_{(\boldsymbol{X}, \boldsymbol{q}(\epsilon t))} \cdot \frac{d\boldsymbol{X}(t)}{dt} + \left.\frac{\partial \Theta(\boldsymbol{X}, \boldsymbol{I})}{\partial \boldsymbol{I}}\right|_{(\boldsymbol{X}, \boldsymbol{q}(\epsilon t))} \cdot \frac{d\boldsymbol{q}(\epsilon t)}{dt}, \tag{A.18}$$

$$\dot{r} = \left.\frac{\partial R(\boldsymbol{X}, \boldsymbol{I})}{\partial \boldsymbol{X}}\right|_{(\boldsymbol{X}, \boldsymbol{q}(\epsilon t))} \cdot \frac{d\boldsymbol{X}(t)}{dt} + \left.\frac{\partial R(\boldsymbol{X}, \boldsymbol{I})}{\partial \boldsymbol{I}}\right|_{(\boldsymbol{X}, \boldsymbol{q}(\epsilon t))} \cdot \frac{d\boldsymbol{q}(\epsilon t)}{dt}. \tag{A.19}$$

Plugging $\boldsymbol{I}(t) = \boldsymbol{q}(\epsilon t) + \sigma \boldsymbol{p}(t)$ into Eq. (A.12) and expanding it to the first order in σ, we can derive

$$\dot{\boldsymbol{X}} = \boldsymbol{F}(\boldsymbol{X}, \boldsymbol{q}(\epsilon t)) + \sigma \boldsymbol{G}(\boldsymbol{X}, \boldsymbol{q}(\epsilon t)) \boldsymbol{p}(t) + O(\sigma^2), \tag{A.20}$$

where the matrix $\boldsymbol{G}$ is defined in the main article. Substituting Eqs. (A.13), (A.14), and (A.20) into Eqs. (A.18) and (A.19), we can obtain

$$\begin{aligned} \dot{\theta} = \omega(\boldsymbol{q}(\epsilon t)) &+ \sigma \left.\frac{\partial \Theta(\boldsymbol{X}, \boldsymbol{I})}{\partial \boldsymbol{X}}\right|_{(\boldsymbol{X}, \boldsymbol{q}(\epsilon t))} \cdot \boldsymbol{G}(\boldsymbol{X}, \boldsymbol{q}(\epsilon t)) \boldsymbol{p}(t) \\ &+ \epsilon \left.\frac{\partial \Theta(\boldsymbol{X}, \boldsymbol{I})}{\partial \boldsymbol{I}}\right|_{(\boldsymbol{X}, \boldsymbol{q}(\epsilon t))} \cdot \dot{\boldsymbol{q}}(\epsilon t) + O(\sigma^2), \end{aligned} \tag{A.21}$$

$$\begin{aligned} \dot{r} = -\lambda(\boldsymbol{q}(\epsilon t)) r &+ \sigma \left.\frac{\partial R(\boldsymbol{X}, \boldsymbol{I})}{\partial \boldsymbol{X}}\right|_{(\boldsymbol{X}, \boldsymbol{q}(\epsilon t))} \cdot \boldsymbol{G}(\boldsymbol{X}, \boldsymbol{q}(\epsilon t)) \boldsymbol{p}(t) \\ &+ \epsilon \left.\frac{\partial R(\boldsymbol{X}, \boldsymbol{I})}{\partial \boldsymbol{I}}\right|_{(\boldsymbol{X}, \boldsymbol{q}(\epsilon t))} \cdot \dot{\boldsymbol{q}}(\epsilon t) + O(\sigma^2), \end{aligned} \tag{A.22}$$

where $\dot{\boldsymbol{q}}(\epsilon t)$ denotes $d\boldsymbol{q}(\epsilon t)/d(\epsilon t)$. For simplicity of notation, we define $\boldsymbol{\zeta}_\theta(\theta, r, \boldsymbol{I}) \in \mathbb{R}^m$, $\boldsymbol{\zeta}_r(\theta, r, \boldsymbol{I}) \in \mathbb{R}^m$, $\boldsymbol{\xi}_\theta(\theta, r, \boldsymbol{I}) \in \mathbb{R}^m$ and $\boldsymbol{\xi}_r(\theta, r, \boldsymbol{I}) \in \mathbb{R}^m$, respectively, as

$$\boldsymbol{\zeta}_\theta(\theta, r, \boldsymbol{I}) = \boldsymbol{G}(\boldsymbol{X}, \boldsymbol{I})^\top \left.\frac{\partial \Theta(\boldsymbol{X}, \boldsymbol{I})}{\partial \boldsymbol{X}}\right|_{\boldsymbol{X} = \boldsymbol{X}(\theta, r, \boldsymbol{I})}, \tag{A.23}$$

$$\boldsymbol{\zeta}_r(\theta, r, \boldsymbol{I}) = \boldsymbol{G}(\boldsymbol{X}, \boldsymbol{I})^\top \left.\frac{\partial R(\boldsymbol{X}, \boldsymbol{I})}{\partial \boldsymbol{X}}\right|_{\boldsymbol{X} = \boldsymbol{X}(\theta, r, \boldsymbol{I})}, \tag{A.24}$$

$$\boldsymbol{\xi}_\theta(\theta, r, \boldsymbol{I}) = \left.\frac{\partial \Theta(\boldsymbol{X}, \boldsymbol{I})}{\partial \boldsymbol{I}}\right|_{\boldsymbol{X} = \boldsymbol{X}(\theta, r, \boldsymbol{I})}, \tag{A.25}$$

$$\boldsymbol{\xi}_r(\theta, r, \boldsymbol{I}) = \left.\frac{\partial R(\boldsymbol{X}, \boldsymbol{I})}{\partial \boldsymbol{I}}\right|_{\boldsymbol{X} = \boldsymbol{X}(\theta, r, \boldsymbol{I})}, \tag{A.26}$$

where $\boldsymbol{X}(\theta, r, \boldsymbol{I}) \in \mathbb{R}^2$ represents an oscillator state with $\theta = \Theta(\boldsymbol{X}, \boldsymbol{I})$, $r = R(\boldsymbol{X}, \boldsymbol{I})$, and parameter $\boldsymbol{I}$. Using Eqs. (A.23), (A.24), (A.25), and (A.26), we can rewrite Eqs. (A.21) and (A.22) as

$$\dot{\theta} = \omega(\boldsymbol{q}(\epsilon t)) + \sigma \boldsymbol{\zeta}_\theta(\theta, r, \boldsymbol{I}) \cdot \boldsymbol{p}(t) + \epsilon \boldsymbol{\xi}_\theta(\theta, r, \boldsymbol{I}) \cdot \dot{\boldsymbol{q}}(\epsilon t) + O(\sigma^2), \tag{A.27}$$

$$\dot{r} = -\lambda(\boldsymbol{q}(\epsilon t)) r + \sigma \boldsymbol{\zeta}_r(\theta, r, \boldsymbol{I}) \cdot \boldsymbol{p}(t) + \epsilon \boldsymbol{\xi}_r(\theta, r, \boldsymbol{I}) \cdot \dot{\boldsymbol{q}}(\epsilon t) + O(\sigma^2). \tag{A.28}$$

Note that $\boldsymbol{\zeta}_\theta(\theta, 0, \boldsymbol{I})$ and $\boldsymbol{\xi}_\theta(\theta, 0, \boldsymbol{I})$ are equivalent to the sensitivity functions $\boldsymbol{\zeta}(\theta, \boldsymbol{I})$ and $\boldsymbol{\xi}(\theta, \boldsymbol{I})$ defined in the main article. The functions $\boldsymbol{\zeta}_r(\theta, r, \boldsymbol{I})$ and $\boldsymbol{\xi}_r(\theta, r, \boldsymbol{I})$ represent sensitivities of the amplitude to the small fluctuations and to the slowly varying component of the applied perturbations, respectively. In the main article, we also assumed that $\boldsymbol{q}(\epsilon t)$ varies sufficiently slowly as compared to the relaxation time of perturbed orbits to C. By using the absolute value of the Floquet exponent $\lambda(\boldsymbol{I})$ and the slowly varying component $\boldsymbol{q}(\epsilon t)$, this assumption can be written as

$$\epsilon \ll \lambda(\boldsymbol{q}(\epsilon t)), \text{ or } \frac{\epsilon}{\lambda(\boldsymbol{q}(\epsilon t))} \ll 1. \tag{A.29}$$

Now, we show that the following relation between the sensitivity functions for the amplitude holds:

$$\boldsymbol{\xi}_r(\theta, 0, \boldsymbol{I}) = -\frac{1}{\omega(\boldsymbol{I})} \int_0^\infty e^{-\lambda(\boldsymbol{I})\phi/\omega(\boldsymbol{I})} \boldsymbol{\zeta}_r(\theta - \phi, 0, \boldsymbol{I}) d\phi \tag{A.30}$$

$$= -\frac{1}{\lambda(\boldsymbol{I})} \int_0^\infty e^{-s} \boldsymbol{\zeta}_r(\theta - \omega(\boldsymbol{I})s/\lambda(\boldsymbol{I}), 0, \boldsymbol{I}) ds, \tag{A.31}$$

where we defined $s = \lambda(\boldsymbol{I})\phi/\omega(\boldsymbol{I})$ in the second line. From Eq. (A.14),

$$\frac{\partial R(\boldsymbol{X}, \boldsymbol{I})}{\partial \boldsymbol{X}} \cdot \boldsymbol{F}(\boldsymbol{X}, \boldsymbol{I}) = -\lambda(\boldsymbol{I}) R(\boldsymbol{X}, \boldsymbol{I}) \tag{A.32}$$

holds. We differentiate Eq. (A.32) with respect to $\boldsymbol{I}$ and plug in $\boldsymbol{X} = \boldsymbol{X}_0(\theta, \boldsymbol{I})$. Then, from the left-hand side of Eq. (A.32), we obtain

$$\begin{aligned}
\frac{\partial}{\partial \boldsymbol{I}} \left[\frac{\partial R(\boldsymbol{X}, \boldsymbol{I})}{\partial \boldsymbol{X}} \cdot \boldsymbol{F}(\boldsymbol{X}, \boldsymbol{I}) \right] \Bigg|_{\boldsymbol{X}=\boldsymbol{X}_0(\theta,\boldsymbol{I})} &= \left[\frac{\partial}{\partial \boldsymbol{I}} \left(\frac{\partial R(\boldsymbol{X}, \boldsymbol{I})}{\partial \boldsymbol{X}} \right) \right]^\top \boldsymbol{F}(\boldsymbol{X}, \boldsymbol{I}) \Bigg|_{\boldsymbol{X}=\boldsymbol{X}_0(\theta,\boldsymbol{I})} \\
&\quad + \frac{\partial \boldsymbol{F}(\boldsymbol{X}, \boldsymbol{I})}{\partial \boldsymbol{I}}^\top \frac{\partial R(\boldsymbol{X}, \boldsymbol{I})}{\partial \boldsymbol{X}} \Bigg|_{\boldsymbol{X}=\boldsymbol{X}_0(\theta,\boldsymbol{I})} \\
&= \left[\frac{\partial}{\partial \boldsymbol{X}} \left(\frac{\partial R(\boldsymbol{X}, \boldsymbol{I})}{\partial \boldsymbol{I}} \right) \right] \boldsymbol{F}(\boldsymbol{X}, \boldsymbol{I}) \Bigg|_{\boldsymbol{X}=\boldsymbol{X}_0(\theta,\boldsymbol{I})} \\
&\quad + \boldsymbol{\zeta}_r(\theta, 0, \boldsymbol{I}),
\end{aligned} \tag{A.33}$$

where $\partial/\partial \boldsymbol{I}$ denotes a differential operator defined as $(\partial/\partial \boldsymbol{I}) f(\boldsymbol{I}) = [\partial f(\boldsymbol{I})/\partial I_1, \ldots, \partial f(\boldsymbol{I})/\partial I_m]^\top \in \mathbb{R}^m$ for a scalar function $f(\boldsymbol{I})$, $\frac{\partial}{\partial \boldsymbol{I}}(\frac{\partial R(\boldsymbol{X},\boldsymbol{I})}{\partial \boldsymbol{X}})$ is a matrix whose (i,j)-th element is given by $\frac{\partial^2 R(\boldsymbol{X},\boldsymbol{I})}{\partial X_i \partial I_j}$, and $\frac{\partial}{\partial \boldsymbol{X}}(\frac{\partial R(\boldsymbol{X},\boldsymbol{I})}{\partial \boldsymbol{I}})$ is the transpose of $\frac{\partial}{\partial \boldsymbol{I}}(\frac{\partial R(\boldsymbol{X},\boldsymbol{I})}{\partial \boldsymbol{X}})$. Here, the first term of the right-hand

side of Eq. (A.33) can be written as

$$\begin{aligned}
&\left[\frac{\partial}{\partial \boldsymbol{X}}\left(\frac{\partial R(\boldsymbol{X},\boldsymbol{I})}{\partial \boldsymbol{I}}\right)\right]\boldsymbol{F}(\boldsymbol{X},\boldsymbol{I})\Big|_{\boldsymbol{X}=\boldsymbol{X}_0(\theta,\boldsymbol{I})} \\
&= \left[\frac{\partial}{\partial \boldsymbol{X}}\left(\frac{\partial R(\boldsymbol{X},\boldsymbol{I})}{\partial \boldsymbol{I}}\right)\right]\Big|_{\boldsymbol{X}=\boldsymbol{X}_0(\theta,\boldsymbol{I})} \frac{d\boldsymbol{X}_0(\omega(\boldsymbol{I})t,\boldsymbol{I})}{dt}\Big|_{t=\theta/\omega(\boldsymbol{I})} \\
&= \omega(\boldsymbol{I})\left[\frac{\partial}{\partial \boldsymbol{X}}\left(\frac{\partial R(\boldsymbol{X},\boldsymbol{I})}{\partial \boldsymbol{I}}\right)\right]\Big|_{\boldsymbol{X}=\boldsymbol{X}_0(\theta,\boldsymbol{I})} \frac{\partial \boldsymbol{X}_0(\theta,\boldsymbol{I})}{\partial\theta} = \omega(\boldsymbol{I})\frac{\partial}{\partial\theta}\left(\frac{\partial R(\boldsymbol{X},\boldsymbol{I})}{\partial \boldsymbol{I}}\right)\Big|_{\boldsymbol{X}=\boldsymbol{X}_0(\theta,\boldsymbol{I})} \\
&= \omega(\boldsymbol{I})\frac{\partial \boldsymbol{\xi}_r(\theta,0,\boldsymbol{I})}{\partial\theta}.
\end{aligned} \tag{A.34}$$

Furthermore, differentiating the right-hand side of Eq. (A.32), we can derive

$$\begin{aligned}
\frac{\partial}{\partial \boldsymbol{I}}\left[-\lambda(\boldsymbol{I})R(\boldsymbol{X},\boldsymbol{I})\right]\Big|_{\boldsymbol{X}=\boldsymbol{X}_0(\theta,\boldsymbol{I})} &= -\left[\frac{d\lambda(\boldsymbol{I})}{d\boldsymbol{I}}R(\boldsymbol{X},\boldsymbol{I}) + \lambda(\boldsymbol{I})\frac{\partial R(\boldsymbol{X},\boldsymbol{I})}{\partial \boldsymbol{I}}\right]\Big|_{\boldsymbol{X}=\boldsymbol{X}_0(\theta,\boldsymbol{I})} \\
&= -\lambda(\boldsymbol{I})\boldsymbol{\xi}_r(\theta,0,\boldsymbol{I}),
\end{aligned} \tag{A.35}$$

where we used $R(\boldsymbol{X}_0(\theta,\boldsymbol{I}),\boldsymbol{I}) = 0$. Thus, from Eqs. (A.32)–(A.35), we can obtain

$$\omega(\boldsymbol{I})\frac{\partial \boldsymbol{\xi}_r(\theta,0,\boldsymbol{I})}{\partial\theta} + \boldsymbol{\zeta}_r(\theta,0,\boldsymbol{I}) = -\lambda(\boldsymbol{I})\boldsymbol{\xi}_r(\theta,0,\boldsymbol{I}) \tag{A.36}$$

Since Eq. (A.36) is a linear first-order ordinary differential equation for $\boldsymbol{\xi}_r(\theta,0,\boldsymbol{I})$, this equation can be solved as follows:

$$\boldsymbol{\xi}_r(\theta,0,\boldsymbol{I}) = -\frac{1}{\omega(\boldsymbol{I})}\int_{-\infty}^{\theta} e^{\lambda(\boldsymbol{I})(\theta'-\theta)/\omega(\boldsymbol{I})}\boldsymbol{\zeta}_r(\theta',0,\boldsymbol{I})d\theta', \tag{A.37}$$

which leads to Eqs. (A.30) and (A.31).

Using the derived Eq. (A.31), we can estimate the order of $\boldsymbol{\xi}_r(\theta,0,\boldsymbol{q}(\epsilon t))$ as

$$\begin{aligned}
\boldsymbol{\xi}_r(\theta,0,\boldsymbol{q}(\epsilon t)) &= \frac{1}{\lambda(\boldsymbol{I})}\int_0^{\infty} e^{-s}\boldsymbol{\zeta}_r(\theta-\omega(\boldsymbol{I})s/\lambda(\boldsymbol{I}),0,\boldsymbol{I})ds\Big|_{\boldsymbol{I}=\boldsymbol{q}(\epsilon t)} \\
&= \frac{1}{\lambda(\boldsymbol{I})}\int_0^{\infty} e^{-s}\boldsymbol{\zeta}_r(\theta,0,\boldsymbol{I})ds\Big|_{\boldsymbol{I}=\boldsymbol{q}(\epsilon t)} + O\left(\frac{1}{\lambda(\boldsymbol{q}(\epsilon t))^2}\right) \\
&= O\left(\frac{1}{\lambda(\boldsymbol{q}(\epsilon t))}\right),
\end{aligned} \tag{A.38}$$

where we expanded $\boldsymbol{\zeta}_r(\theta,r,\boldsymbol{I})$ in θ in the second line. For simplicity of notation, we introduce $\tilde{\boldsymbol{\xi}}_r(\theta,\boldsymbol{I})$ as follows:

$$\tilde{\boldsymbol{\xi}}_r(\theta,\boldsymbol{I}) = \lambda(\boldsymbol{I})\boldsymbol{\xi}_r(\theta,0,\boldsymbol{I}) = \int_0^{\infty} e^{-s}\boldsymbol{\zeta}_r(\theta-\omega(\boldsymbol{I})s/\lambda(\boldsymbol{I}),0,\boldsymbol{I})ds. \tag{A.39}$$

Note that $\tilde{\boldsymbol{\xi}}_r(\theta,\boldsymbol{I})$ is of the order $O(1)$.

To evaluate the order of $r(t)$, we approximate the solution to Eq. (A.28) describing the oscillator amplitude in a small neighborhood of $t = t'$. We introduce a small parameter $\tilde{\epsilon} := \epsilon/\lambda(\boldsymbol{q}(\epsilon t'))$, which is sufficiently small ($\ll 1$) by the assumption that $\epsilon \ll \lambda(\boldsymbol{q}(\epsilon t))$. Then, using the small parameters σ and $\tilde{\epsilon}$, we expand the solutions to Eqs. (A.27) and (A.28) as follows:

$$\theta(t) = \theta_0(t) + \sigma\theta_{\sigma,1}(t) + \tilde{\epsilon}\theta_{\epsilon,1}(t) + \cdots, \tag{A.40}$$

$$r(t) = r_0(t) + \sigma r_{\sigma,1}(t) + \tilde{\epsilon} r_{\epsilon,1}(t) + \cdots, \tag{A.41}$$

where $\theta_0(t)$ and $r_0(t)$ are the lowest order solutions and $\theta_{\sigma,j}(t)$, $r_{\sigma,j}(t)$, $\theta_{\epsilon,j}(t)$, and $r_{\epsilon,j}(t)$ are jth order perturbations. The lowest order solutions are given by $\theta_0(t) = \theta(t') + \omega(\boldsymbol{q}(\epsilon t'))(t - t')$ and $r_0(t) = 0$ in the neighborhood of $t = t'$. By introducing a rescaled time $s = \Phi(t) := \int_0^t \lambda(\boldsymbol{q}(\epsilon t'))dt'$ (i.e., $ds = \lambda(\boldsymbol{q}(\epsilon t))dt$), we can rewrite Eq. (A.28) as

$$\frac{dr}{ds} = -r + \frac{\sigma\boldsymbol{\zeta}_r(\theta, r, \boldsymbol{q}(\epsilon t))}{\lambda(\boldsymbol{q}(\epsilon t))} \cdot \boldsymbol{p}(t) + \frac{\epsilon\boldsymbol{\xi}_r(\theta, r, \boldsymbol{q}(\epsilon t))}{\lambda(\boldsymbol{q}(\epsilon t))} \cdot \dot{\boldsymbol{q}}(\epsilon t). \tag{A.42}$$

We also expand $\boldsymbol{q}(\epsilon t)$ around $t = t'$ ($s = \Phi(t')$) as $\boldsymbol{q}(\epsilon t) = \boldsymbol{q}(\epsilon t') + \epsilon\boldsymbol{q}'(\epsilon t')(t - t') + \cdots$. Plugging $\theta(t) = \theta_0(t) + O(\sigma, \tilde{\epsilon})$, $r(t) = r_0(t) + O(\sigma, \tilde{\epsilon})$ and $\boldsymbol{q}(\epsilon t) = \boldsymbol{q}(\epsilon t') + O(\epsilon)$ into Eq. (A.42), we can derive

$$\begin{aligned}
\frac{dr}{ds} &= -r + \sigma\frac{\boldsymbol{\zeta}_r(\theta_0(t) + O(\sigma,\tilde{\epsilon}), 0 + O(\sigma,\tilde{\epsilon}), \boldsymbol{q}(\epsilon t') + O(\epsilon))}{\lambda(\boldsymbol{q}(\epsilon t') + O(\epsilon))} \cdot \boldsymbol{p}(t) \\
&\quad + \epsilon\frac{\boldsymbol{\xi}_r(\theta_0(t) + O(\sigma,\tilde{\epsilon}), 0 + O(\sigma,\tilde{\epsilon}), \boldsymbol{q}(\epsilon t') + O(\epsilon))}{\lambda(\boldsymbol{q}(\epsilon t') + O(\epsilon))} \cdot \dot{\boldsymbol{q}}(\epsilon t) \\
&= -r + \sigma(1 + O(\epsilon))\frac{\boldsymbol{\zeta}_r(\theta_0(t) + O(\sigma,\tilde{\epsilon}), 0 + O(\sigma,\tilde{\epsilon}), \boldsymbol{q}(\epsilon t') + O(\epsilon))}{\lambda(\boldsymbol{q}(\epsilon t'))} \cdot \boldsymbol{p}(t) \\
&\quad + \epsilon(1 + O(\epsilon))\frac{\boldsymbol{\xi}_r(\theta_0(t) + O(\sigma,\tilde{\epsilon}), 0 + O(\sigma,\tilde{\epsilon}), \boldsymbol{q}(\epsilon t') + O(\epsilon))}{\lambda(\boldsymbol{q}(\epsilon t'))} \cdot \dot{\boldsymbol{q}}(\epsilon t) \\
&= -r + \sigma(1 + O(\epsilon))\frac{\boldsymbol{\zeta}_r(\theta_0(t), 0, \boldsymbol{q}(\epsilon t') + O(\epsilon))}{\lambda(\boldsymbol{q}(\epsilon t'))} \cdot \boldsymbol{p}(t) \\
&\quad + \epsilon(1 + O(\epsilon))\frac{\boldsymbol{\xi}_r(\theta_0(t), 0, \boldsymbol{q}(\epsilon t') + O(\epsilon))}{\lambda(\boldsymbol{q}(\epsilon t'))} \cdot \dot{\boldsymbol{q}}(\epsilon t) + O(\sigma^2, \sigma\tilde{\epsilon}, \tilde{\epsilon}^2).
\end{aligned} \tag{A.43}$$

Substituting Eq. (A.39) into the above equation, we obtain

$$\begin{aligned}
\frac{dr}{ds} &= -r + \sigma(1 + O(\epsilon))\frac{\boldsymbol{\zeta}_r(\theta_0(t), 0, \boldsymbol{q}(\epsilon t') + O(\epsilon))}{\lambda(\boldsymbol{q}(\epsilon t'))} \cdot \boldsymbol{p}(t) \\
&\quad + \epsilon(1 + O(\epsilon))\frac{\tilde{\boldsymbol{\xi}}_r(\theta_0(t), \boldsymbol{q}(\epsilon t') + O(\epsilon))}{\lambda(\boldsymbol{q}(\epsilon t'))\lambda(\boldsymbol{q}(\epsilon t') + O(\epsilon))} \cdot \dot{\boldsymbol{q}}(\epsilon t) + O(\sigma^2, \sigma\tilde{\epsilon}, \tilde{\epsilon}^2) \\
&= -r + \sigma(1 + O(\epsilon))\frac{\boldsymbol{\zeta}_r(\theta_0(t), 0, \boldsymbol{q}(\epsilon t')) + O(\epsilon)}{\lambda(\boldsymbol{q}(\epsilon t'))} \cdot \boldsymbol{p}(t) \\
&\quad + \epsilon(1 + O(\epsilon))\frac{\tilde{\boldsymbol{\xi}}_r(\theta_0(t), \boldsymbol{q}(\epsilon t')) + O(\epsilon)}{\lambda(\boldsymbol{q}(\epsilon t'))^2} \cdot \dot{\boldsymbol{q}}(\epsilon t) + O(\sigma^2, \sigma\tilde{\epsilon}, \tilde{\epsilon}^2) \\
&= -r + \sigma\frac{\boldsymbol{\zeta}_r\big(\theta(t') + \omega(\boldsymbol{q}(\epsilon t'))(t - t'), 0, \boldsymbol{q}(\epsilon t')\big)}{\lambda(\boldsymbol{q}(\epsilon t'))} \cdot \boldsymbol{p}(t)
\end{aligned}$$

$$+\epsilon\frac{\tilde{\boldsymbol{\xi}}_r\big(\theta(t')+\omega(\boldsymbol{q}(\epsilon t'))(t-t'),\boldsymbol{q}(\epsilon t')\big)}{\lambda(\boldsymbol{q}(\epsilon t'))^2}\cdot\dot{\boldsymbol{q}}(\epsilon t)+O(\sigma^2,\sigma\tilde{\epsilon},\tilde{\epsilon}^2). \tag{A.44}$$

By integrating Eq. (A.44), we can estimate the order of $r(t')$ as

$$\begin{aligned} r(t') &= \frac{\sigma}{\lambda(\boldsymbol{q}(\epsilon t'))}\int_{-\infty}^{\Phi(t')} e^{s-\Phi(t')}\boldsymbol{\zeta}_r\big(\theta(t')+\omega(\boldsymbol{q}(\epsilon t'))(t-t'),0,\boldsymbol{q}(\epsilon t')\big)\cdot\boldsymbol{p}(t)\big|_{t=\Phi^{-1}(s)}ds \\ &+ \frac{\epsilon}{\lambda(\boldsymbol{q}(\epsilon t'))^2}\int_{-\infty}^{\Phi(t')} e^{s-\Phi(t')}\tilde{\boldsymbol{\xi}}_r\big(\theta(t')+\omega(\boldsymbol{q}(\epsilon t'))(t-t'),\boldsymbol{q}(\epsilon t')\big)\cdot\dot{\boldsymbol{q}}(\epsilon t)\big|_{t=\Phi^{-1}(s)}ds \\ &+ O(\sigma^2,\sigma\tilde{\epsilon},\tilde{\epsilon}^2) \\ &= O\left(\frac{\sigma}{\lambda(\boldsymbol{q}(\epsilon t'))},\frac{\epsilon}{\lambda(\boldsymbol{q}(\epsilon t'))^2}\right). \end{aligned} \tag{A.45}$$

Now, by expanding Eq. (A.21) in r, we can obtain

$$\begin{aligned} \dot{\theta} &= \omega(\boldsymbol{q}(\epsilon t))+\sigma\boldsymbol{\zeta}_\theta(\theta,0,\boldsymbol{q}(\epsilon t))\cdot\boldsymbol{p}(t)+\epsilon\boldsymbol{\xi}_\theta(\theta,0,\boldsymbol{q}(\epsilon t))\cdot\dot{\boldsymbol{q}}(\epsilon t) \\ &\quad +\sigma r\frac{\partial\boldsymbol{\zeta}_\theta(\theta,0,\boldsymbol{q}(\epsilon t))}{\partial r}\cdot\boldsymbol{p}(t)+\epsilon r\frac{\partial\boldsymbol{\xi}_\theta(\theta,0,\boldsymbol{q}(\epsilon t))}{\partial r}\cdot\dot{\boldsymbol{q}}(\epsilon t)+O(r^2). \end{aligned} \tag{A.46}$$

Substituting Eq. (A.45) into Eq. (A.46) and neglecting higher order terms in r, we can derive the generalized phase equation (4.8) in the main article,

$$\begin{aligned} \dot{\theta} &= \omega(\boldsymbol{q}(\epsilon t))+\sigma\boldsymbol{\zeta}_\theta(\theta,0,\boldsymbol{q}(\epsilon t))\cdot\boldsymbol{p}(t)+O\left(\frac{\sigma^2}{\lambda(\boldsymbol{q}(\epsilon t))},\frac{\sigma\epsilon}{\lambda(\boldsymbol{q}(\epsilon t))^2}\right) \\ &\quad +\epsilon\boldsymbol{\xi}_\theta(\theta,0,\boldsymbol{q}(\epsilon t))\cdot\dot{\boldsymbol{q}}(\epsilon t)+O\left(\frac{\sigma\epsilon}{\lambda(\boldsymbol{q}(\epsilon t))},\frac{\epsilon^2}{\lambda(\boldsymbol{q}(\epsilon t))^2}\right). \end{aligned} \tag{A.47}$$

Equation (A.47) reveals that our phase equation well approximates the exact phase dynamics under the conditions that

$$\frac{\sigma^2}{\lambda(\boldsymbol{q}(\epsilon t))}\ll\sigma,\ \ \frac{\sigma\epsilon}{\lambda(\boldsymbol{q}(\epsilon t))^2}\ll\sigma,\ \ \frac{\sigma\epsilon}{\lambda(\boldsymbol{q}(\epsilon t))}\ll\epsilon,\ \text{ and }\ \frac{\epsilon^2}{\lambda(\boldsymbol{q}(\epsilon t))^2}\ll\epsilon. \tag{A.48}$$

Here, we compared the first two error terms $\frac{\sigma^2}{\lambda(\boldsymbol{q}(\epsilon t))}$ and $\frac{\sigma\epsilon}{\lambda(\boldsymbol{q}(\epsilon t))^2}$ with σ, and the last two $\frac{\sigma\epsilon}{\lambda(\boldsymbol{q}(\epsilon t))}$ and $\frac{\epsilon^2}{\lambda(\boldsymbol{q}(\epsilon t))^2}$ with ϵ, because the first and last two error terms arose when we expanded the second term $\sigma\boldsymbol{\zeta}_\theta(\theta,r,\boldsymbol{q}(\epsilon t))\cdot\boldsymbol{p}(t)$ $(=O(\sigma))$ and the third term $\epsilon\boldsymbol{\xi}_\theta(\theta,r,\boldsymbol{q}(\epsilon t))\cdot\dot{\boldsymbol{q}}(\epsilon t)$ $(=O(\epsilon))$ of Eq. (A.27) in r, respectively. because the first two terms arise from the expansion of the second term $\sigma\boldsymbol{\zeta}_\theta(\theta,r,\boldsymbol{q}(\epsilon t))\cdot\boldsymbol{p}(t)$ $(=O(\sigma))$ of Eq. (A.27) in r, and the last two terms arise from the third term $\epsilon\boldsymbol{\xi}_\theta(\theta,r,\boldsymbol{q}(\epsilon t))\cdot\dot{\boldsymbol{q}}(\epsilon t)$ $(=O(\epsilon))$, respectively. These conditions are satisfied when

$$\frac{\epsilon}{\lambda(\boldsymbol{q}(\epsilon t))^2}\ll 1\ \text{ and }\ \frac{\sigma}{\lambda(\boldsymbol{q}(\epsilon t))}\ll 1, \tag{A.49}$$

namely, when (i) the timescale of the slowly varying component $\boldsymbol{q}(\epsilon t)$ is much larger than the relaxation time of perturbed orbits to C, and (ii) the remaining fluctuations $\sigma \boldsymbol{p}(t)$ is sufficiently weak, as we assumed in the main article.

For limit-cycle oscillators with higher-dimensional state variables ($n \geq 3$), we can also derive a phase equation corresponding to Eq. (A.47). In higher-dimensional cases, the system of Eq. (A.12) has n (≥ 3) Floquet exponents. Let $\lambda_j(\boldsymbol{I})$ denote the absolute value of the j-th largest Floquet exponent of the oscillator for a given constant $\boldsymbol{I}$ ($\lambda_1(\boldsymbol{I}) = 0 > \lambda_2(\boldsymbol{I}) \geq \cdots \geq \lambda_n(\boldsymbol{I})$). In these exponents, the second largest exponent $\lambda_2(\boldsymbol{I})$ dominates the relaxation time of perturbed orbits. Thus, using the absolute value of the second largest Floquet exponent $\lambda_2(\boldsymbol{q}(\epsilon t))$ instead of $\lambda(\boldsymbol{q}(\epsilon t))$, we can obtain the same results as Eq. (A.47); that is, we can obtain the following phase equation also for the higher-dimensional cases ($n \geq 3$):

$$\begin{aligned} \dot{\theta} &= \omega(\boldsymbol{q}(\epsilon t)) + \sigma \boldsymbol{\zeta}_\theta(\theta, 0, \boldsymbol{q}(\epsilon t)) \cdot \boldsymbol{p}(t) + \epsilon \boldsymbol{\xi}_\theta(\theta, 0, \boldsymbol{q}(\epsilon t)) \cdot \dot{\boldsymbol{q}}(\epsilon t) \\ &\quad + O\left(\frac{\epsilon^2}{\lambda_2(\boldsymbol{q}(\epsilon t))^2}, \frac{\sigma\epsilon}{\lambda_2(\boldsymbol{q}(\epsilon t))}, \frac{\sigma^2}{\lambda_2(\boldsymbol{q}(\epsilon t))} \right). \end{aligned} \tag{A.50}$$

A.5 Relations among Different Sensitivity Functions

This section gives a derivation of Eqs. (4.11)–(4.13) in the main article. These relations are essentially important in understanding the properties of the sensitivity functions and in developing methods to calculate and estimate the sensitivity functions. In this section, for simplicity of notation, the sensitivity functions are denoted by $\boldsymbol{\zeta}(\theta, \boldsymbol{I})$ and $\boldsymbol{\xi}(\theta, \boldsymbol{I})$ as in the main article.

A.5.1 Derivation of Eq. (4.11)

As we shown in Eq. (4.11) in the main article, the sensitivity function $\boldsymbol{\xi}(\theta, \boldsymbol{I})$ can be written as

$$\boldsymbol{\xi}(\theta, \boldsymbol{I}) = -\frac{\partial \boldsymbol{X}_0(\theta, \boldsymbol{I})}{\partial \boldsymbol{I}}^\top \boldsymbol{Z}(\theta, \boldsymbol{I}). \tag{A.51}$$

This equation relates the change in the shape of the limit-cycle orbit $\boldsymbol{X}_0(\theta, \boldsymbol{I})$ and the phase sensitivity function $\boldsymbol{Z}(\theta, \boldsymbol{I})$ to the sensitivity function $\boldsymbol{\xi}(\theta, \boldsymbol{I})$. From the definition of $\Theta(\boldsymbol{X}, \boldsymbol{I})$,

$$\Theta(\boldsymbol{X}_0(\theta, \boldsymbol{I}), \boldsymbol{I}) = \theta \tag{A.52}$$

holds. By differentiating Eq. (A.52) with respect to $\boldsymbol{I}$, we can obtain

$$\begin{aligned} \frac{\partial}{\partial \boldsymbol{I}} \Theta(\boldsymbol{X}_0(\theta, \boldsymbol{I}), \boldsymbol{I}) &= \frac{\partial \boldsymbol{X}_0(\theta, \boldsymbol{I})}{\partial \boldsymbol{I}}^\top \left. \frac{\partial \Theta(\boldsymbol{X}, \boldsymbol{I})}{\partial \boldsymbol{X}} \right|_{\boldsymbol{X}=\boldsymbol{X}_0(\theta, \boldsymbol{I})} + \left. \frac{\partial \Theta(\boldsymbol{X}, \boldsymbol{I})}{\partial \boldsymbol{I}} \right|_{\boldsymbol{X}=\boldsymbol{X}_0(\theta, \boldsymbol{I})} \\ &= \frac{\partial \boldsymbol{X}_0(\theta, \boldsymbol{I})}{\partial \boldsymbol{I}}^\top \boldsymbol{Z}(\theta, \boldsymbol{I}) + \boldsymbol{\xi}(\theta, \boldsymbol{I}) = 0, \end{aligned} \tag{A.53}$$

which leads to Eq. (A.51).

A.5.2 Derivation of Eqs. (4.12) and (4.13)

As we shown in Eqs. (4.12) and (4.13) in the main article, the sensitivity functions $\boldsymbol{\zeta}(\theta, \boldsymbol{I})$ and $\boldsymbol{\xi}(\theta, \boldsymbol{I})$ are mutually related as follows:

$$\boldsymbol{\xi}(\theta, \boldsymbol{I}) = \boldsymbol{\xi}(\theta_0, \boldsymbol{I}) - \frac{1}{\omega(\boldsymbol{I})} \int_{\theta_0}^{\theta} [\boldsymbol{\zeta}(\phi, \boldsymbol{I}) - \bar{\boldsymbol{\zeta}}(\boldsymbol{I})] d\phi, \tag{A.54}$$

$$\boldsymbol{\zeta}(\theta, \boldsymbol{I}) = \bar{\boldsymbol{\zeta}}(\boldsymbol{I}) - \omega(\boldsymbol{I}) \frac{\partial \boldsymbol{\xi}(\theta, \boldsymbol{I})}{\partial \theta}, \tag{A.55}$$

and

$$\bar{\boldsymbol{\zeta}}(\boldsymbol{I}) := \frac{1}{2\pi} \int_0^{2\pi} \boldsymbol{\zeta}(\theta, \boldsymbol{I}) d\theta = \frac{d\omega(\boldsymbol{I})}{d\boldsymbol{I}}, \tag{A.56}$$

where $\theta_0 \in [0, 2\pi)$ is an arbitrary phase and $\bar{\boldsymbol{\zeta}}(\boldsymbol{I})$ is the average of $\boldsymbol{\zeta}(\theta, \boldsymbol{I})$ with respect to θ and is a function of $\boldsymbol{I}$. Equation (A.54) (or (A.55)) represents the sensitivity function $\boldsymbol{\xi}(\theta, \boldsymbol{I})$ characterizing the phase response caused by a small constant shift in $\boldsymbol{I}$ as an integral of the phase response to the instantaneous change in $\boldsymbol{I}$ at each θ, and Eq. (A.56) relates the change in the frequency $\omega(\boldsymbol{I})$ of the limit-cycle orbit to the average of the sensitivity function $\boldsymbol{\zeta}(\theta, \boldsymbol{I})$, i.e., the net phase shift caused by the a small constant shift in $\boldsymbol{I}$ during one period of oscillation. Using these relations, we can obtain the sensitivity function $\boldsymbol{\xi}(\theta, \boldsymbol{I})$ for each $\boldsymbol{I}$. Namely, we can calculate the sensitivity function $\boldsymbol{\zeta}(\theta, \boldsymbol{I})$, e.g., by using the adjoint method, and then integrate $\boldsymbol{\zeta}(\theta, \boldsymbol{I})$ with respect to θ to obtain the sensitivity function $\boldsymbol{\xi}(\theta, \boldsymbol{I})$.

Since we can straightforwardly derive Eq. (A.54) by integrating Eq. (A.55) with respect to θ, we only describe derivations of Eq. (A.55) and Eq. (A.56). From the definition of $\Theta(\boldsymbol{X}, \boldsymbol{I})$,

$$\frac{\partial \Theta(\boldsymbol{X}, \boldsymbol{I})}{\partial \boldsymbol{X}} \cdot \boldsymbol{F}(\boldsymbol{X}, \boldsymbol{I}) = \omega(\boldsymbol{I}) \tag{A.57}$$

holds. By differentiating Eq. (A.57) with respect to $\boldsymbol{I}$ and plugging in $\boldsymbol{X} = \boldsymbol{X}_0(\theta, \boldsymbol{I})$, we can obtain

$$\begin{aligned}
\frac{\partial}{\partial \boldsymbol{I}} \left[\frac{\partial \Theta(\boldsymbol{X}, \boldsymbol{I})}{\partial \boldsymbol{X}} \cdot \boldsymbol{F}(\boldsymbol{X}, \boldsymbol{I}) \right] \Bigg|_{\boldsymbol{X}=\boldsymbol{X}_0(\theta,\boldsymbol{I})} &= \left[\frac{\partial}{\partial \boldsymbol{I}} \left(\frac{\partial \Theta(\boldsymbol{X}, \boldsymbol{I})}{\partial \boldsymbol{X}} \right) \right]^{\top} \boldsymbol{F}(\boldsymbol{X}, \boldsymbol{I}) \Bigg|_{\boldsymbol{X}=\boldsymbol{X}_0(\theta,\boldsymbol{I})} \\
&\quad + \frac{\partial \boldsymbol{F}(\boldsymbol{X}, \boldsymbol{I})}{\partial \boldsymbol{I}}^{\top} \frac{\partial \Theta(\boldsymbol{X}, \boldsymbol{I})}{\partial \boldsymbol{X}} \Bigg|_{\boldsymbol{X}=\boldsymbol{X}_0(\theta,\boldsymbol{I})} \\
&= \left[\frac{\partial}{\partial \boldsymbol{X}} \left(\frac{\partial \Theta(\boldsymbol{X}, \boldsymbol{I})}{\partial \boldsymbol{I}} \right) \right] \boldsymbol{F}(\boldsymbol{X}, \boldsymbol{I}) \Bigg|_{\boldsymbol{X}=\boldsymbol{X}_0(\theta,\boldsymbol{I})} + \boldsymbol{\zeta}(\theta, \boldsymbol{I}) \\
&= \frac{d\omega(\boldsymbol{I})}{d\boldsymbol{I}},
\end{aligned} \tag{A.58}$$

where $\frac{\partial}{\partial \boldsymbol{I}}(\frac{\partial \Theta(\boldsymbol{X},\boldsymbol{I})}{\partial \boldsymbol{X}})$ is a matrix whose (i,j)-th element is given by $\frac{\partial^2 \Theta(\boldsymbol{X},\boldsymbol{I})}{\partial X_i \partial I_j}$, and $\frac{\partial}{\partial \boldsymbol{X}}(\frac{\partial \Theta(\boldsymbol{X},\boldsymbol{I})}{\partial \boldsymbol{I}})$ is the transpose of $\frac{\partial}{\partial \boldsymbol{I}}(\frac{\partial \Theta(\boldsymbol{X},\boldsymbol{I})}{\partial \boldsymbol{X}})$. Here, the first term of the third line in Eq. (A.58) can be written as

$$\begin{aligned}
&\left[\frac{\partial}{\partial \boldsymbol{X}}\left(\frac{\partial \Theta(\boldsymbol{X},\boldsymbol{I})}{\partial \boldsymbol{I}}\right)\right]\boldsymbol{F}(\boldsymbol{X},\boldsymbol{I})\Big|_{\boldsymbol{X}=\boldsymbol{X}_0(\theta,\boldsymbol{I})} \\
&= \left[\frac{\partial}{\partial \boldsymbol{X}}\left(\frac{\partial \Theta(\boldsymbol{X},\boldsymbol{I})}{\partial \boldsymbol{I}}\right)\right]\Big|_{\boldsymbol{X}=\boldsymbol{X}_0(\theta,\boldsymbol{I})} \frac{d\boldsymbol{X}_0(\omega(\boldsymbol{I})t,\boldsymbol{I})}{dt}\Big|_{t=\theta/\omega(\boldsymbol{I})} \\
&= \omega(\boldsymbol{I})\left[\frac{\partial}{\partial \boldsymbol{X}}\left(\frac{\partial \Theta(\boldsymbol{X},\boldsymbol{I})}{\partial \boldsymbol{I}}\right)\right]\Big|_{\boldsymbol{X}=\boldsymbol{X}_0(\theta,\boldsymbol{I})} \frac{\partial \boldsymbol{X}_0(\theta,\boldsymbol{I})}{\partial \theta} = \omega(\boldsymbol{I})\frac{\partial}{\partial \theta}\left(\frac{\partial \Theta(\boldsymbol{X},\boldsymbol{I})}{\partial \boldsymbol{I}}\right)\Big|_{\boldsymbol{X}=\boldsymbol{X}_0(\theta,\boldsymbol{I})} \\
&= \omega(\boldsymbol{I})\frac{\partial \boldsymbol{\xi}(\theta,\boldsymbol{I})}{\partial \theta}. \qquad \text{(A.59)}
\end{aligned}$$

Then, from Eqs. (A.58) and (A.59), we can derive Eq. (A.55) and Eq. (A.56) as

$$\frac{d\omega(\boldsymbol{I})}{d\boldsymbol{I}} = \frac{1}{2\pi}\int_0^{2\pi}\left[\omega(\boldsymbol{I})\frac{\partial \boldsymbol{\xi}(\theta,\boldsymbol{I})}{\partial \theta} + \boldsymbol{\zeta}(\theta,\boldsymbol{I})\right]d\theta = \frac{1}{2\pi}\int_0^{2\pi}\boldsymbol{\zeta}(\theta,\boldsymbol{I})d\theta, \qquad \text{(A.60)}$$

where the first term in the integral vanishes due to 2π-periodicity of $\boldsymbol{\xi}(\theta,\boldsymbol{I})$.

A.6 Relation between Conventional and Generalized Phase Equations

Here we compare the generalized phase equation with the conventional phase equation using the near-identity transformation. As stated in the main article, the conventional phase equation can be written as

$$\dot{\tilde{\theta}} = \omega(\boldsymbol{q}_c) + \sigma_c \boldsymbol{\zeta}(\tilde{\theta},\boldsymbol{q}_c)\cdot\boldsymbol{p}_c(t) + O(\sigma_c^2), \qquad \text{(A.61)}$$

where $\boldsymbol{q}_c \in A$ is a constant, $\boldsymbol{p}_c(t)$ is an external input defined as $\sigma_c \boldsymbol{p}_c(t) = \boldsymbol{I}(t) - \boldsymbol{q}_c$, and σ_c is a parameter representing the intensity of the external input. We decompose the external input $\boldsymbol{p}_c(t)$ into two terms, $\boldsymbol{p}_1(t)$ and $\boldsymbol{p}_2(t)$, as

$$\boldsymbol{p}_c(t) = \boldsymbol{p}_1(t) + \boldsymbol{p}_2(t), \qquad \text{(A.62)}$$

and introduce a slightly deformed phase $\phi(t)$ as

$$\phi(t) = \tilde{\theta}(t) + \sigma_c \boldsymbol{\xi}(\tilde{\theta}(t),\boldsymbol{q}_c)\cdot\boldsymbol{p}_1(t). \qquad \text{(A.63)}$$

By applying the above near-identity transformation to the phase equation (A.61), we can derive the following phase equation for $\phi(t)$:

$$\dot{\phi} = \omega(\boldsymbol{q}_c) + \sigma_c \left.\frac{d\omega(\boldsymbol{I})}{d\boldsymbol{I}}\right|_{\boldsymbol{I}=\boldsymbol{q}_c}\cdot\boldsymbol{p}_1(t) + \sigma_c\boldsymbol{\zeta}(\phi,\boldsymbol{q}_c)\cdot\boldsymbol{p}_2(t) + \sigma_c\boldsymbol{\xi}(\phi,\boldsymbol{q}_c)\cdot\dot{\boldsymbol{p}}_1(t) + O(\sigma_c^2). \qquad \text{(A.64)}$$

Without loss of generality, we can regard the input terms $\sigma_c \boldsymbol{p}_1(t)$ and $\sigma_c \boldsymbol{p}_2(t)$ in Eq. (A.64) as the slowly varying part $\boldsymbol{q}(\epsilon t)$ and the weak fluctuations $\sigma \boldsymbol{p}(t)$ in the main article, because we can choose the decomposition of $\boldsymbol{p}_c(t)$ arbitrarily. Then, Eq. (A.64) can be considered an approximation to the generalized phase equation (2) in the main article. In other words, the first term of Eq. (A.64) represents the first-order (linear) approximation in $\boldsymbol{q}$ around $\boldsymbol{q} = \boldsymbol{q}_c$ to the first term of the generalized phase equation, while the second and third terms of Eq. (A.64) are zeroth-order (constant) approximations in $\boldsymbol{q}$ around $\boldsymbol{q} = \boldsymbol{q}_c$ to the second and third terms of the generalized phase equation.

In this sense, the generalized phase equation (2) in the main article can be considered a nonlinear generalization of the conventional phase equation (A.64). For the modified Stuart-Landau oscillator defined in the main article, the frequency $\omega(I)$ and the sensitivity functions $\zeta(\theta, I)$ and $\xi(\theta, I)$ are explicitly given by

$$\omega(I) = e^{2I} = 1 + 2I + 2I^2 + \frac{4I^3}{3} + \cdots , \tag{A.65}$$

$$\zeta(\theta, I) = 2e^{2I} - e^I \cos\theta = 1 - \cos\theta + (4 - \cos\theta)I + \left(4 - \frac{\cos\theta}{2}\right) I^2 + \cdots , \tag{A.66}$$

$$\xi(\theta, I) = e^{-I} \sin\theta = \sin\theta - (\sin\theta)I + \frac{\sin\theta}{2} I^2 + \cdots . \tag{A.67}$$

When the temporal variation in the input $I(t)$ is sufficiently small, we can truncate $\omega(I)$ at the first order, and $\zeta(\theta, I)$ and $\xi(\theta, I)$ at the zeroth order, which is equivalent to using the conventional phase equation. However, when the input $I(t)$ varies largely with time and the shape of the limit-cycle orbit is significantly deformed, the above approximation is no longer valid. In such cases, the conventional phase equation would fail to predict the actual oscillator dynamics and the generalized phase reduction method should be used.

A.7 Accuracy and Robustness of Generalized Phase Equation

In the main article, we briefly demonstrated that the generalized phase equation can accurately predict the time series of the oscillation phase as compared to the conventional phase equation. Here, we examine the accuracy and robustness of the generalized phase equation in more detail with numerical simulations. We use a modified Stuart-Landau oscillator defined as

$$\dot{x} = e^{2I(t)}(\lambda_0 x - y - \lambda_0 I(t)) - \lambda_0[(x - I(t))^2 + y^2](x - I(t)), \tag{A.68}$$

$$\dot{x} = e^{2I(t)}(x + \lambda_0 y - I(t)) - \lambda_0[(x - I(t))^2 + y^2]y, \tag{A.69}$$

whose amplitude relaxation rate can explicitly be specified by the parameter λ_0. Here, x and y are state variables representing the oscillator state, $I(t)$ is an external input, and λ_0 is a parameter that

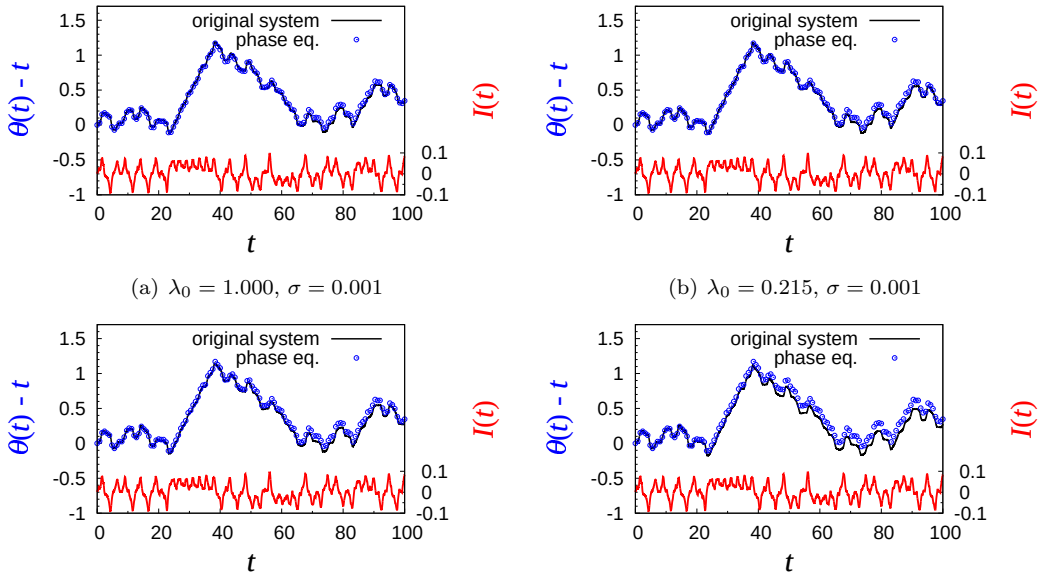

(a) $\lambda_0 = 1.000$, $\sigma = 0.001$

(b) $\lambda_0 = 0.215$, $\sigma = 0.001$

(c) $\lambda_0 = 0.046$, $\sigma = 0.001$

(d) $\lambda_0 = 0.010$, $\sigma = 0.001$

Figure A.1: Accuracy and robustness of the generalized phase equation. A modified Stuart-Landau oscillator (Eqs. (A.68) and (A.69)) is driven by a periodically varying parameter $I(t)$ (red lines, Eq. (A.70)). The time series of the phase $\theta(t) = \Theta(\boldsymbol{X}(t), \boldsymbol{q}(\epsilon t))$ measured directly from the original system (black lines) and predicted by the direct numerical simulation of the generalized phase equation (blue circles) are plotted. The parameter σ is fixed at 0.001 and λ_0 is varied between 1 and 0.01.

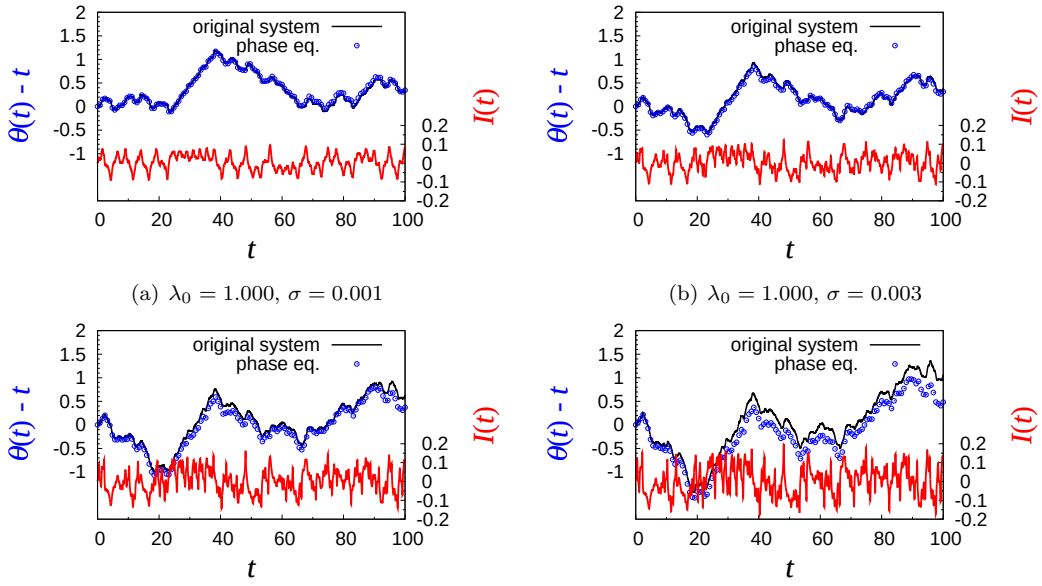

(a) $\lambda_0 = 1.000$, $\sigma = 0.001$

(b) $\lambda_0 = 1.000$, $\sigma = 0.003$

(c) $\lambda_0 = 1.000$, $\sigma = 0.005$

(d) $\lambda_0 = 1.000$, $\sigma = 0.007$

Figure A.2: Accuracy and robustness of the generalized phase equation. A modified Stuart-Landau oscillator (Eqs. (A.68) and (A.69)) is driven by a periodically varying parameter $I(t)$ (red lines, Eq. (A.70)). The time series of the phase $\theta(t) = \Theta(\boldsymbol{X}(t), \boldsymbol{q}(\epsilon t))$ measured directly from the original system (black lines) and predicted by the direct numerical simulation of the generalized phase equation (blue circles) are plotted. The parameter λ_0 is fixed at 1 and σ is varied between 0.001 and 0.007.

controls the timescale of the amplitude relaxation. For this model, one can explicitly define the amplitude $r = \sqrt{(x - I(t))^2 + y^2}$, which decays exponentially as $\dot{r} = -2\lambda_0 r$. As stated in the main article, the small parameter ϵ represents the relative timescale of the slowly varying component $\boldsymbol{q}(\epsilon t)$ to the amplitude relaxation time of the oscillator (which was assumed to be $O(1)$ in the main article). Thus, by varying the parameter λ_0, we can effectively control the parameter ϵ.

We applied a periodically varying parameter

$$I(t) = 0.005L_1(0.3t) + \sigma L_2(t) \tag{A.70}$$

to the oscillator, where $L_1(t)$ and $L_2(t)$ are independently generated time series of the variable x of the chaotic Lorenz model [3], $\dot{x} = 10(y - x)$, $\dot{y} = x(28 - z) - y$, and $\dot{z} = xy - 8z/3$, and σ is a parameter controlling the intensity of the high-frequency components in $I(t)$. Since the parameters λ_0 and σ play important roles in the proposed phase reduction method, we examine the accuracy and robustness of the generalized phase equation for varying values of λ_0 and σ.

Figures A.1 and A.2 shows the results of numerical simulations, where one of the parameters is kept fixed and the other is varied. In Figs. A.1 (a)–(d), σ is fixed and λ_0 is varied. The accuracy of the proposed phase reduction method is deteriorated as λ_0 is decreased. In this case, when $\lambda_0 > 0.01$, the generalized phase equation can predict the temporal evolution of the actual phase of the oscillator. Similarly, when λ_0 is fixed and σ is varied (Figs. A.2 (a)–(d)), the accuracy of the proposed method becomes worse as σ is increased. In this case, when $\sigma < 0.007$, the generalized phase equation can predict the temporal evolution of the actual phase.

A.8 Phase Locking of Morris-Lecar Model Driven by Periodic Forcing

In the main article, we analyzed the phase locking of a modified Stuart-Landau oscillator to periodic forcing and demonstrated the usefulness of the proposed phase reduction method. In this section, we further analyze another type of limit-cycle oscillator, i.e., the Morris-Lecar model [5], which describes periodic firing of a neuron. We theoretically analyze the phase locking dynamics of the Morris-Lecar model to periodic external forcing and compare the theoretical predictions with direct numerical simulations.

A.8.1 Morris-Lecar Model

The Morris-Lecar model [5] of a periodically firing neuron has a two-dimensional state variable $\boldsymbol{X}(t) = [V(t), w(t)]^\top$. The vector field $\boldsymbol{F}(\boldsymbol{X}, I) = [F_1(V, w, I), F_2(V, w, I)]^\top$ is given by

$$C_{\rm m}F_1 = g_{\rm L}(V_L - V) + g_{\rm K}w(V_K - V) + g_{\rm Ca}m_\infty(V_{\rm Ca} - V) + I, \tag{A.71}$$

$$F_2 = \lambda_w(w_\infty - w), \tag{A.72}$$

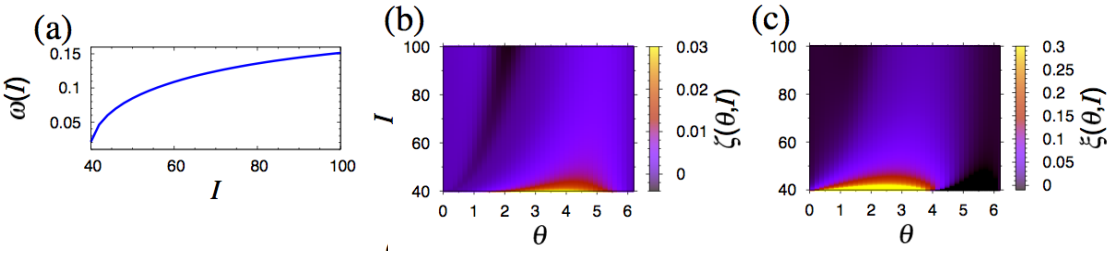

Figure A.3: Dynamical properties of the Morris-Lecar model exhibiting smooth oscillations. (a) Natural frequency $\omega(I)$. (b), (c) Sensitivity functions $\zeta(\theta, I)$ and $\xi(\theta, I)$.

where $m_\infty(V) = 0.5\{1 + \tanh[(V - V_1)/V_2]\}$ and $w_\infty(V) = 0.5\{1 + \tanh[(V - V_3)/V_4]\}$ are the conductance functions, I is the parameter to which the forcing is applied, and $V_{\rm K}$, $V_{\rm L}$, $V_{\rm Ca}$, $g_{\rm K}$, $g_{\rm L}$, $g_{\rm Ca}$, C, V_1, V_2, V_3, V_4, and λ_w are constant parameters. This model exhibits stable limit-cycle oscillations when the parameter values are chosen appropriately.

A.8.2 Smooth Oscillations

We set the parameters as $V_{\rm K} = -84$, $V_{\rm L} = -60$, $V_{\rm Ca} = 120$, $g_{\rm K} = 8$, $g_{\rm L} = 2$, $g_{\rm Ca} = 4$, $C = 20$, $V_1 = -1.2$, $V_2 = 18$, $V_3 = 12$, $V_4 = 17$, and $\lambda_w = 0.0667$. For these parameters, a stable limit cycle emerges via a saddle-node on invariant circle (SNIC) bifurcation at $I \simeq 50$, and vanishes via a Hopf bifurcation at $I \simeq 115$. The oscillation remains generally smooth for all values of I. The phase sensitivity function has the type-I shape with a positive lobe near the SNIC bifurcation, and a sinusoidal type-II shape with both positive and negative lobes near the Hopf bifurcation [5]. Thus, when the external forcing $I(t)$ is time-varying, the shape of the orbit, frequency, and phase response properties of the oscillator can vary significantly with time.

Numerically calculated $\omega(I)$, $\zeta(\theta, I)$, and $\xi(\theta, I)$ are shown in Figs. A.3 (a)–(c), and phase-locked dynamics of the variable $V(t)$ to the periodic forcing $I(t)$ is shown in Figs. A.4(d)–(f). Note that the oscillations are significantly deformed due to strong periodic forcing. Figures A.4 (g)–(i) compare the results of the reduced phase equations with those of the direct numerical simulations. We can confirm that the generalized phase reduction theory nicely predicts the stable phase differences ψ, while the conventional method does not. The orbits of the oscillator and the cylinder C of the limit cycles in three-dimensional space (V, w, I) are plotted in Figs. A.4 (j)–(l), showing synchronous [(j) and (k)] or asynchronous (l) dynamics with the periodic forcing.

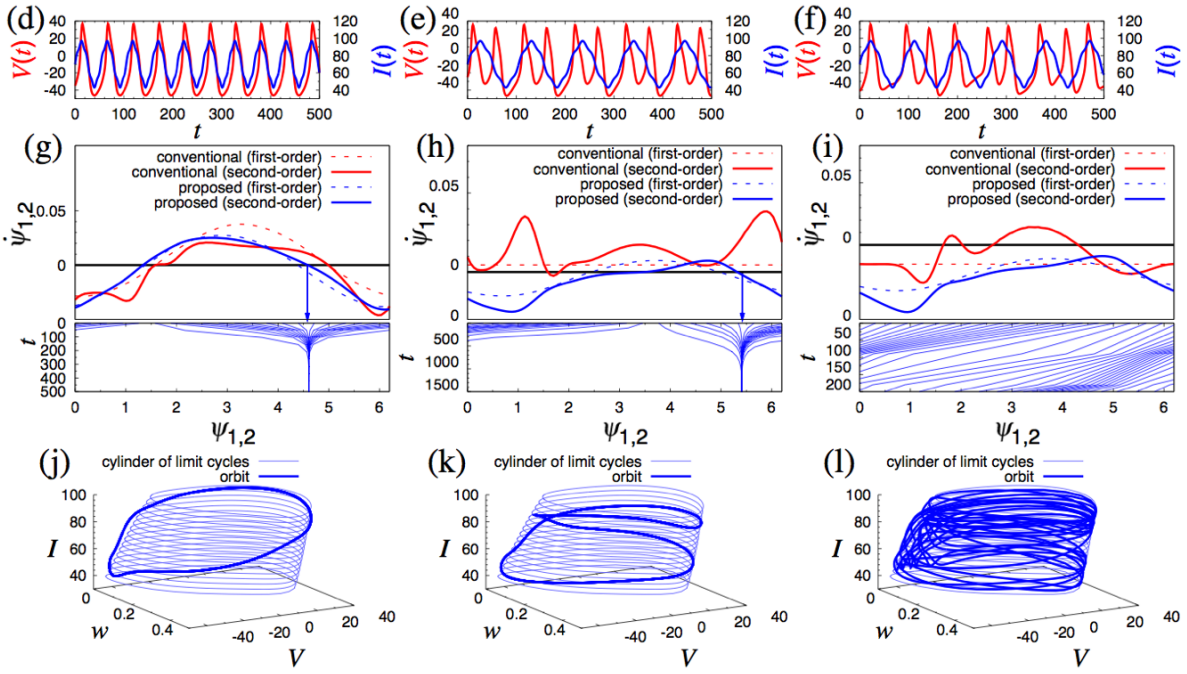

Figure A.4: Phase locking of the Morris-Lecar model exhibiting smooth oscillations. Three sets of periodically varying parameters, $I^{(j)}(t)$: $q^{(j)}(\epsilon t) = 70 + 25\sin(\omega_I^{(j)} t)$ and $\sigma p^{(j)}(t) = 2\sin(5\omega_I^{(j)} t)$ with $\omega_I^{(1,2,3)} = 0.12,\ 0.06,\ 0.07$ are used, which lead to $1:1$ or $1:2$ phase locking to $q(\epsilon t)$; $1:1$ phase locking to $I^{(1)}(t)$ [(d), (g), and (j)], $1:2$ phase locking to $I^{(2)}(t)$ [(e), (h), and (k)], and failure of phase locking to $I^{(3)}(t)$ [(f), (i), and (l)]. (a) Natural frequency $\omega(I)$. (b), (c) Sensitivity functions $\zeta(\theta, I)$ and $\xi(\theta, I)$. (d)–(f) Time series of the state variable $V(t)$ of a periodically driven oscillator (red) and the periodic external forcing (blue). (g)–(i) Dynamics of the phase difference ψ. The averaged dynamics of ψ is shown in the top panel, where the stable phase difference predicted by the second-order averaging of the generalized phase equation is indicated by an arrow, and evolution of ψ from 20 different initial states are plotted in the bottom panel. (j)–(l) Orbits of the periodically driven oscillator (blue) and I-dependent stable limit-cycle solutions (light blue) plotted in three-dimensional space (V, w, I).

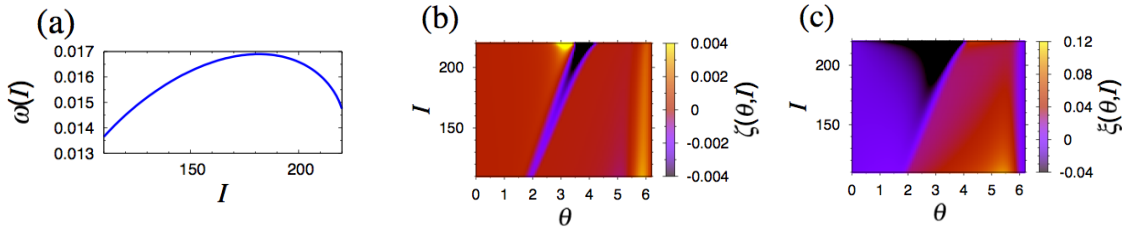

Figure A.5: Dynamical properties of the Morris-Lecar model exhibiting relaxation oscillations. (a) Natural frequency $\omega(I)$. (b), (c) Sensitivity functions $\zeta(\theta, I)$ and $\xi(\theta, I)$.

A.8.3 Relaxation Oscillations

We set the parameters as $V_{\mathrm{K}} = -84$, $V_{\mathrm{L}} = -60$, $V_{\mathrm{Ca}} = 120$, $g_{\mathrm{K}} = 8$, $g_{\mathrm{L}} = 2$, $g_{\mathrm{Ca}} = 4.4$, $C = 20$, $V_1 = -1.2$, $V_2 = 18$, $V_3 = 2$, $V_4 = 30$, and $\lambda_w = 0.004$. For these parameters, the ML model exhibits relaxation oscillations consisting of fast and slow dynamics in an appropriate range of I, and correspondingly the phase sensitivity function takes an impulse-like shape. Numerically calculated $\omega(I)$, $\zeta(\theta, I)$, and $\xi(\theta, I)$ are shown in Figs. A.5 (a)–(c), and the phase-locked dynamics of $V(t)$ to the periodic forcing $I(t)$ are shown in Figs. A.6 (d)–(f). Figures A.6 (g)–(i) compare the results of the reduced phase equations with those of the direct numerical simulations. The parameter I was varied between 140 and 200. In this case, both the conventional and generalized phase equations seem to nicely predict the stable phase difference. As shown below, however, the conventional phase equation may actually fail to predict the oscillator dynamics in such cases.

To investigate whether the two phase equations can accurately predict dynamics of the original limit-cycle oscillator, we further calculate the phase maps [3], corresponding to the numerical simulations shown in Fig. A.6. The phase map is a one-dimensional map from the phase $\theta(nT_I)$ at $t = nT_I$ to the phase $\theta((n+1)T_I)$ after one period of the external forcing, where $n \in \mathbb{N}$ is an integer and T_I is the period of external forcing. Figure A.7 compares the phase maps calculated by direct numerical simulations of the original limit-cycle oscillator with those obtained by the conventional and generalized phase equations. These results indicate that the generalized phase equation well captures the dynamics of the oscillator, while the conventional equation does not; it turns out that the conventional phase equation could not actually predict the oscillator dynamics in the numerical simulation of Fig. A.6, and the seemingly correct prediction of the stable phase difference was a coincidence.

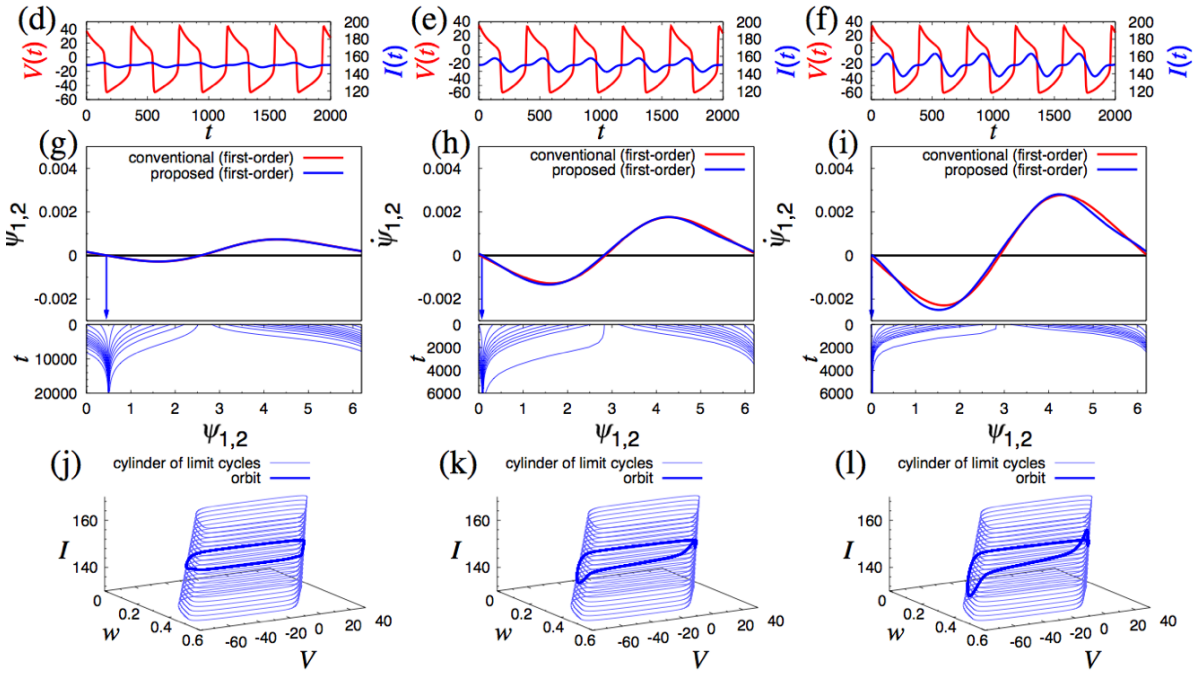

Figure A.6: Phase locking of the Morris-Lecar model (relaxation oscillation). Three types of periodically varying parameters, $I^{(j)}(t)$: $q^{(j)}(\epsilon t) = 150 + \alpha^{(j)} \sin(\omega_I t) - \alpha^{(j)} \sin(2\omega_I t)$ and $\sigma p^{(j)}(t) = 0$ with $\alpha^{(4,5,6)} = 10$, 15, 20 and $\omega_I = 0.016$ are used, which lead to $1:1$ phase locking to $I^{(4)}(t)$ [(d), (g), and (j)], $I^{(5)}(t)$ [(e), (h), and (k)], and $I^{(6)}(t)$ [(f), (i), and (l)]. (d)–(f) Time series of the state variable $V(t)$ of a periodically driven oscillator (red) and periodic external forcing (blue). (g)–(i) Dynamics of the phase difference ψ with an arrow representing the stable phase difference (top panel) and evolution of ψ from 20 different initial states (bottom panel). (j)–(l) Orbits of a periodically driven oscillator (blue) and I-dependent stable limit-cycle solutions (light blue) plotted in three-dimensional space (V, w, I).

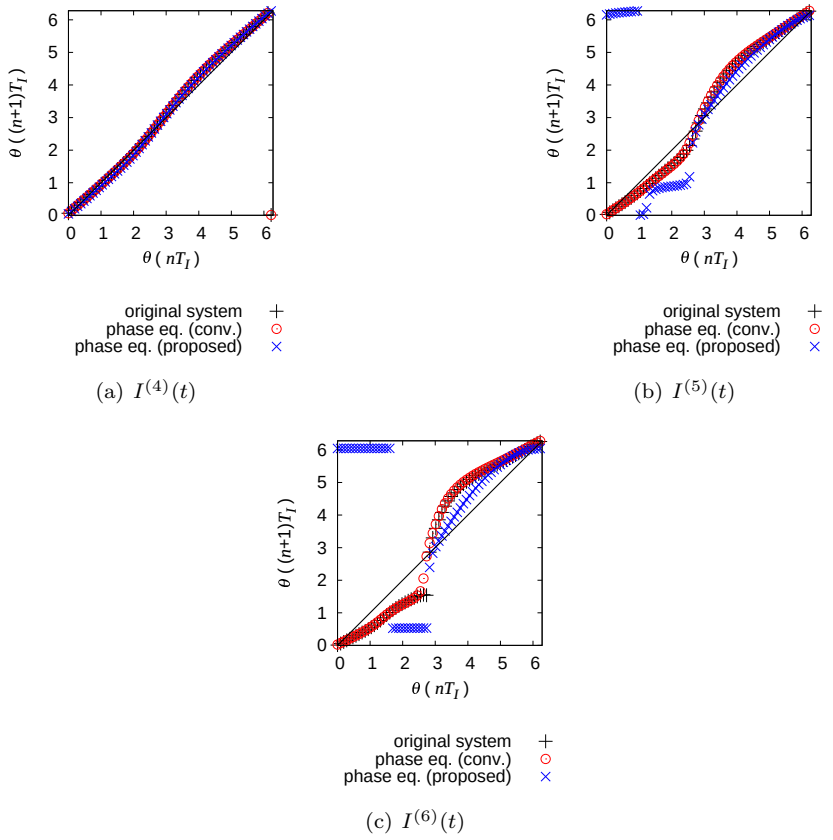

(a) $I^{(4)}(t)$ (b) $I^{(5)}(t)$

(c) $I^{(6)}(t)$

Figure A.7: Phase maps calculated by direct numerical simulations of the original limit-cycle oscillator (black crosses) and by the conventional (red circles) and generalized (blue circles) phase equations. Results for the three types of the periodic forcing used in Fig. A.5, i.e., (a) $I^{(4)}(t)$, (b) $I^{(5)}(t)$, and (c) $I^{(6)}(t)$, are shown.

A.9 Criterion for Decomposition of External Forcing

When we use the generalized phase reduction method, we need to decompose the input $\boldsymbol{I}(t)$ to the slowly varying component $\boldsymbol{q}(\epsilon t)$ and remaining weak fluctuations $\sigma \boldsymbol{p}(t)$ as follows:

$$\boldsymbol{I}(t) = \boldsymbol{q}(\epsilon t) + \sigma \boldsymbol{p}(t). \tag{A.73}$$

How to decompose the input $\boldsymbol{I}(t)$ is an important problem, which significantly affects the approximation accuracy of the phase equations.

In this section, we propose a simple criterion for choosing the threshold frequency Ω_d that gives a reasonable decomposition of the input for approximating the dynamics of the oscillator. Here, we define the decomposition by a linear filter $f(\tau)$ as follows:

$$\boldsymbol{q}(\epsilon t) = \int_{-\infty}^{+\infty} \boldsymbol{I}(t-\tau) f(\tau) d\tau, \tag{A.74}$$

$$\sigma \boldsymbol{p}(t) = \boldsymbol{I}(t) - \boldsymbol{q}(\epsilon t), \tag{A.75}$$

where $f(\tau)$ is assumed to be an ideal low-pass filter with the cutoff frequency Ω_d, *i.e.*, the amplitude response $A(\Omega)$ $(:= |\int_{-\infty}^{+\infty} f(\tau) e^{-i\Omega\tau} d\tau|)$ of $f(\tau)$ is given by

$$A(\Omega) = \begin{cases} 1 & (|\Omega| < \Omega_d), \\ 0 & (\text{otherwise}). \end{cases} \tag{A.76}$$

As discussed in Sec. A.4, we can describe the dynamics of a limit-cycle oscillator by phase and amplitude variables, where the amplitude variable represents the deviation of the oscillator state from the periodic orbit. If we assume that the state of the oscillator state $\boldsymbol{X}(t)$ is two-dimensional, it can be fully described by a phase variable $\theta(t)$ and an amplitude variable $r(t)$ defined as

$$r(t) = R(\boldsymbol{X}(t), \boldsymbol{q}(\epsilon t)), \tag{A.77}$$

where the function $R(\boldsymbol{X}, \boldsymbol{I})$ of $\boldsymbol{X} \in \mathbb{R}^n$ and $\boldsymbol{I} \in \mathbb{R}^m$ is defined as

$$\frac{\partial R(\boldsymbol{X}, \boldsymbol{I})}{\partial \boldsymbol{X}} \cdot \boldsymbol{F}(\boldsymbol{X}, \boldsymbol{I}) = -\lambda(\boldsymbol{I}) R(\boldsymbol{X}, \boldsymbol{I}). \tag{A.78}$$

In Sec. A.4, we derived the following dynamical equation of the amplitude variable $r(t)$:

$$\frac{dr(t)}{dt} = -\lambda(\boldsymbol{q}(\epsilon t)) r + \sigma \boldsymbol{\zeta}_r(\theta, r, \boldsymbol{q}(\epsilon t)) \cdot \boldsymbol{p}(t) + \epsilon \boldsymbol{\xi}_r(\theta, r, \boldsymbol{q}(\epsilon t)) \cdot \dot{\boldsymbol{q}}(\epsilon t) + O(\sigma^2), \tag{A.79}$$

where $\boldsymbol{\zeta}_r(\theta, r, \boldsymbol{q}) = \boldsymbol{G}(\boldsymbol{X}, \boldsymbol{q})^\top \frac{\partial R(\boldsymbol{X}, \boldsymbol{q})}{\partial \boldsymbol{X}}\big|_{\boldsymbol{X}=\tilde{\boldsymbol{X}}(\theta, r, \boldsymbol{q})}$, $\boldsymbol{\xi}_r(\theta, r, \boldsymbol{q}) = \frac{\partial R(\boldsymbol{X}, \boldsymbol{q})}{\partial \boldsymbol{q}}\big|_{\boldsymbol{X}=\tilde{\boldsymbol{X}}(\theta, r, \boldsymbol{q})}$, and $\tilde{\boldsymbol{X}}(\theta, r, \boldsymbol{q})$ is a state point in $\mathbb{R}^n$ satisfying $\Theta(\tilde{\boldsymbol{X}}, \boldsymbol{q}) = \theta$ and $R(\tilde{\boldsymbol{X}}, \boldsymbol{q}) = r$.

As discussed in Sec. A.4, the approximation error of the generalized phase equation (**??**) is of the order $O(r)$. Thus, we can minimize the approximation error by minimizing the amplitude $|r|$,

i.e., the deviation from the periodic orbit. From Eq. (A.38), we can approximate $\boldsymbol{\xi}_r(\theta, 0, \boldsymbol{I})$ by $\boldsymbol{\zeta}_r(\theta, 0, \boldsymbol{I})$ as follows:

$$\boldsymbol{\xi}_r(\theta, 0, \boldsymbol{I}) = \frac{1}{\lambda(\boldsymbol{I})}\boldsymbol{\zeta}_r(\theta, 0, \boldsymbol{I}) + O\left(\frac{1}{\lambda(\boldsymbol{I})^2}\right). \tag{A.80}$$

In addition, the order of r can be evaluated as follows (see Eq. (A.45)):

$$r = O\left(\frac{\epsilon}{\lambda(\boldsymbol{q}(\epsilon t))^2}, \frac{\sigma}{\lambda(\boldsymbol{q}(\epsilon t))}\right). \tag{A.81}$$

Thus, by plugging Eqs. (A.80) and (A.81) into Eq. (A.79), we can obtain

$$\begin{aligned}\frac{dr(t)}{dt} = &-\lambda(\boldsymbol{q}(\epsilon t))r + \boldsymbol{\zeta}_r(\theta, 0, \boldsymbol{q}(\epsilon t)) \cdot \left[\sigma \boldsymbol{p}(t) + \frac{\epsilon}{\lambda(\boldsymbol{q}(\epsilon t))}\dot{\boldsymbol{q}}(\epsilon t)\right] \\ &+ O\left(\frac{\epsilon^2}{\lambda(\boldsymbol{q}(\epsilon t))^2}, \frac{\epsilon\sigma}{\lambda(\boldsymbol{q}(\epsilon t))}, \frac{\epsilon\sigma}{\lambda(\boldsymbol{q}(\epsilon t))^2}, \frac{\sigma^2}{\lambda(\boldsymbol{q}(\epsilon t))}, \frac{\epsilon}{\lambda(\boldsymbol{q}(\epsilon t))^2}, \right).\end{aligned} \tag{A.82}$$

This equation indicates that, if $\lambda(\boldsymbol{q}(\epsilon t))$ can be assumed constant, we can minimize the amplitude $|r|$ by minimizing the amplitude of

$$\tilde{I}_j(t) := \sigma p_j(t) + \frac{\epsilon}{\lambda(\boldsymbol{q}(\epsilon t))}\dot{q}_j(\epsilon t), \tag{A.83}$$

where $j = 1, \ldots, m$ represents vector components.

As a measure for choosing the threshold value Ω_d, we define the variance $V_j(\Omega_d)$ of $\tilde{I}_j(t)$ as

$$V_j(\Omega_d) = \lim_{\tau\to\infty}\frac{1}{\tau}\int_0^\tau [\tilde{I}_j(t)]^2 dt. \tag{A.84}$$

We assume that the absolute value of the second largest Floquet exponent $\lambda(\boldsymbol{q}(\epsilon t))$ does not vary largely and replace $\lambda(\boldsymbol{q}(\epsilon t))$ by a constant λ_c defined as

$$\lambda_c := \lambda\left(\lim_{\tau\to\infty}\frac{1}{\tau}\int_0^\tau \boldsymbol{I}(t)dt\right). \tag{A.85}$$

Under this approximation, Eq. (A.84) can be written as follows:

$$V_j(\Omega_d) \approx 2\int_0^{\Omega_d}\frac{\Omega^2}{\lambda_c^2}P_j(\Omega)d\Omega + 2\int_{\Omega_d}^\infty P_j(\Omega)d\Omega, \tag{A.86}$$

where $P_j(\Omega)$ is the power spectrum of $I_j(t)$.

The optimal threshold frequency Ω_d that minimizes this approximate variance $V_j(\Omega_d)$ can be obtained as

$$\Omega_d = \lambda_c, \tag{A.87}$$

because this Ω_d satisfies

$$\frac{dV_j(\Omega_d)}{d\Omega_d} = \left(\frac{\Omega_d^2}{\lambda_c^2} - 1\right) P_j(\Omega_d) = 0, \tag{A.88}$$

and

$$\frac{d^2V_j(\Omega_d)}{d\Omega_d^2} = \left(\frac{\Omega_d^2}{\lambda_c^2} - 1\right) \frac{dP_j(\Omega_d)}{d\Omega_d} + \frac{2\Omega_d}{\lambda_c^2} P_j(\Omega_d) > 0. \tag{A.89}$$

Thus, the optimal timescale for the decomposition of the input to minimize the approximate variance $V_j(\Omega_d)$ coincides with the amplitude relaxation time of the oscillator.

We propose Eq. (A.87) as a simple criterion for choosing the value of the threshold frequency Ω_d. It gives an optimal Ω_d for predicting the oscillator dynamics when $\lambda(\boldsymbol{q}(\epsilon t))$ is strictly constant, and is expected to provide nearly optimal prediction even if $\lambda(\boldsymbol{q}(\epsilon t))$ slightly varies. Although we assumed that the state of the oscillator is two-dimensional, our result can be generalized to higher-dimensional cases by regarding $\lambda(\boldsymbol{q})$ as the absolute value of the second largest Floquet exponent among the n Floquet exponents of the oscillator, because the deviation from the periodic orbit is dominated by the slowest amplitude mode characterized by the second largest Floquet exponent.